CAPACITIVE TECHNOLOGY FOR ENERGY EXTRACTION FROM CHEMICAL POTENTIAL DIFFERENCES

Bruno Bastos Sales

Thesis committee

Promotor
Prof. Dr C.J.N. Buisman
Professor of Biological Recovery and Re-use Technology
Wageningen University

Co-promotor
Dr. H.V.M. Hamelers
Program Director
Wetsus – Centre of Excellence for Sustainable Water Technology, Leeuwarden

Other members
Prof. Dr J.H. Bitter, Wageningen University
Prof. Dr D.C. Nijmeijer, University of Twente, Enschede
Prof. Dr A.V. Delgado, Granada University, Spain
Prof. S. Tennison, MAST Carbon International Ltd., Basingstoke, United Kingdom

This research was conducted under the auspices of the Graduate School SENSE (Netherlands Research School for the Socio-Economic and Natural Sciences of the Environment)

CAPACITIVE TECHNOLOGY FOR ENERGY EXTRACTION FROM CHEMICAL POTENTIAL DIFFERENCES

Bruno Bastos Sales

Thesis
submitted in fulfilment of the requirements for the degree of doctor
at Wageningen University
by the authority of the Rector Magnificus
Prof. Dr M.J. Kropff,
in the presence of the
Thesis Committee appointed by the Academic Board
to be defended in public
on Friday 1 November 2013
at 10:30 a.m. in the Grand Hotel Post Plaza, Leeuwarden.

Bruno Bastos Sales
Capacitive Technology for Energy Extraction from Chemical Potential Differences, 120 pages

PhD thesis Wageningen University, Wageningen , NL (2013)
With references, with summaries in Dutch and English

ISBN 978-94-6173-738-0

Table of Contents

1. General Introduction 6

2. Direct Power Production from a Water Salinity Difference in a Membrane-Modified Supercapacitor Flow Cell 20

3. Electrochemical characterization of a supercapacitor flow cell for power production from salinity gradients 33

4. Auto Generative Capacitive Mixing for Power Conversion of Sea and River Water by the Use of Membranes 52

5. Impact of Wire Geometry in Energy Extraction from Salinity Differences Using Capacitive Technology 73

6. Capacitive Technology for Extracting Power from Low Temperature Waste Heat 88

7. General Discussion and Perspectives 96

References 104

Summary 111

Samenvatting 114

Chapter 1

General Introduction

1.1 Introduction

Both salinity and temperature differences constitute a potential renewable energy source (Wick and Schmitt 1977). This thesis reports the invention, together with scientific and technological developments, of a capacitive technology capable of electricity production from these salinity and temperature differences. The capacitive technology is based on the use of capacitive porous electrodes covered with ion exchange membranes. The ion exchange membranes are driving the process as they give an electrical potential when exposed to a difference in salinity or temperature. As the Donnan potential lies at the basis of the membrane potential, this technology is called Capacitive energy extraction based on Donnan Potential (CDP). The thesis is mainly concerned with energy extractions from salinity gradients, and in the end an initial account about the use of CDP for temperature gradients is presented. This introduction therefore focuses on salinity gradient energy.

CDP exploits the differences of salinity between two water bodies to produce electricity in a sustainable manner. A naturally occurring example is the delta areas, i.e. when rivers meet the sea, frequently and widely found around the world. In this chapter we: (i) discuss the need for a society using renewable energy, (ii) describe the potential role of marine sources in achieving this goal, (iii) introduce the capacitive technology of this thesis.

1.2 The current Energy Challenge

The rapid increase of economic and life standards around the globe, requires an accelerated energy supply (Kamat 2007). Already during the last century, the worldwide energy use went up 16 times while the human population went up 4 times. Current energy production is mainly based on fossil fuels that are polluting when combusted and which resources are depleting. Yet, a sustainable worldwide

economic growth crucially depends on the availability of cheap and cleaner energy. For example, the largest emerging markets in the world, with their large number of new consumers buying new cars, are India and China. Since these fleets depend on burning fossil fuels for their mobility, these countries have more than 50% of their air pollution primarily caused by CO2 emissions from the automotive industry (Myers and Kent 2003). Such cases demonstrate the harmful impact on the environment of this increasing energy demand when fossil energy sources are simply scaled up in production and use. In addition to this disadvantage, fossil fuels belong to the family of non-renewable resources due to their slow formation, taking ages (in geochronological terms) to complete. Another great additional concern at the moment is global warming, which has a significant contribution from greenhouse gases released during use of fossil fuels (Figure 1.1).

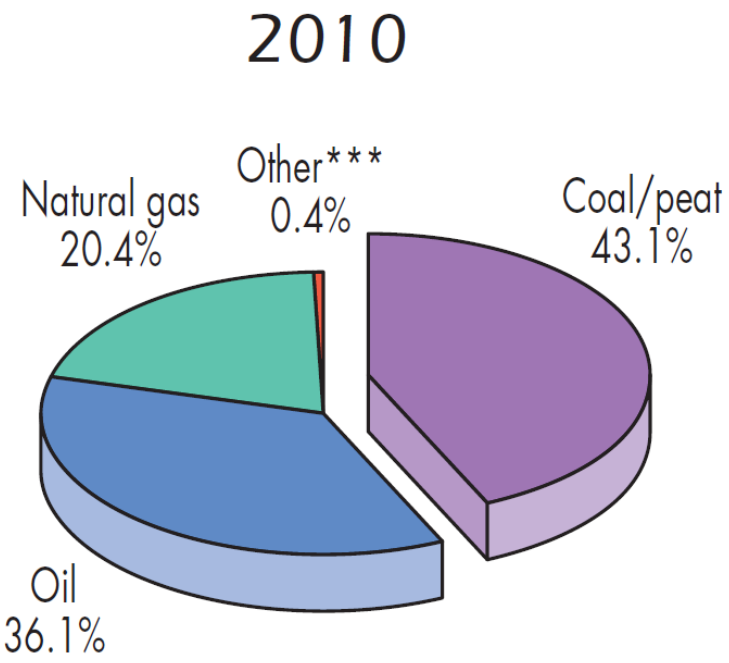

Figure 1.1 Contribution of different fossil fuels to CO2 emissions in 2010 (source: IEA 2012)

In the last decades, a global mobilization around climate change has started and culminated in a recent call of the United Nations Framework Convention on Climate Change (UNFCCC): “stabilization of greenhouse-gas (GHG) concentrations in the atmosphere at a level that would prevent dangerous anthropogenic interference with the climate system implies that 10 TW (10 x 10^{12} watts) of carbon-emission-free power needs to be produced by the year 2050, almost equivalent to the power provided by all of today's energy sources combined” (Hoffert, Caldeira et al. 2002). The current energy challenge is to maintain the present lifestyle, during the next decades, in a sustainable and cleaner way. Therefore the so-called green renewable sources are a solution. This motivates the development of renewable and environmentally clean alternatives to fossil fuel, either for its imminent peak production limitation (and its unavoidable complete depletion), or its heavy environmental outcome (Campbell 2002).

Next to the debate on energy sources, there’s also the debate on the future energy infrastructure driven by the need of a higher efficiency of energy conversion and transport. For example, in the Europe Union (EU), an increase is expected from 20% to 45.5% in the proportion of electricity in end-use applications by 2050. This reflects a paradigm shift on the demand side, where in an extremely developed region, direct use of fossil fuels is replaced by efficient electric technologies in the residential and transport sectors (Birol 2013). The increase in electricity demand alone could lead to a simple rise in the conversion of fossil fuels into electricity, but due to the EU directives to lower GHG emissions, new sustainable methods to access clean and reliable electricity production are required.

1.3 Renewable Sources

We are currently experiencing the second wave of strong interest in renewables. The first happened during the energy crisis of the mid-1970s, when the global oil production peaked and the risk of compromising prosperity due to lack of energy

emerged (Turner 1999). A boom of renewables' research and innovation followed the fear of fossil fuel limitations, but it was short lived since the oil supply quickly resumed meeting the continuous high demand. The 1990s brought the present attention to the consequences of burning fossil fuels in terms of pollution and climate change (Mann, Bradley et al. 1998).

The main renewable sources for electricity generation are: solar, wind, geothermal, bioenergy, marine and hydro. Figure 1.2 shows the recent trend in the investment in energy generation from different sources and the 2012 global generation. It shows a continuous predominance of investment in solar energy, which has received more than 50% of all investments in the last few years, while negligible funding has been allocated to marine resources. Larger part of these investments are supplied by governmental subsidies to renewable energy (Dincer 2000; Huys, Eshel et al. 2012; Kostevšek, Cizelj et al. 2013). Despite the increase in the role of non-hydro renewables, marine resources are consistently overlooked regardless its immense global potential and environmentally friendly characteristics (Jones and Rowley 2002).

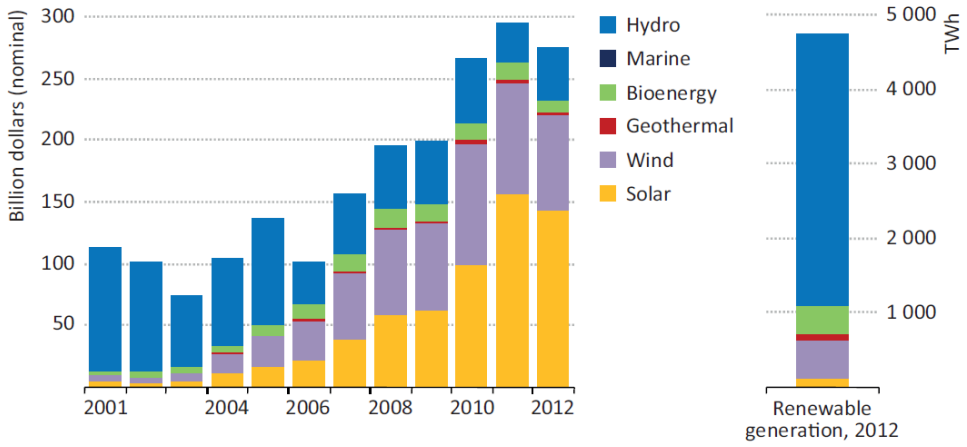

Figure 1.2 World renewables-based power sector investments by type and total generation (source: IEA 2013).

Table 1 (Wick and Schmitt 1977) shows the several possibilities for producing sustainable electricity from our vast oceans. Salinity and thermal gradients are clearly the outstanding candidates both in terms of global power potential and energy density. Salinity difference is particularly interesting in locations with nearby Delta areas, where rivers meet the sea, and other energy sources have less potential, e.g. solar and wind. Other marine competitors like ocean waves lack a substantial energy density to be viably exploited.

TABLE 1.
MARINE RENEWABLE RESOURCES

Resource	Power (TW)	Energy Density (m)
Ocean Currents	0.05	0.05
Ocean Waves	2.7	1.5
Tides	0.03	10
Thermal Gradient	2.0	210
Salinity Gradient	2.6	240

Our ambition is to make salinity gradients, or the so-called Blue Energy (Boon and van Roij 2011), a key player in the field of renewables. The first ever mention of this energy resource was in the 1950s (Pattle 1954), although it remained latent as simple scientific curiosity till the energy crisis (Levenspiel and Nevers 1974; Norman 1974; Loeb and Norman 1975). From that day, several distinct techniques and principles were suggested (Jones, Finley et al. 2003; Post, Veerman et al. 2007; Logan and Elimelech 2012). Pressure-Retarded Osmosis (PRO) and Reverse Electrodialysis (RED) are the furthest developed among them, each of these principles contain its own advantages and bottlenecks to achieve commercial relevance.

The thermodynamic upper limit for extractable work in Blue Energy processes is defined (Eq. 1.1) by the difference in the Gibbs free energy (ΔE_{mix}), or simply energy of mixing. When we mix two solutions with different salt concentration, e.g. sea and river, the energy of mixing is the sum of the chemical potentials times moles of the initial separated solutions minus those of the final mixed volume:

$$\Delta E_{mix} = 2RT\left[c_{sea} \ln \frac{c_{sea}\left(1+\frac{V_{river}}{V_{sea}}\right)}{c_{sea}+\left(\frac{V_{river}}{V_{sea}}\cdot c_{river}\right)} + \left(\frac{V_{river}}{V_{sea}}\cdot c_{river}\right) \ln \frac{c_{river}\left(1+\frac{V_{river}}{V_{sea}}\right)}{c_{sea}+\left(\frac{V_{river}}{V_{sea}}\cdot c_{river}\right)} \right] \quad \text{Eq. 1.1}$$

where R is the universal gas constant (J/K·mol), T is the absolute temperature (K), c_{sea} and c_{river} are the NaCl concentrations in sea and river (mol), finally V_{sea} and V_{river} are the volumes of sea and river water (m^3). This equation allows an estimate of the total global size of this energy source ~ 2.6 TW (Weinstein and Leitz 1976). Having a more conservative approach and taking into consideration the envisioned engineering constraints and actual efficiencies, still ~ 1 TW was calculated (Ramon, Feinberg et al. 2011).

1.4 Main principles for Blue Energy

We present the principles of PRO and RED and discuss the specific advantages and challenges (financial and engineering) of those techniques. This discussion will define the rationale for proposing and investigating our new capacitive technology.

1.4.1 Pressure-Retarded Osmosis

The principle of PRO is based on the osmotic driving force through a semipermeable membrane, i.e. a membrane allowing only water molecules to pass

and retaining the salt. Two compartments are separated by the membrane, of which one is filled with river and the other with sea water (Figure 1.3A). The osmotic potential makes water molecules diffuse through the membrane and increase the water volume in the sea water compartment (Figure 1.3B) while decreasing the water volume in the river compartment. For the operation of a PRO apparatus the sea water compartment volume is fixed and a hydraulic pressure is applied on the sea water. This applied pressure decreases the osmotic driving force and retards the osmotic process, thus the name pressure-retarded osmosis. As the sea water compartment is fixed and a pressure applied, the water volume transported through the membrane will leave the compartment under pressure and can then be used to generate electricity in a turbine.

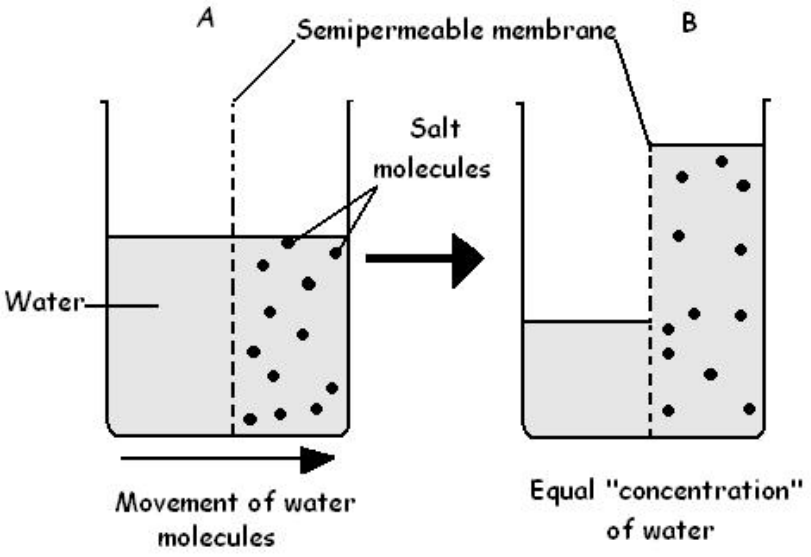

Figure 1.3 Schematics of the PRO principle. A) A compartment of river water is separated by a semipermeable membrane from the sea water compartment. B) Water molecules permeate the membrane and moves to the sea water compartment (source: Statkraft 2013).

The major constraint of PRO continues to be the search for a robust and dependable membrane capable of resisting high osmotic pressures (when in contact with high concentration brines) and preventing partial clogging due to fouling. An efficient pressure exchanger is also a component to be improved. Lowering the costs and further development of the characteristics of available commercial membranes are required to allow the process to operate more reversibly (Thorsen and Holt 2009).

1.4.2 Reverse Electrodialysis

Different from PRO, RED employs a different type of separator namely ion exchange membranes, i.e. membranes only allowing either cations or anions to pass while retaining water. The membranes are stacked in an alternating pattern of anion exchange membrane (AEM) and cation exchange membrane (CEM). This stack is placed between a pair of electrodes where a reversible redox couple generates an electric current, through the external load where energy is harvested. The cell potential is the result of the sum of the electrochemical potential over each membrane, simply named the membrane potential. This acts as the driving force for ionic flux via the membranes from the sea water compartment to the river water compartment. The direction of the ions is dictated by their polarity: anions move towards the anode where an oxidation happens; and cations move to the cathode where a reduction occurs (Figure 1.4).

The major constraint in RED is the need of further development of ion exchange membranes in terms of selectivity, price and resistance; together with spacer improvement to avoid viscous dissipation, i.e. the lowering of effective membrane surface area (the so-called “shadow effect”) (Długołęcki, Gambier et al. 2009); and the proper selection of electrode systems to avoid other losses related to optimal electrode segmentation for overall performance (Veerman, Saakes et al. 2010).

Continuous research is on progress tackling every one of these bottlenecks and several possible solutions have been suggested (Nijmeijer and Metz 2010).

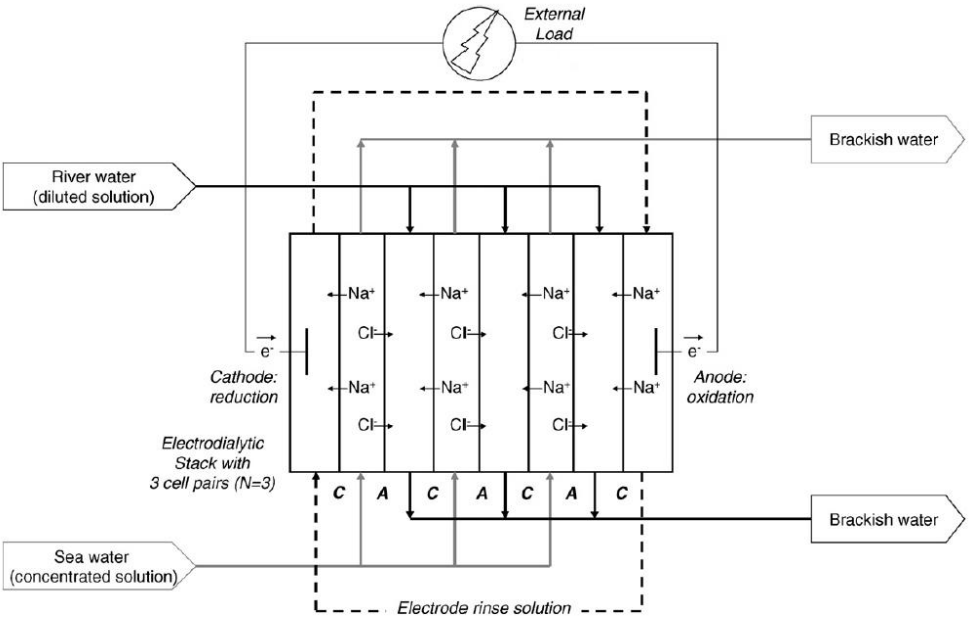

Figure 1.4 Schematics of a full RED conversion scheme. Anion exchange membranes (A) are alternated with cation exchange membranes (C), separating compartments for river and sea water. Source: (Post, Veerman et al. 2007).

1.5 Capacitive Technology for Energy Extraction

A principle combining supercapacitor technology and ion exchange membranes was introduced in 2009 proposing a new route for extracting energy from salinity gradients (Sales, Saakes et al. 2010). Figure 1.5 shows the typical apparatus construction to investigate this alternative. A single cell (Fig. 1.5A) comprises the sandwich combination of an electronic current collector, attached to a capacitive carbon layer for ionic adsorption/desorption, which in turn is covered by an ion exchange membrane (cationic and anionic) for selectivity and driving force due to

the Donnan potential (Donnan 1911), finally separated by a spacer. This cell is then connected to an external resistor (Fig. 1.5B), where electricity is harvested and analyzed by monitoring the voltage evolution over time by a multimeter.

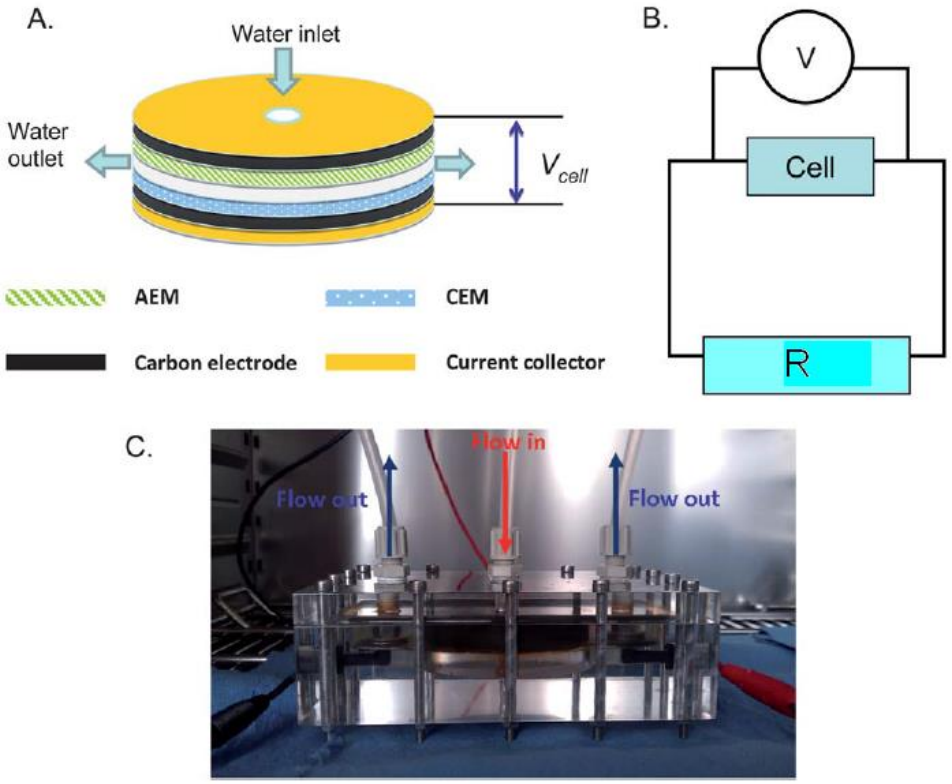

Figure 1.5 Schematic drawing of one cell pair (A), the electric circuit that the cells are incorporated into (B), and a photograph of the cell, showing where the saline solutions enter and leave the cell (C). Source: (Liu, Schaetzle et al. 2012)

The operation of the setup (Fig. 1.6) starts by alternating the flow of sea water and river water through the cell. During the flow of sea water, the Donnan potential acts as the driving force for ionic migration through the membranes and consequent adsorption (Fig. 1.6A) in the capacitive carbon layer, causing an electric current via

the external resistor to achieve electroneutrality. When these electrodes reach saturation, river water is then pumped and the reverse process occurs (Fig. 1.6B), releasing the ions from the electrodes back into the flow compartment and thus regenerating the cell to restart this two step cyclic process. The advantages of this capacitive technique ranges from presumed less sensitivity to fouling, to simplicity added to lack of secondary converters (turbines, batteries, parasitic redox reactions, etc.) A more detailed theoretical and practical description of this technology can be found in the subsequent chapters of this thesis.

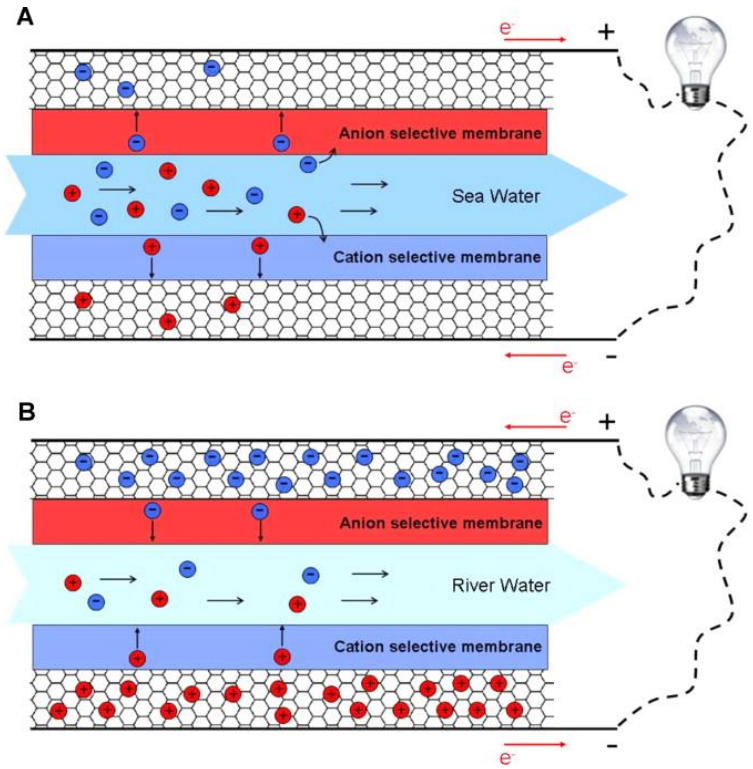

Figure 1.6 Working principle of Capacitive energy extraction based on Donnan Potential. (A) Sea water is flushed in the system allowing ions to diffuse in the electrodes and thus generate a current in the external load. (B) River water is flushed in the system allowing ions to diffuse out of the electrodes and thus generate an opposite current.

1.4 Outline of this thesis

The goal of this thesis is to introduce and develop a new principle for energy extraction from salinity gradients, named Capacitive energy extraction based on Donnan Potential (CDP) and show its possible application exploiting thermal gradients.

Chapter 2 introduces the principle and theoretical understanding in terms of of the adsorption/desorption cycles in CDP. A flow through cell was used to perform the experiments, resulting in a peak power around 70 mW/m^2 of membrane surface area. This study also highlights the benefits of using a design with ion exchange membranes.

Chapter 3 seeks to characterize and distinguish the individual contributions of the components in a CDP cell: carbon electrodes and ion exchange membranes, via electrochemical characterization. The methods cyclic voltammetry and galvanostatic charge-discharge were employed to determine the capacitive behavior of the cell and its capacitance in different conditions: varied concentration, different materials and impact of flow rate during operation.

To improve power density, Chapter 4 investigates in depth the hydrodynamics in the prototype CDP cell used in the previous studies. It analysis the disadvantages of using a flat plate electrode configuration, and concludes that optimizing the feed fluid flow is among the most beneficial paths to improve the technology and make it a viable competitor for energy extraction from gradients.

In **Chapter 5** a cylindrical shape for the electrodes a new is proposed, We theoretically investigate the benefits of such geometry, followed by experiments showing for the first time a decrease in internal resistance while at the same time of achieving lower hydrodynamic resistance. The advantages continue with faster

time response for the change of Donnan potential during operation. We also made the system mobile for stationary water bodies, instead of the contrary.

Chapter 6 shows for the first time the possibility of employing the CDP system for thermal gradients. In the case of streams with same concentration, but different temperatures, it is possible to cause ionic migration and adsorption/desorption cycles due to the principle of thermo membrane potential acting as driving force. We summarize the initial experiments confirming the electricity production from a difference of temperature with this setup.

In conclusion, in **Chapter 7** the aim of the discussion is to identify the current obstacles for the technology and suggest possible routes for overcoming restrains.

Chapter 2

Direct Power Production from a Water Salinity Difference in a Membrane-Modified Supercapacitor Flow Cell

The entropy increase of mixing two solutions of different salt concentrations can be harnessed to generate electrical energy. Worldwide, the potential of this resource, the controlled mixing of river and seawater, is enormous, but existing conversion technologies are still complex and expensive. Here we present a small-scale device that directly generates electrical power from the sequential flow of fresh and saline water, without the need for auxiliary processes or converters. The device consists of a sandwich of porous "supercapacitor" electrodes, ion-exchange membranes, and a spacer and can be further miniaturized or scaled-out. Our results demonstrate that alternating the flow of saline and fresh water through a capacitive cell allows direct autogeneration of voltage and current and consequently leads to power generation. Theoretical calculations aid in providing directions for further optimization of the properties of membranes and electrodes.

This chapter has been published as:

Sales, B. B.; Saakes, M.; Post, J. W.; Buisman, C. J. N.; Biesheuvel, P. M.; Hamelers, H. V. M., Direct Power Production from a Water Salinity Difference in a Membrane-Modified Supercapacitor Flow Cell. *Environmental Science & Technology* **2010**, 44, (14), 5661-5665.

2.1 Introduction

Fossil fuel depletion and carbon dioxide emissions drive the quest for renewable energy resources. One option is to harvest energy from the inevitable entropy increase when fresh and saline waters mix. In a suitable process work can be extracted, up to a maximum equal to the entropy increase. When work is extracted, simultaneously the aqueous streams cool down to the same amount; thus effectively heat is converted into work, driven by the entropy increase. The theoretical available amount of energy from mixing 1 m^3 river water with a large surplus of seawater is 2.5 MJ, corresponding to the hydraulic energy of a dam of a height of over 250 m. In terms of total power, the effluent of all fresh water streams combined has the potential to satisfy the current global electricity demand (2 TW) (Wick and Schmitt 1977; Post, Hamelers et al. 2008).

Existing technologies require auxiliary devices to harvest the energy. Unfortunately, such devices increase the complexity of the system and reduce the energy efficiency. Here we show how placing thin ion-exchange membranes in the flow cell leads to direct electricity production, without requiring auxiliary processes or converters. Existing technologies comprise pressure-retarded osmosis (PRO) (Achilli, Cath et al. 2009; Thorsen and Holt 2009), reverse electrodialysis (RED) (Pattle 1954; Weinstein and Leitz 1976; Długołęcki, Gambier et al. 2009; Veerman, Saakes et al. 2009), and a capacitive technology based on double-layer expansion (CDLE) (Brogioli 2009). PRO makes use of the osmotic pressure difference between fresh and saline water, which leads to flow of water through a water-permeable (but necessarily salt-impermeable) membrane, and the development of a pressure differential which using a turbine and pressure exchanger can be converted into electrical power. PRO can use any solution of dissolved particles, but for aqueous solutions, it is also possible to make explicit use of the charge of the ions as is done in RED and CDLE. RED is a continuous process in which a large number of cation and anion exchange membranes form chambers through which fresh and saline water is alternately fed. All membrane potentials add up and

combined with two electrodes at each end, electrical power can be continuously extracted. A suitable redox solution must circulate between the two electrode chambers at each end of the stack to inhibit large electrode overpotentials and allow for the required electrochemical reactions. When using CDLE, based on electrostatic double layer “super”-capacitors (Chmiola, Yushin et al. 2006; Simon and Gogotsi 2008; Stoller, Park et al. 2008; Levi, Salitra et al. 2009), fresh and saline water sequentially flow in between or along two blocking (i.e., nonfaradaic) electrodes electrically connected via an external power source (which ideally is a rechargeable battery with very low overpotential). While saline water flows through the cell, the electrodes are charged up, one relative to the other. Switching to flow of fresh water, the double layers in the electrode expand, the cell voltage spontaneously increases, and the electron current spontaneously reverses, leading to power production.

All of these technologies need auxiliary equipment (turbines and pressure exchangers in PRO; redox solutions in RED; secondary batteries in CDLE) reducing overall efficiency and increasing complexity and costs. Here we introduce a new technology that combines elements of RED and CDLE, namely the generation of an electrical potential over an ion-exchange membrane separating salt solutions of different concentration, and the capacity of porous electrodes to store large quantities of ionic and electronic charge, see Figure 2.1a,b. As we will show this leads to a process in which we can simply alternate the fresh and saline water flow through the device and spontaneously generate a current both during contacting with fresh water (with current running in one direction) and during the subsequent step of contacting with saline water (with current now running in the other direction), without requiring a secondary battery. This is possible because the ion-exchange membranes only allow passage of one ion type (either the cation or the anion), thereby setting up an ionic current in one direction leading at the same time to an electronic current in the external circuit to compensate the ionic charge that forms within the porous electrodes. Combined with the Donnan potentials that

develop across each membrane, electrical power can be extracted from this cell. As electrochemical reactions are not required (electron and ion flow is purely of a capacitive nature) we do not need to add a chemical redox couple to the system.

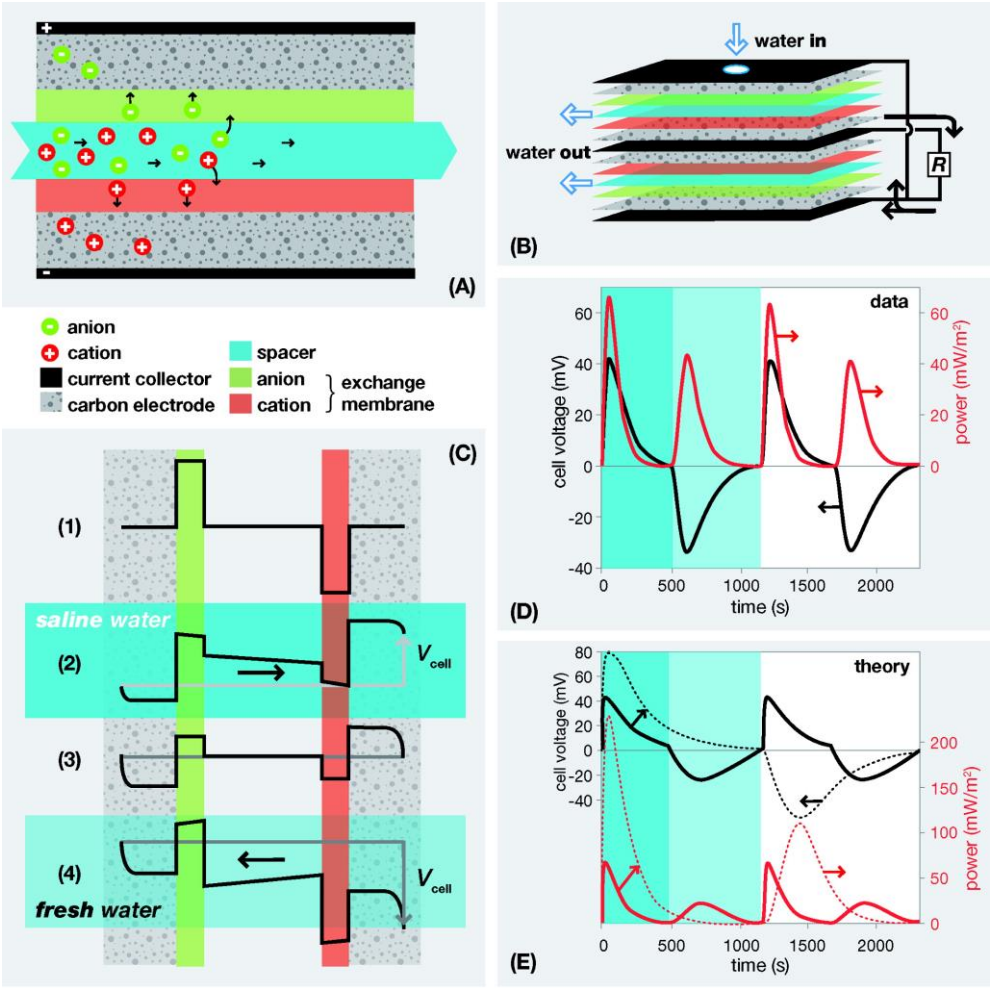

Figure 2.1 (A) Schematic representation of anion and cation transport from spacer channel through ion-exchange membranes into the porous electrodes. (B) Sandwich structure of two adjacent cells and direction of current through a resistance R when saline water flows through the cell (stage (2) of panel C). (C) Electrostatic potential profiles across the cell. Horizontal arrows show direction of

current. From the initial situation (1), during flow of saline water (2), the membrane potentials are perturbed leading to a positive cell voltage. (3) Formation of electrostatic double layers ultimately cancels the membrane potential. (4) Flowing fresh water, the membrane potentials are again perturbed and negative cell voltages and currents result, until we arrive back in (1). Both during stage 2 and 4 electrical work is performed in the external circuit. (D) Experimental data for cell voltage, Vcell, and power in two subsequent cycles (R = 1 Ω). (E) Theoretical results (solid lines: with leakage; dashed lines: no leakage).

To prove the feasibility of the idea we constructed a device consisting of a spacer compartment through which the water flows and two porous carbon electrodes electrically connected through a resistance R. In between the spacer and the electrodes, cation and anion exchange membranes are placed. We alternate the flow of saline and fresh water through the device, in this manner allowing continuous autogeneration of voltage and power in the external resistance. For a proof-of-principle that energy production is possible, a simple electrical circuit was used with a fixed resistance in series with the cell.

2.2 Materials and Methods

The experiments were performed in a homemade stack consisting of 8 parallel cells. Figure 2.1a presents a sketch of one cell, while Figure 2.1b schematically shows how two cells out of the full stack are electrically connected. Each current collector is in contact with two porous electrode layers in adjacent cells. With the current collectors alternatingly positively or negatively biased, the direction of ion transport is also reversed from one to the next cell, which importantly implies that also the sequence of ion-exchange membrane must be reversed from cell to cell.

Each cell consists of a sandwich of graphite (dense) current collectors (Cixi Sealing Spacer Material Factory, Ningbo City, China, thickness δcc = 250 μm), porous carbon electrodes (type CR-B, Axion Power Intl., Delaware, USA, δe = 270 μm, 8.5

g total mass in the stack), cation and anion exchange membranes (Neosepta AMX and CMX, Tokuyama, Japan, δm ~ 160 μm), and a polymer spacer (Glass fiber prefilter, cat no. AP2029325, Millipore, Ireland, δsp = 400 μm). All materials are cut in pieces of 6 × 6 cm^2 dimension and are assembled, after which the entire stack of all layers is firmly pressed together and placed in a Teflon housing. An aqueous NaCl solution is pumped through a small hole (1.5 × 1.5 cm^2) located in the exact middle of the stack and flows radially outward through the spacer layers. The generated electrical current runs through an external resistance, across which voltage is measured using a high-impedance potentiostat (Iviumstat, IVIUM Technologies, Eindhoven, the Netherlands). Synthetic fresh water is based on a clow = 10 mM ionic strength NaCl solution (which is about the lower range of brackish water) and for saline water a salinity of chigh = 510 mM is used. The water flow rate is set to Φtot = 60 mL/min.

Theory

To evaluate and optimize the process we set up a theoretical model which describes both ion transport and storage as well as the ion-exchange membranes and the electrostatic double layers (EDLs) formed inside of the porous electrodes (Bazant, Thornton et al. 2004; Zhao, Biesheuvel et al. 2009; Biesheuvel and Bazant 2010). We make the following assumptions: 1. Perfect symmetry, i.e., the anion (exchange membrane) behaves exactly the same as the cation (exchange membrane), except for the obvious difference in sign; 2. The spacer compartment (flow channel) is ideally mixed, thus absence of ion concentrations gradients in any direction; 3. The membranes are perfectly blocking for co-ions; 4. The salt concentration, ce, in the pores of the electrodes is independent of position and changes in time because of expulsion of co-ions from the EDLs that gradually form, while a leakage flow of part of the solution through the electrode (instead of through the spacer) further modifies ce; 5. The Gouy−Chapman-Stern (GCS) model describes the equilibrium EDLs formed inside of the electrode (Biesheuvel

2004; Biesheuvel and van der Wal 2010; Jiang and Stein 2010). With these assumptions we can set up the following theoretical model.

First of all, an overall salt balance is given for the spacer compartment by

$$v_{sp}\frac{dc_{sp}}{dt} = \Phi_{sp}\left(c_0 - c_{sp}\right) - A\cdot\frac{J}{F} \qquad \text{Eq. 2.1}$$

where c_0 is the inlet salt concentration (in mM; either c_{low} for fresh water intake; or c_{high} for saline water), c_{sp} is the salt concentration in the spacer channel, v_{sp} is the spacer open volume, t is time, Φ_{sp} is the flow rate through the spacer, A is the projected area of all electrodes of one bias, J is the current density (in A/m^2) and F is the Faraday constant. Current density relates to the cell voltage V_{cell} and the external resistance R_{ext} according to

$$V_{cell} = J\cdot A\cdot R_{ext} \qquad \text{Eq. 2.2}$$

while within the cell J relates to the dimensionless potential drop across half the spacer channel and one membrane, $\Delta\Phi_{tr+mem}$, according to

$$J = -K\cdot F\cdot\Delta\phi_{tr+mem} \qquad \text{Eq. 2.3}$$

with K being an effective transfer coefficient (multiply Φ with V_T = RT/F to obtain the dimensional voltage, V). The cell voltage V_{cell} is given by

$$\frac{1}{2}\frac{V_{cell}}{V_T} = \Delta\phi_{tr+mem} + \Delta\phi_{donnan} + \Delta\phi_d + \Delta\phi_{st} \qquad \text{Eq. 2.4}$$

where $\Delta\Phi_d$ is the diffuse layer potential of the EDLs in the electrode, $\Delta\Phi_{st}$ is the Stern layer potential, and $\Delta\Phi_{donnan}$ is the membrane potential given by a summation of the two Donnan potentials established on each side of the membrane, resulting in (Biesheuvel and van der Wal 2010)

$$\Delta\phi_{donnan} = \ln\left(\frac{c_{sp}}{c_e}\right) \qquad \text{Eq. 2.5}$$

where c_e is salt concentration in the (charge-neutral) pores within the electrode. According to GCS-theory, $\Delta\Phi_d$ and $\Delta\Phi_{st}$ relate to the electrode charge density q as

$$q = 4\lambda_D c_e F \sinh\left(\frac{1}{2}\Delta\phi_d\right) \qquad \text{Eq. 2.6}$$

$$q = C_{st} \cdot \Delta\phi_{st} \cdot V_T \qquad \text{Eq. 2.7}$$

where λ_D is the Debye length

$$\lambda_D = \left(8\pi \cdot c_e \cdot N_{av} \cdot \lambda_B\right)^{-\frac{1}{2}} \qquad \text{Eq. 2.8}$$

and where λ_B is the Bjerrum length (λ_B = 0.72 nm in water at room temperature), N_{av} is Avogadro's number, and C_{st} is the Stern layer capacity. Surface charge q relates to J according to

$$\frac{dq}{dt} = -J \cdot \frac{A}{a} \qquad \text{Eq. 2.9}$$

where a is the internal electrode area of all electrodes of one bias. Finally, a salt balance for each of the electrode compartments is given by

$$v_e \cdot \frac{dc_{eff}}{dt} = \Phi_e \cdot \left(c_0 - c_e\right) \qquad \text{Eq. 2.10}$$

where v_e is the electrode open volume, Φ_e is the solution flow rate through each of the electrodes, and c_{eff} is an effective pore co-ion concentration given by (Grahame 1947)

$$c_{eff} = c_e - 2\lambda_D \cdot h_p^{-1} \cdot c_e\left(1 - \exp\left(\frac{1}{2}\Delta\phi_d\right)\right) \qquad \text{Eq. 2.11}$$

i.e., c_{eff} equals the pore salt concentration, c_e, reduced by co-ion expulsion from the EDLs. Here, h_p is an effective pore size (pore volume/internal area).

Based on (Zhao, Biesheuvel et al. 2009) we use the following parameter settings for the theoretical model which describes the stack of 8 cells, namely: electrode projected area A = 270 cm^2, open spacer volume v_{sp} = 70 mL, total solution flow rate Φ_{tot} = 1 mL/s, internal electrode area a = 3820 m^2, and Stern capacity C_{st} = 0.1 F/m^2 (both a and A are defined for all electrodes of one bias). For h_p we use h_p = 1.06 nm based on the specific area for ion adsorption a_m = 900 m^2/g, porosity p = 0.55, and electrode mass density ρ = 0.58 g/mL, where $h_p = p/(a_m \cdot \rho)$. The transfer

coefficient K in μmol/(m^2·s) is empirically described as $K^{-1} = K_m^{-1} + (0.5 \cdot c_{sp}+10)^{-1}$ with c_{sp} in mM and K_m representing the transfer coefficient of the membrane, for which K_m = 35 μmol/(m^2·s) is used, while the second term describes the transfer coefficient in the spacer channel which for sufficiently high salt concentrations, becomes proportional to c_{sp}.

The calculation is repeated for several cycles, until the system stabilizes and a dynamic steady-state is reached. Without leakage through the electrode chamber (α=0), we require as input a value for the effective co-ion electrode concentration, c_{eff}, though the chosen value does not have a large influence on the outcome of the calculation. We base the calculation on $c_{eff} = (c_{low} \cdot c_{high})^{1/2}$ ~ 71 mM. With leakage, c_{eff} changes in time and does not have to be prescribed. Instead, we require a value for the electrode open volume, which we estimate as v_e = 4 mL (=$A \cdot p \cdot \delta_e$). We fit the theory to the data by varying the fraction of the total flow rate Φ_{tot} that inadvertently flows (i.e., leaks) through each of the electrodes, instead of flowing through the spacer channel, given by $\alpha = \Phi_e/\Phi_{tot}$. The solution flow through the spacer compartment is given by $\Phi_{sp} = (1-2\alpha) \cdot \Phi_{tot}$.

2.3 Results and Discussion

The process is based on sequentially flowing fresh and saline water through the cell. Starting with a cell that is equilibrated in fresh water (stage 1 in Figure 2.1c), when we now switch to flow of saline water, a positive membrane potential rapidly develops, leading to a positive cell voltage and (ionic and electron) current (stage 2). The current leads to the gradual formation of electrostatic double layers in the porous electrodes, which over time leads to the decay to zero of the externally measurable cell voltage (stage 3). Upon switching back to fresh water, the membrane potentials are reversed, and both the direction of the current and the sign of the cell voltage are reversed (stage 4) until the electrostatic double layers are again uncharged and we are back in stage 1. Both during charging (stage 2) and discharging (stage 4) electrical power is produced. Figure 2.1d shows two

cycles (out of a larger sequence) with experimental data, for an external resistance of 1 Ω. During charging the voltage increases to >40 mV with a maximum power around 60 mW/m^2, while during discharge these numbers are somewhat lower (35 mV and 40 mW/m^2). Results at other values of the external resistance are presented in Table 1. The charge transferred from one to the other electrode can be calculated as 8.0 C, while 0.4 J energy is extracted.

TABLE 1. Experimental Results for Maximum Voltage, Maximum Power Density, and Cycle Energy Efficiency

load (Ω)	max voltage (mV)	power density (mW/m^2)	energy efficiency (%)
100	119	5.3	47
11	98	32.6	56
1	42	66	27
0.5	29	72	22

Figure 2.1e shows theoretical results of our process model for the flow cell, based on two value of α, the fraction of the solution that inadvertently flows through (each of) the electrodes, i.e., a leakage flow. For α = 0.02 we can fit the model to a very reasonable extent to the data (solid lines), suggesting that part of the ingoing solution indeed flows through the electrode structure, and not through the spacer. This electrode flow reduces the concentration difference between the electrode region and the spacer region and thus reduces the membrane potential and consequently the cell voltage and power. Making a calculation for a cell design where the electrode is blocked off on all sides and thus leakage is zero (α = 0), we obtain the second set of curves in Figure 2.1e (dashed lines) showing that making this design improvement has the potential to increase the maximum voltage by more than a factor of 2 and the maximum power by over a factor of 4. The theoretical stored charge increases by a factor of 3.

It is interesting to note that in all of these theoretical curves the voltage and power are lower during contacting with fresh water (stage 4) than during contacting with saline water (stage 2) as also observed in the data. At first thought, one might perhaps consider this difference to be due to the higher resistance in the spacer channel during flushing with fresh water. However, in a separate calculation where K was independent of salt concentration, interestingly the difference between the two states only diminished slightly, see Figure 2.2. Thus, this difference is an informative fingerprint of the processes that take place in the spacer channel and in the electrode, captured in first-order by the present model.

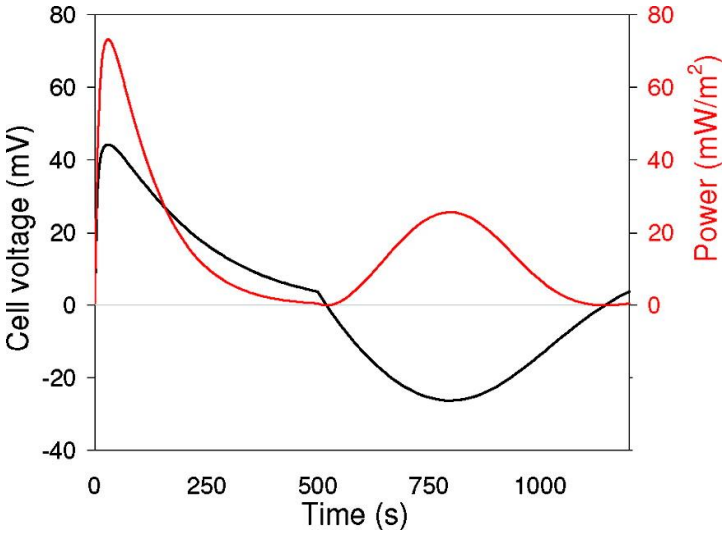

Figure 2.2 Theoretical results for cell voltage and power in a full cycle where in stage 2 (0 < time (s) < 500) the cell is flushed with saline water while in stage 4 (500 < time (s) < 1200) the cell is contacted with fresh water. In this calculation the transfer coefficient K is assumed to be independent of salt concentration, and the same difference remains between stages 2 and 4 as experimentally observed, with voltage and power lower in stage 4. Thus, it is strongly suggested that this difference is not simply the effect of a difference in spacer resistance because of different salt concentrations.

The theoretical analysis furthermore suggests that next to reducing electrode leakage, we can increase performance of the system by reducing the spacer resistance by placing the anion and cation exchange membranes closer together as well as by increasing the ion and electron adsorption capacity of the electrodes. A reduced spacer volume will also lead to more rapid and sharp switching between the flow of fresh water and that of saline water, without the rather lengthy period in which the internal volume must be replaced (the period where cell voltage slowly increases to the maximum) and the two solutions become intermixed.

The potential of the technology can be underscored by comparing the energy production with the entropy increase of the aqueous streams. In an ideal case, this entropy increase follows from the amount of salt adsorbed during stage 2 which is released again in stage 4 (which for a membrane that is perfectly blocking for co-ions directly relates to the stored charge q) and its ideal transfer from the saline solution to the fresh water solution. This calculation results for the experiment discussed above (resistance of 1 Ω) in an efficiency of 27%, which even increases further to values above 50% at resistances of 10 and 100 Ω, see Appendix B. Taking instead the worst case that all water flowing out of the cell is discarded into a common reservoir, then per cycle there is an entropy increase equivalent to 1 kJ while the extracted work is less by a factor of 1 in 2000. Thus theoretically it is feasible to extract a factor of 103 more energy from the same water flow as at present. One option for an optimized technology to achieve this aim is to step away from the present approach where fresh water and saline water are intermittently fed to the same cell but instead to remove and dip the electrode-membrane assemblies (which are overall charge-neutral) alternatingly in continuous water streams of low and high salinity.

In conclusion, we have demonstrated that the direct extraction of electrical work from water salinity differences can be achieved in a flow cell based on ion-exchange membranes and porous supercapacitor electrodes, without the need for

secondary energy converters or batteries, a development which has the potential to bring the cost-efficient harvesting of this renewable source of energy closer to realization.

Chapter 3

Electrochemical characterization of a supercapacitor flow cell for power production from salinity gradients

Salinity gradients could be a great source of energy in the future. Capacitive energy extraction based on Donnan Potential (CDP) is a new technique to directly convert this energy into electricity. CDP uses a supercapacitor-like device combining ion exchange membranes and capacitive materials to adsorb and desorb ions with the Donnan Potential of the membranes as only driving force. The resulting current can be extracted through an external load. In this study, traditional electrochemical techniques: galvanostatic charge–discharge and cyclic voltammetry were used to investigate intrinsic properties of this open system. This study demonstrates the feasibility to characterize the capacitive behavior of the cell in low concentration (0.5 M). Presence of membranes, as well as the possibility of having the electrolyte flowing through the cell was investigated. In the studied cell, the presence of membranes showed a limitation by the anion exchange membrane at low current densities but no effect at high current densities. The flow rate did not influence the capacitance of the system either.

This chapter has been published as:

Sales, B. B.; Liu, F.; Schaetzle, O.; Buisman, C. J. N.; Hamelers, H. V. M., Electrochemical characterization of a supercapacitor flow cell for power production from salinity gradients. *Electrochimica Acta* **2012**, 86, 298-304.

3.1 Introduction

Renewable energy can be harvested from the salinity gradient difference between river and sea water. The mixing of fresh and sea water increases the entropy of the mixture and dissipates free energy. Globally, the total flow of rivers into the seas has a power potential of 2.6 TW (Wick and Schmitt 1977). Different methods were studied to extract energy from this source (Jones, Finley et al. 2003; Post, Veerman et al. 2007; Brogioli 2009), all facing great technical challenges. Recently, capacitive techniques have been developed to extract this energy (Sales, Saakes et al. 2010; Boon and van Roij 2011; Brogioli, Zhao et al. 2011). Among these techniques, the Capacitive energy extraction based on Donnan Potential (CDP), a technique combining carbon electrodes and ion-exchange membranes in a supercapacitor flow cell was proposed with desirable advantages. Fig. 3.1 illustrates the working principle of this technique.

First, when a concentrated salt solution (e.g. sea water) is flushed in the cell, ions diffuse through the ion exchange membranes into the capacitive electrodes. An electronic current is generated from the anion-adsorbing electrode to the cation-adsorbing electrode through an external load (Fig. 3.1A). When the system reaches equilibrium, a diluted salt solution (river water) is flushed in the system. The adsorbed ions are diffusing out of the electrodes generating an electronic current flowing from the cation-desorbing electrode to the anion-desorbing electrode (Fig. 3.1B). When the system reaches equilibrium the complete cycle can start over by switching back to sea water.

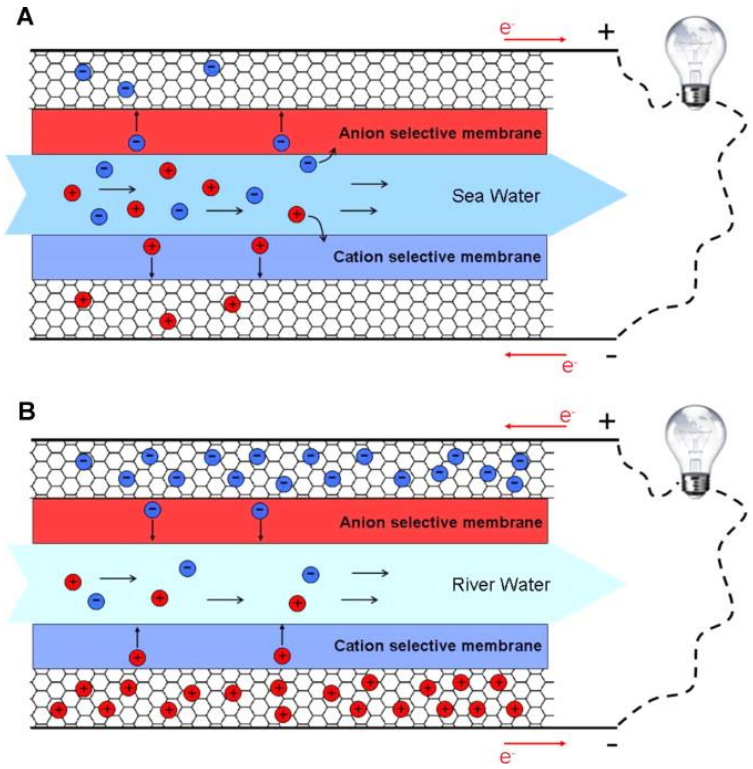

Figure 3.1 Working principle of CDP. (A) Sea water is flushed in the system allowing ions to diffuse in the electrodes and thus generate a current in the external load. (B) River water is flushed in the system allowing ions to diffuse out of the electrodes and thus generate an opposite current.

Similar to a capacitor, the total electrical energy extracted and stored in a CDP device is directly proportional to the capacitance and voltage squared of this device. The overall performance of CDP increases with the optimization of these parameters. The electrolytes are restricted to neutral aqueous solutions simulating river and sea water, theoretically having a practical operating voltage about 0.6–0.8 V (Khomenko, Raymundo-Piñero et al. 2010). In our proposed operation, the operating voltage is rather low (<0.2 V). This potential is determined by the Donnan equilibrium potential (Pivonka, Smith et al. 2007) induced by the presence of the membranes and acts as only the driving force of the process without any energy

input (other than the energy required for pumping). Therefore the selection of electrode material and construction of electrodes becomes a major path leading to breakthroughs for this technology.

The research on capacitive energy extraction from salinity gradients is still young with only few papers published so far. The performances of the materials in such system are not yet well studied or characterized. In comparison with the supercapacitor studies, where different optimization techniques are suggested to improve the capacitance of the electrodes (Frackowiak, Delpeux et al. 2002; Simon and Gogotsi 2008; Choi and Choi 2010; Kim and Choi 2010; Demarconnay, Raymundo-Piñero et al. 2011), we would like to introduce standardized measurement methods in order to avoid wide variation in published values (Stoller and Ruoff 2010). For that reason a reliable characterization cell and methodology to test and confirm the performance of suitable materials for CDP is still needed.

CDP has several characteristics very different from traditional supercapacitors. First, CDP uses ion-exchange membranes (anion exchange at one side and cation exchange at the other) that are of course completely absent in traditional supercapacitors. Second, the electrolytes used have relatively low concentrations compared to typical supercapacitors (Conway 1999; Björnbom 2007) (0.017 M and 0.5 M for CDP compared to typically several molar for standard supercapacitors). Finally, the system is open, allowing a hydraulic flow between the electrodes.

For these reasons, this study is aiming at using for the first time standard electrochemical characterization methods on a CDP system. The presence of membranes, the flow and different salt concentrations were tested regarding their effects on the capacitance of the system.

3.2 Experimental

3.2.1 Carbon Electrodes

Carbon electrodes were prepared with the composition of 90% activated carbon (Super 30, Norit, The Netherlands) and 10% polyvinylidene fluoride (PVDF) (KYNAR HSV 900, Arkema Inc., Philadelphia, USA). The production procedure was as follows: a carbon slurry was obtained by mixing activated carbon powder with a solution of PVDF in 1-methyl 2-pyrrolidone (NMP) (Merck Schuchardt OHG, Hohenbrunn, Germany) in a ball mill grinder (PM 100, Retsch, Haan, Germany) for 30 min at 450 rpm to produce a carbon slurry. The carbon slurry was casted with the Doctor Blade method on a graphite paper foil (1.0 g/cm3 density, 99% purity, Coidan Graphite Products Ltd., York, UK) and was dried for 24h in a fume hood.

3.2.2 Research Setup

The cell used during our previous chapter presented several drawbacks like uneven flow repartition and water leakages between the membrane and the electrode. Thus, we designed a new flow through cell different from the previously reported one by a more linear flow pattern and by a better integration of the different components. The CDP flow-through cell used in this study consisted of a flow through compartment (10 cm × 2.2 cm × 1.5 cm). At each side of the cell a stack containing an ion exchange membrane, a capacitive electrode and a current collector was placed. At one of the side a cation exchange membrane is used (FKS, Fumatech, Germany) and at the opposite side an anion exchange membrane is used (Fumasep FAS, Fumatech, Germany). Graphite plates were used as current collectors (Muller & Rossner GmbH, Troisdorf, Germany). The total amount of activated carbon material in the cell was around 2g and the total geometric area of the electrode was 44 cm^2 for one cell. Fig. 3.2 shows a picture and a drawing of the experimental setup.

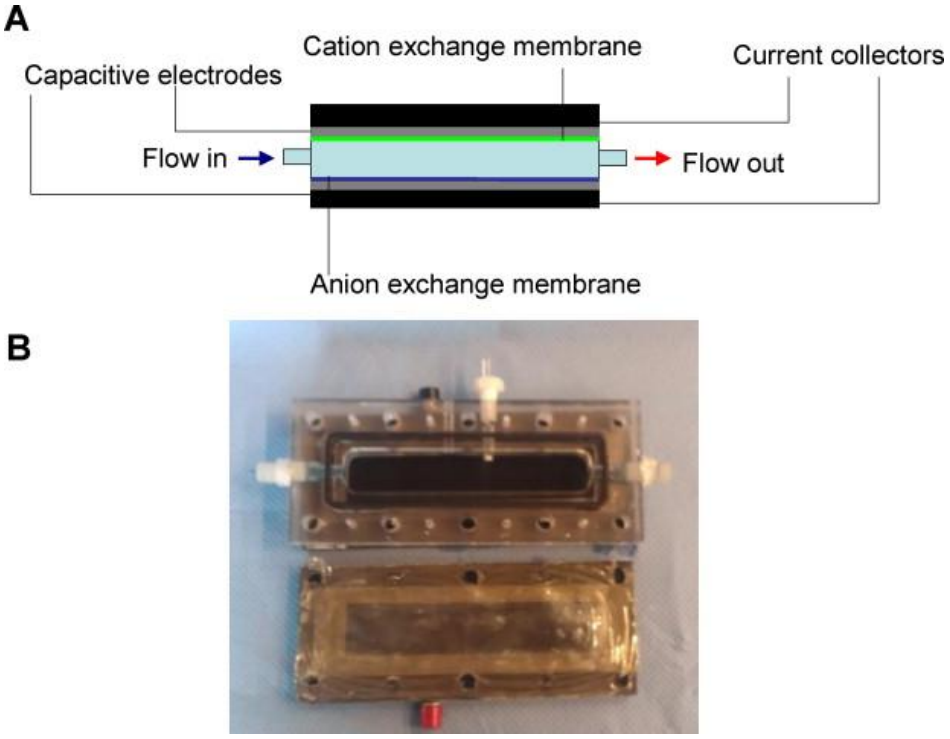

Figure 3.2 Drawing (A) and picture (B) of the CDP cell used in this study.

3.2.3 Operation

The electrolyte solutions were 0.5 M NaCl solution (concentrated salt solution) and 0.017 M NaCl solution (diluted salt solution), which were fed into the cell alternatively with three flow rates, 0 mL/min, 60 mL/min, and 450 mL/min. All the experiments were conducted at 25 °C in a thermostatic incubator (Friocell, MMM Medcenter, Munich, Germany). NaCl was from ESCO-salt (Harlingen, The Netherlands).

3.2.4 Electrochemical measurement and analyses

In this study, the cell was investigated by cyclic voltammetry and galvanostatic charge–discharge, using a potentiostat (IviumStat, Ivium Technologies, The Netherlands). Cyclic voltammetry measurements were performed at 1 mV/s from

0.4 V to −0.4 V between both electrodes. Capacitance was calculated in each case by integrating the current between 0.0 V and +0.3 V where all the obtained voltammograms showed good capacitive behavior.

Galvanostatic charge–discharge was done at different current densities: 0.45 A/m^2, 11 A/m^2, 22.7 A/m^2 and 45.4 A/m^2. The internal resistance was calculated by using the voltage drops before and after each charging/discharging step. The capacitance was calculated by dividing the amount of charges stored or released during each step by the corresponding ΔV according to the formula:

$$C = \frac{Q}{\Delta V} \qquad \text{Eq. 3.1}$$

where C is the capacitance (F), Q the amount of charges (C) and ΔV (V) the difference between the potential before and after the charging/discharging step. By default, the electrolyte concentration used for these experiments was 0.5 M (e.g. sea water concentration). Concentrations of 1, 2, 3, and 6 M were also investigated.

3.3 Results and Discussion

3.3.1 Electricity extraction cycle

Even though the cell was designed to characterize the materials and the effect of the flow and the membranes, we first tested its performances for energy extraction in order to check if the characterization would match the conditions of actual operation of such system. For this, we proceeded with the same two-step process as previously reported. Fig. 3.3 displays the evolution of the cell potential over time. In this operation, step one consists of a “charging” step where the cell was filled with the concentrated salt solution. The ions were diffusing through the ion exchange membranes into the electrodes. The charge separation led to an increase of the cell potential known as the Donnan potential. The electrons repelled at the anion exchanging side were flowing through an external load (R = 15 Ω) before reaching the cation exchanging side where they allowed the sodium

ions to adsorb. The cell potential is progressively decreasing with the flow of electrons until reaching 0 V. The concentrated salt solution in the cell was then replaced by the diluted salt solution to start the second step of the process. The salinity gradient made the ions to leave the electrodes and to go through the membranes in the other direction toward the flow channel. This led the cell potential to suddenly decrease toward the negative values. The electrons were then flowing back from the cation adsorbing side, through the load and finally to the anion adsorbing side. The resulting cell potential progressively reached 0 V allowing a new cycle to start.

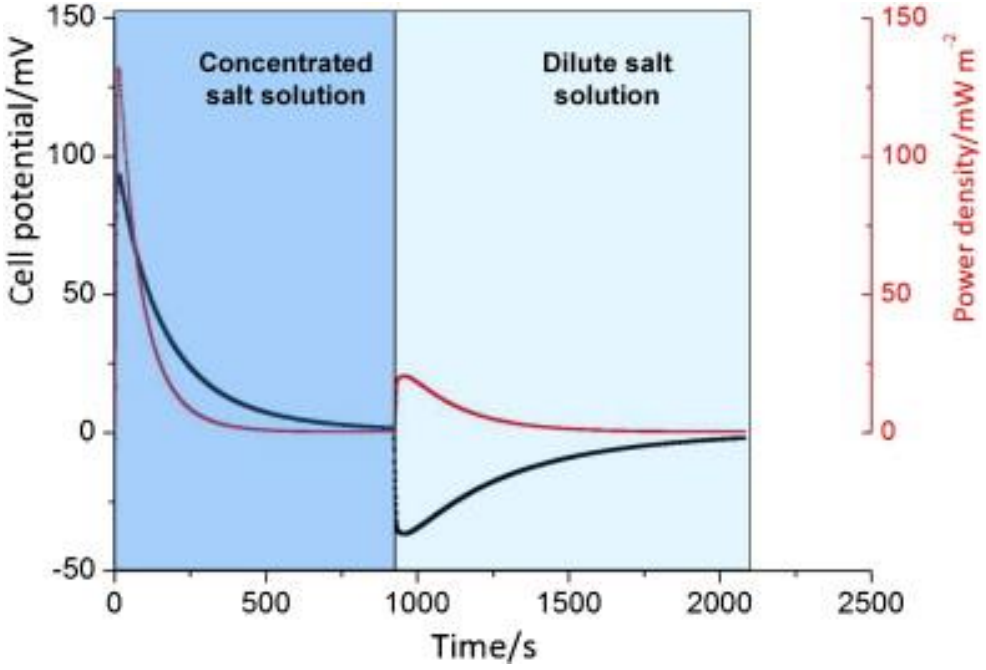

Figure 3.3 Cell potential versus time and peak power density (mW/m^2) for one cycle with “charging” in the concentrated salt solution and “discharging” in the diluted salt solution.

The amount of charges exchanged in a single cycle was 1.17 coulombs during the charging step and 1 coulomb during the discharge. The difference between these

values is related to a self-discharge effect common to supercapacitors (Ricketts and Ton-That 2000). The overall performances of the system studied here was the extraction of 75.6 mJ per cycle (37.8 mJ/g of activated carbon or 17.18 J/m^2 of electrode geometric surface area) for a maximum power density of 131.7 mW/m^2 during the charging step (and 20.3 mW/m^2 peak power density during the discharging step). The average power produced through the whole cycle was 8.36 mW/m^2. In comparison, the previous chapter reported peaks of respectively 60 and 40 mW/m^2 for the charging and the discharging steps and 6.9 mW/m^2 average power. However, direct comparisons are difficult as cell designs were very different (different amounts of carbon, surface area and channel volume). For more optimal energy extraction a smaller distance between the two electrodes is needed. Moreover, in this study, the energy input (pumping and flow control) was not taken into account as the purpose is the investigation of the effect of the materials and not the energy extraction itself. The large channel used in the present studies explains the rather low average power as the cycle had to last longer due to the distance between the electrodes (the cycles were twice as long as the ones previously reported).

3.3.2 Electrochemical characterization of the device

3.3.2.1 Feasibility of the characterization

As these systems use rather low concentrations of electrolyte compared to supercapacitors (typically 0.5 M for the artificial sea water) we first proceeded with preliminary tests of the characterization methods. For this, we used galvanostatic charge–discharge and cyclic voltammetry. Fig. 3.4 shows the obtained results for the studied cell when concentrated salt solution is in the cell compartment and in the absence of flow.

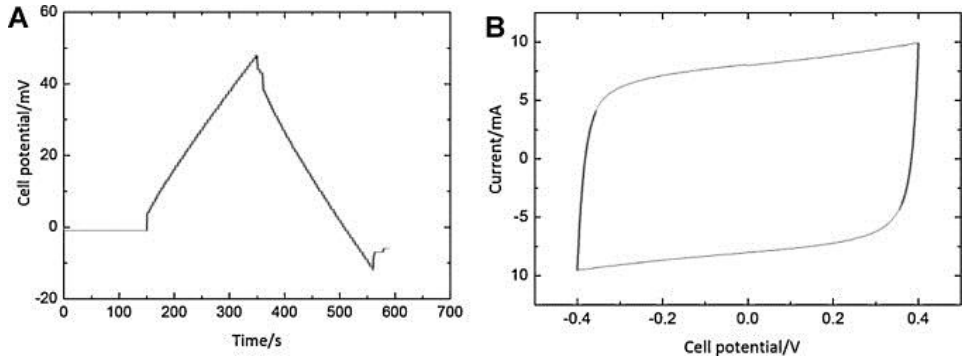

Figure 3.4 Galvanostatic charge and discharge (2 mA) (A) and cyclic voltammetric (1 mV/s) (B) investigations of our system in concentrated salt solution without flow.

These methods proved to be very reproducible with our system and gave consistent results. With both methods we could evaluate comparable specific capacitances over triplicate experiments (4.58 ± 0.1 F/g using the galvanostatic charge, 4.2 ± 0.1 F/g using the galvanostatic discharge and 4.89 ± 0.1 F/g using cyclic voltammetry).

In term of reproducibility, the standard deviation measured for consecutive duplicates was around 0.05 F/g for galvanostatic charge and discharge and 0.1 F/g for cycling voltametry. However, when experiments were repeated after one day, the standard deviation for both methods was 0.3 F/g.

Moreover, the galvanostatic charge–discharge method was used to evaluate the internal resistance (through the potential drop before and after charging at constant current). The 2 Ω internal resistance that was calculated this way was comparable to the values obtained by directly measuring this resistance with an AC-milliohmmeter (Agilent Technolgies, mention type meter).

Finally, the capacitance behavior was slightly different during the charging and the discharging step. We systematically obtained lower specific capacitance during the discharge than during the charge (Table 1).

Table 1. Specific capacitances (F/g) measured with different methods for different flow rate, different currents and different cell configurations at 0.5 M NaCl.

	Galvanostatic charge–discharge at 0.45 A/m^2		Galvanostatic charge–discharge at 11 A/m^2		Cyclic voltammetry
	Charge	Discharge	Charge	Discharge	
Both membranes					
0 mL/min	4.59	4.24	4.27	3.89	4.32
60 mL/min	4.58	4.2	4.28	3.88	4.89
450 mL/min	4.55	3.9	4.32	3.88	4.96
No membranes (60 mL/min)	4.65	4.31	4.64	4.21	4.56
Only CEM (60 mL/min)	4.65	4.47	4.72	4.42	4.96
Only AEM (60 mL/min)	4.81	4.08	4.45	4.05	5.35

A possible explanation for this is the self discharge of the system. During the charge the self-discharge of the system limit the potential increase and thus induce and overestimation of the capacitance. During the discharge however, the self-discharge induces a higher potential change and thus an underestimation of the capacitance.

The “self-discharge” of the system is more complex than the one occurring in standard supercapacitors. Ion exchange membranes are typically not 100% selective. This results in a slow equilibration of the charges at both sides of the membrane that leads to a slow voltage drop over time occurring in parallel with the self-discharge of the capacitor. A more precise evaluation of the capacitance of the system would be the average specific capacitance between charge and discharge.

3.3.2.2 Effect of the concentration

To further address the electrolyte concentration effect, we measured the specific capacitance obtained at different concentrations using galvanostatic charge and discharge with a 2 mA current (0.45 A/m^2 current density). The low concentration at river water concentration inducing high resistive behavior in the cyclic voltammogram, thus, cyclic voltammetry was not used to investigate the effect of concentration. Figure 3.5 shows the relation between the specific capacitance and the electrolyte concentration. We observed that the specific capacitance slightly increased with the electrolyte concentration. However, the specific capacitance at 6 M is only 12.5% higher than the one measured at sea water concentration (0.5 M).

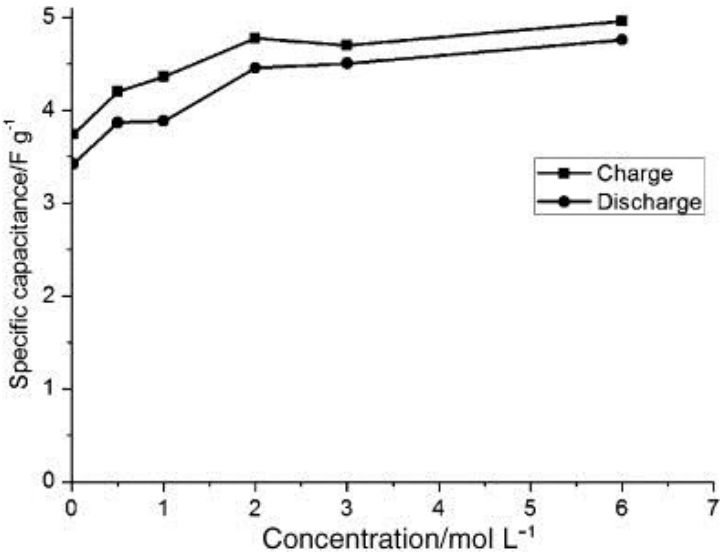

Figure 3.5 Specific capacitances measured for different NaCl concentrations.

This result suggests that the carbon material can be relatively safely characterized at sea water concentration. This statement is of importance regarding the fact that the operational process of energy production uses these lower concentrations to extract energy.

We also investigated the internal resistances relatively to the electrolyte concentration. Fig. 3.6 shows that the internal resistance is particularly important at the lowest concentration (15.5 Ω at 0.017 M NaCl). Such resistance is directly related to the rather high distances between the electrodes (1.5 cm). However, the purpose of the studied cell being the characterization of the carbon materials, the internal resistance of the system is of less importance. An actual operating system for energy extraction would need smaller space between the electrodes and thus hydrodynamics of the system would be of particular importance.

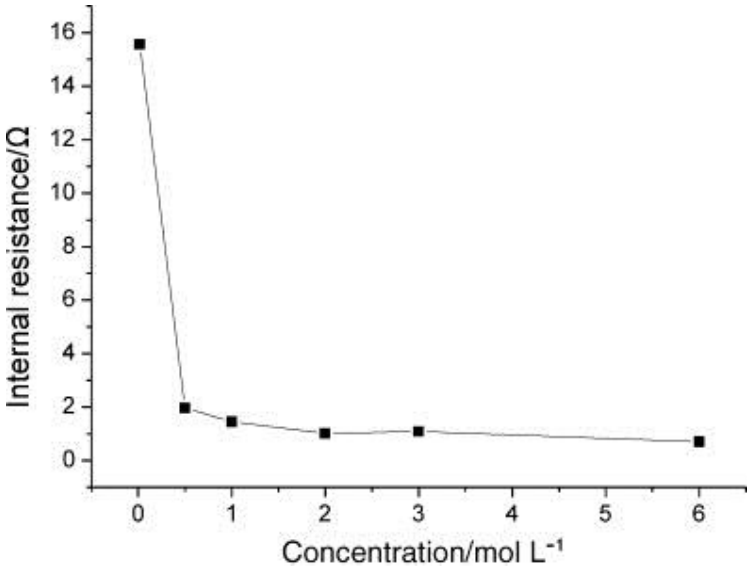

Figure 3.6 Relation between internal resistance and electrolyte concentration.

3.3.2.3 Effect of the membranes

One of the main differences between the studied system and a traditional supercapacitor is the presence of ion selective membranes. To investigate the effect of the membranes on the capacitive behavior of our system we tested different cell configurations: (i) the cell without membrane, (ii) the cell with only one anion exchange membrane, (iii) the cell with only one cation exchange membrane

and (iv) the cell with both anion and cation exchange membranes. Fig. 3.7 shows the results obtained by cyclic voltammetry for these 4 configurations.

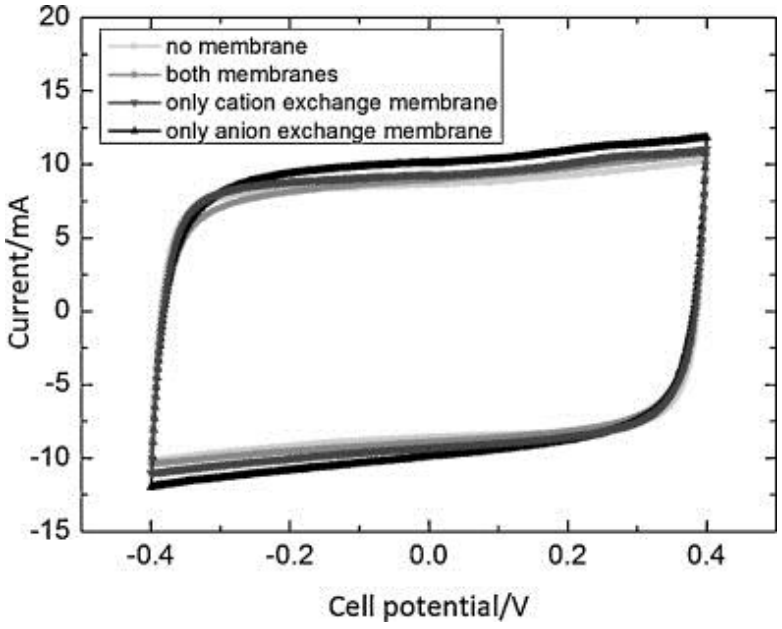

Figure 3.7 Cyclic voltammograms obtained at 1 mV/s for 4 cell configurations.

The specific capacitances calculated from these measurements did not show very significant differences between the different configurations (Table 1).

This result is confirmed by the galvanostatic charge–discharge method. Fig. 3.8 shows the results obtained for two different current densities (11 A/m^2 and 0.45 A/m^2). We can observe that in the experiment with the lower current density, the discharge behavior differs slightly between the different cell configurations. We can see that at lower current densities, the discharge step presents lower performances when the anion exchange membrane is present. A possible explanation for this is the lower permselectivity of anion exchange membranes compared to cation exchange membranes. The explanation for this effect being more visible at lower current densities relies in the amount of charge exchanged and the relative effect

of the self discharge. Indeed, the amount of charges exchanged at 11 A/m^2 was 10 times higher than the measurement at 0.45 A/m^2 (respectively 4C and 0.4C). Thus, the relative contribution of the leakage (dV_{self}) compared to the potential increase (ΔV) is more important as the charge/discharge cycle was slower during the lower current density experiment, leading to larger self discharge.

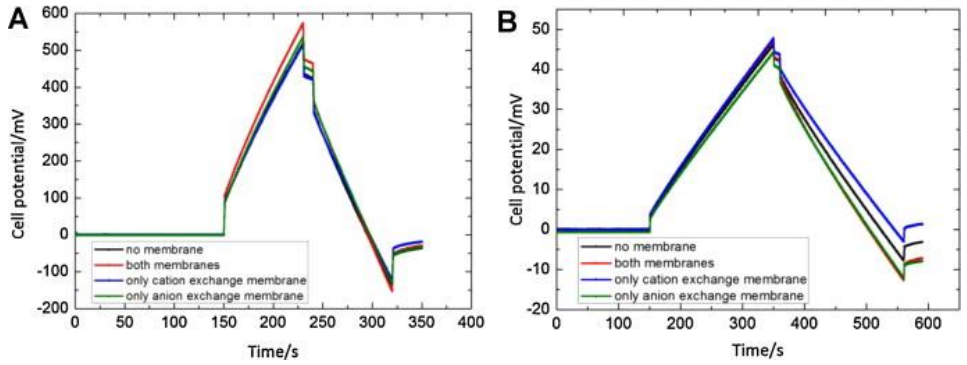

Figure 3.8 Galvanostatic charge and discharge for different cell configuration at different current densities: 11 A/m^2 (A) and 0.45 A/m^2 (B).

As electricity extraction process has a peak current around 6 mA, the relative limitation of the anion exchange membrane must still be important. Improving either the membrane quality or increasing the current density could improve the overall process (by increasing the amount of charges exchanged and decreasing the amount of charges leaked through time).

Moreover, Fig. 3.9 shows the relation between the specific capacitance and the charge–discharge current density. The capacitance slightly decreases with the current but stabilizes around 4 F/g. This again, suggests that increasing the current density in the process could be beneficial for the overall performance of our system. More charges could thus be stored at a higher rate leaving less time to the system to leak charges.

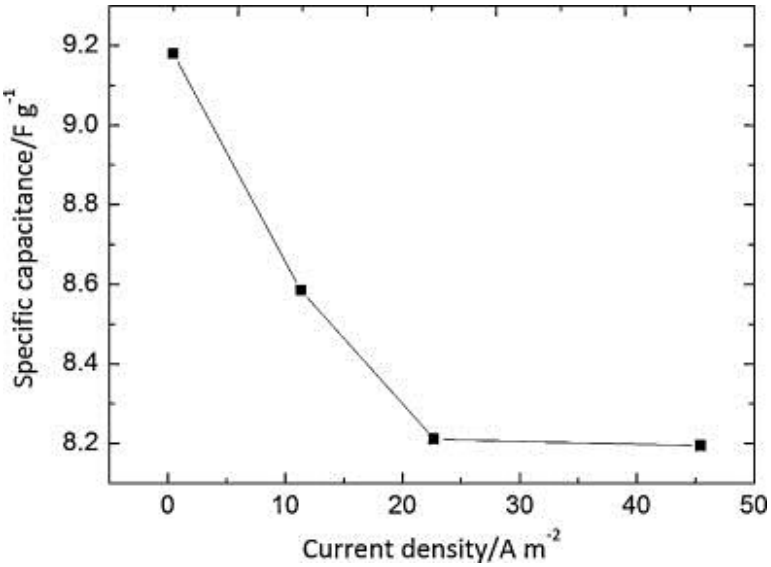

Figure 3.9 Relation between the specific capacitance (F/g) and the charge/discharge current density (A/m^2).

3.3.2.4 Effect of the flow

Another major difference of such system compared to traditional supercapacitors is the possibility to have the electrolyte flowing through the system. Fig. 3.10 shows the results obtained by galvanostatic charge–discharge with different flow rates.

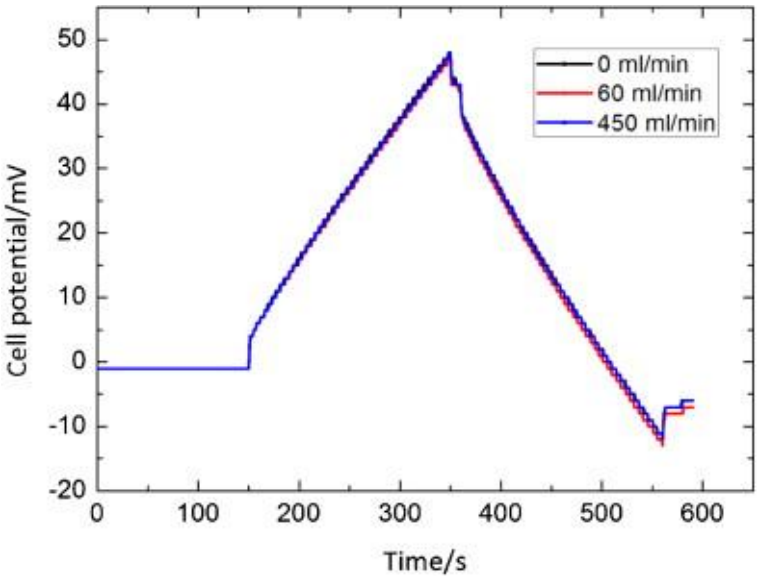

Figure 3.10 Galvanostatic charge and discharge at 0.45 A/m^2 under different flow rates.

We can see that, in the studied system, the flow rate had no influence at all on the performance of the cell. This result suggests that mass transport is not limiting the operation of our system. To verify this we can calculate the thickness of the hydrodynamic boundary layer and thus evaluate the relative amount of salt that adsorbed from this source. This can be calculated to be 257 μm for the sodium adsorbing side and 311 μm for the chloride adsorbing side at 60 mL/min using (Hayes and Kolaczkowski 1994):

$$Sh = 3.66\left(\frac{1+0.095 D_T P_e}{L}\right)^{0.45} \quad \text{Eq. 3.2}$$

$$P_e = \frac{D_T \nu}{D} \quad \text{Eq. 3.3}$$

$$Sh = \frac{k D_T}{D} \quad \text{Eq. 3.4}$$

$$\delta = \frac{D}{k} \quad \text{Eq. 3.5}$$

where Sh is the Sherwood number, D_T is the hydraulic diameter (m) = 2WH/(W + H) (with W = width = 2 cm, H = height = 1.5 cm), L = channel length = 12 cm, P_e is the Peclet number, v is the flow velocity = 0.36 cm/s, D is the diffusion coefficient for the considered ion = 1.33×10^{-9} m^2/s for sodium and 2.03×10^{-9} m^2/s for chloride (Samson, Marchand et al. 2003), k is the mass transfer coefficient (m/s), and δ is the thickness of the hydrodynamic boundary layer (m). The Reynolds number: $R_e = D_T v\rho/\mu = 69$, where ρ is the density = 1 × 103 kg/m^3, and μ the viscosity = 8.9 × 10−4 Pa/s ensure that the flow is laminar.

First we use (Eq. 3.3) to calculate P_e that can then be used to calculate Sh in (Eq. 3.2). From this k can then be deducted from (Eq. 3.4) and finally δ can be calculated from (Eq. 3.5).

With the calculated thicknesses we can determine that in sea water concentrations we have 2.83 × 10−4 moles of sodium and 3.42 × 10−4 moles of chloride available within this boundary. With the amount of charge that we exchanged (maximum of 4C) during our galvanostatic experiments the corresponding amount of ions would be 4.15 × 10−5 moles. This amount being one order of magnitude less than the amount of salt present in the boundary layer it is no-surprise that the mass transport is not limiting. Moreover, in operation, only 1.17C was exchanged making the mass transport even less limiting.

In the perspective of an operational device this result is very positive as it implies that less water can be used for the same results, thus increasing the fuel efficiency of the system.

3.4 Conclusions

A CDP device was investigated using electrochemical methods traditionally used in the study of supercapacitors. The new cell used showed performances of 131.7 mW/m^2 comparable to the one previously described in the literature.

The characterization methods showed to be very reproducible and allowed to evaluate a specific capacitance of the system around 4.6 F/g. The study of the effect of salt concentration revealed that the system could be reasonably characterized in sea water. The presence of membranes showed no significant effect at higher current and a limitation from anion exchange membranes at lower current. The internal resistance was considerably high under lower concentrations (15 Ω at 0.017 M) because of the considerable distance between the electrodes (1.5 cm). However this is of limited impact on the characterization of the materials and is only of importance for the operation of the device. Future studies will have to focus on how to optimize the distance between the electrodes in regard to the hydrodynamics of the flow.

Finally, the flow showed no effect on the capacitive behavior of the cell. All these results combined suggest that the designed cell is appropriate to test different carbon materials without being influenced by the presence of membranes or by the flow. Materials can thus be tested in such cell before being implemented in an optimized operational CDP design to be developed in the future.

Chapter 4

Auto Generative Capacitive Mixing for Power Conversion of Sea and River Water by the Use of Membranes

The chemical potential (free energy) of mixing two aqueous solutions can be extracted via an auto generative capacitive mixing (AGCM) cell using anionic and cationic exchange membranes together with porous carbon electrodes. Alternately, feeding sea and river water through the unit allows for the system to spontaneously deliver charge and discharge the capacitive electrodes so that dc electric work is supplied. Having a stack of eight cells coupled in parallel demonstrated the viability of this technology. An average power density of 0.055W/m^2 was obtained during the peak of the different cycles, though reasonable optimization suggests an expectation of 0.26W/m^2 at 6.2 A/m^2. It was found that 83 ± 8% of the theoretical driving potential was obtained during the operating process. By studying the polarization curves during charging and discharging cycles, it was found that optimizing the feed fluid flow is currently among the most beneficial paths to make AGCM a viable salinity difference power source. Another parallel route for increasing the efficiency is lowering the internal ohmic resistances of the cell by design modifications.

This chapter has been published as:

Burheim, O.; Sales, B. B.; Schaetzle, O.; Liu, F.; Hamelers, H. V. M., Auto Generative Capacitive Mixing for Power Conversion of Sea and River Water by the Use of Membranes. *Journal of Energy Resources Technology* **2012**, 135, (1), 011601.

4.1 Introduction

All renewable power sources are somehow initially solar driven. Among these, vast solar driven energy cycles are the onshore fresh water supply. During the last centuries, this energy cycle has mainly been utilized for hydroelectric power generation. When this water cycle ends and rivers pour into the oceans, the chemical potential difference between sea water and river water is dissipated by mixing. The world wide power source potential, of this naturally occurring process of mixing, is in the order of 2.6 TW (Wick and Schmitt 1977; Wick and Isaacs 1978). River water mixed with infinite amount of sea water offers 2.5 MJ/m^3 and 1.7 MJ/m^3 for equal volumetric mixing (Veerman, Saakes et al. 2009).

In order to have a sustainable economy, energy supply, and environmental preservation, the human society needs a gradual conversion to renewable energy sources (Fronk, Neal et al. 2010) and shortly to CO_2-neutral energy supply (Vellini and Tonziello 2010). In the light of energy supply and the need for more renewable energy resources, salinity gradient energy technologies hold many advantages. For instance, currently most energy markets are dominated by peak demand during daytime and a market electric surplus during night time. Though large amounts of plug-in hybrid vehicles charging during night time can take up some of these variations (Himelic and Kreith 2011), many renewable energy sources are less dynamic - such as wind power which is present when wind is present - and a need for dynamic energy supplies are needed. The first large scale efforts of salinity energy will be located at dikes with large buffers allowing for a highly dynamic supply (Post, Goeting et al. 2010) - similar to that of hydroelectricity. In comparison to CO_2-capture and storage, some new infrastructure is also needed and thus one can say that building salinity difference energy infrastructure offers renewable and carbon neutral electricity supply where CO2-neutral infrastructure construction only offers the latter. Another argument for salinity gradient energy technologies is that, in comparison to, e.g., wind energy, it is hardly not developed, it has a very low visual impact and is typically close to urban district at river deltas.

Using the potential of salinity gradients as a renewable power source was first proposed by (Pattle 1954). Currently, two technologies for exploiting these power sources are well established in the literature; pressure retarded osmosis (PRO) and reverse electrodialysis (RED) both using membranes of specific kinds.

An osmotic power generator was proposed by (Norman 1974) as predecessor for today's pressure retarded osmosis (Thorsen and Holt 2009). The principle of this salinity power technology is contrary to all others as the process leans on the driving potential of transport of water rather than the salt. For PRO, there is a pressure buildup across a water permeable membrane which induces streaming water out of the chosen membrane assembly such that a water turbine can generate AC electric power. The classic and most common description of the potential is van't Hoff equation. This equation, a simplification of the chemical potential of water in two solutions containing sodium chloride, and states that the osmotic pressure of two solutions is equal to the salt concentration difference of the two solutions multiplied with a membrane specific constant. (Achilli and Childress 2010) recently summarized the history of PRO.

Reverse electrodialysis was brought forward by (Weinstein and Leitz 1976) as the first of many electrochemical techniques to harvest the potential power of mixing sea and river water. Lacey developed the first thorough model of such systems but concluded at the time that the lack of feasibility was due to membrane costs (Lacey 1980). Since then membrane prices were lowered by a factor ten and the price of raw materials suggests another factor ten or more, as these materials become subject to large volume products. The electrochemical potential of RED is commonly given by the chemical potential difference of sodium chloride in two aqueous solutions, divided by the Faraday constant and multiplied by a membrane selectivity coefficient, as to express the power potential as an electrochemical dc electric power source. This can be seen in Eqs. (4.1)–(4.3).

One of the main reasons why power extraction from mixing sea and river water has received a renewed attention lately is the development of membranes over the last decades. Furthermore, the scale up of plants (reverse osmosis (RO), RED, and PRO) requires mass production of membranes (Gerstandt, Peinemann et al. 2008). With PRO and RED as the two dominating salinity difference power source technologies, Post et al. concluded that, in evaluating energy efficiencies and power extraction, RED is favored over PRO for the process of mixing sea and river water. While the opposite is expected to be the case when the salinity difference is further enlarged, i.e., when replacing sea water with brines (Post, Veerman et al. 2007).

In addition to these two techniques, less established technologies for power extraction deploying membranes and nonmembrane processes have also been suggested recently. La Mantia et al. suggested to apply solid state electrochemical electrodes of similar reversible half-cell potential, where one of the reversible half-cell potential is sensitive to the chloride concentration and the other one to the sodium concentration (La Mantia, Pasta et al. 2011). This technique was termed Nano-Batteries at first. In this technique, a dc current is spontaneously generated when the concentrations replace each other. The challenges with this technology are to develop nonsoluble electrodes that consist of sodium or chloride, with promising electrochemical kinetics, and which do not include precious or environmentally unfriendly metals (e.g. AgCl or PbCl2).

Brogioli et al. suggested extracting the potential energy of mixing sea and river water by deploying activated carbon capacitors and utilizing the response in the capacitive double layer expansion (CDLE) effect from solution interchange (Brogioli 2009; Boon and van Roij 2011; Brogioli, Zhao et al. 2011; Rica, Brogioli et al. 2012). This approach requires, first, that the capacitor is charged from an external power source while the electrodes are submerged in sea water. Next, when these are charged, the set of capacitors is subsequently submerged in river water, more

energy (net electric work) can be returned during the corresponding discharge process (same amount of charge is returned but at a higher potential). Finally, the pair of capacitors is returned to sea water and the cycle restarts.

Sales et al. demonstrated that, when correctly assembled, supercapacitor materials in combination with ion exchange membranes, the energy of mixing sea and river water can be harvested (Sales, Saakes et al. 2010). This technology offers an auto generative power source by mixing sea and river water with materials that are already established within the research field and commercially available. Deploying carbon for electrodes in salinity difference power systems have been suggested and proven viable for RED, although AGCM deploys differently (Veerman, Saakes et al. 2010; Burheim, Seland et al. 2012).

One advantage of capacitive mixing technologies (Bijmans, Burheim et al. 2012) have compared to other competing techniques is the possible capability to sustain exposure to biologic fouling. For RED, it was observed that over 26 weeks the performance drops linearly in time (Ratkje, Holt et al. 1986). Replacing the river water feed with sea water for 15 min after several days in operation was demonstrated to kill 90% of the algae fouling in PRO (Lee and Elimelech 2007; Mi and Elimelech 2010). Thus, compared to the other membrane technologies, since alternating the feed solutions and ionic currents are mandatory for AGCM, many biological fouling mechanisms are considered to be significantly impeded. Another advantage the AGCM holds relates to short circuiting and cell design. Though electrode segmentation might become a necessity for the AGCM, as well for RED (Veerman, Saakes et al. 2011), ionic short circuiting (Veerman, Post et al. 2008) is far less likely because the cells are coupled in parallel rather than in series (and thus there is much lower feed channel short circuit potential present).

The aim of this paper is to focus on how the power is generated in an AGCM and the characteristics of the transport phenomena. The novelty of this study lies in that

we aim to study the AGCM system by traditional electrochemical means and that we pay attention to transport of momentum, i.e., the hydrodynamic mixing.

4.2 Theory

In this section, we describe the AGCM process, the thermodynamic potential (exergy) and the exergy losses (Kotas 2012) related to the running cell. Exergy is usually considered for machines that deal with heat and mechanical work (Margarone, Magi et al. 2011; Demirkaya, Besarati et al. 2012) though the term is also valid for electrochemical systems (Khazaee 2012) and is the electric work that is available when considering the process as a whole. Exergy efficiency is then defined as how much of the available work one gets out of the system when accounting for all losses.

4.2.1 AGCM Process

The details of an AGCM process are given in more detail in Chapter 2, and is therefore only briefly repeated here.

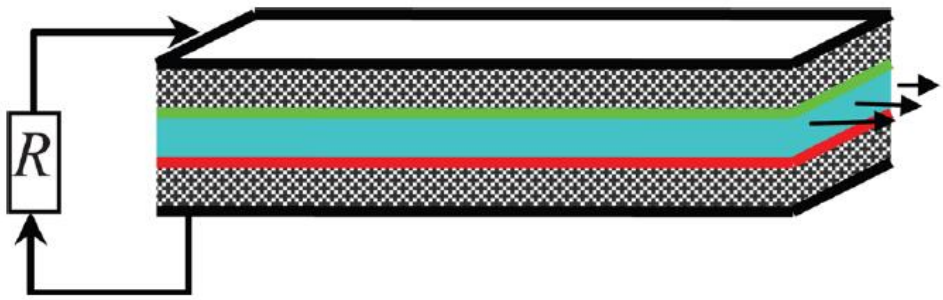

Figure 4.1 The AGCM cell, consisting (f.t.) of a CPEC, a CEM (green line), a water flow compartment, an AEM (red line), and one more CPEC. The two electrodes are connected to an external load (R).

Figure 4.1 depicts an AGCM single cell and its cross section. Assuming that the starting point of the process is sea water flowing through, the capacitive porous electrode compartment (CPEC) materials are charged by filling the electrode surface double layer with ions. When the sea water flow is replaced by flowing river water, the cell is brought out of physical–chemical equilibrium. The cell will respond to this by discharging the double layers of each of the two electrode compartments. Due to the ionic selectivity of the membranes, anion exchange membrane (AEM) and cation exchange membrane (CEM), one electrode will release mainly anions and the opposite electrode cations. Thus, a DC power is dissipated in the resistor, R, in the external circuit, see Fig. 4.1. This process is dynamic and carried out while the solutions are being replaced. Hence, as the average salt concentration decreases, the power will increase up to the point when the driving potential starts to deplete and the power dissipation in the external resistor will decrease until physical–chemical equilibrium is reestablished. The next step in this process is feeding sea water. The process is thus operated in a reversed manner.

4.2.2 Reversible Potential of Mixing in AGCM

The reversible potential of mixing sea and river water solution is dictated by the difference in chemical potential of NaCl between the two solutions, $\Delta\mu_{NaCl}$ (Kjelstrup and Bedeaux 2008; Newman and Thomas-Alyea 2012) and is given by

$$E_{mix}^{rev} = \frac{\Delta\mu_{NaCl_{diss}}}{F} = \frac{RT}{F}\ln\frac{a_{NaCl}^{s.w.}}{a_{NaCl}^{r.w.}} \qquad \text{Eq. 4.1}$$

where

$$a_{NaCl} = \frac{m_{Na^+}\cdot m_{Cl^-}}{m_0^2}\gamma_{\pm}^2 \qquad \text{Eq. 4.2}$$

where R is the ideal gas constant, T is the temperature in K, F is the Faraday constant, ai is the activity of component i, m is the molal concentration, and c6 is the mean molal activity coefficient. Equations (4.1) and (4.2) give a reversible potential of 0.16 V at 25 °C for the solutions applied in the experiments of this

paper. It is the potential as defined by Eq. (4.1) that defines the maximal exergy potential of the AGCM (and RED) process(es).

4.2.3 Open Circuit Potential

AEM and CEM separate the flow compartment from the porous capacitor electrode compartments (PCEC). If the concentration of the bulk solution in the PCEC is kept constant, the open circuit potential change (or difference) between the two electrodes as a response to the electrolyte replacement can be described by the same equations as the open circuit potential for a reverse electrodialysis unit cell, $RED_{u.c.}$ (Lacey 1980)

$$E_{mix}^{OCP} = E_{RED_{u.c.}}^{OCP} = \alpha_{mean} \frac{RT}{F} \ln \frac{a_{NaCl}^{s.w.}}{a_{NaCl}^{r.w.}} \qquad \text{Eq. 4.3}$$

Equation (4.3) can be recognized as the Nernst equation multiplied by the mean permselectivity coefficient, α_{mean}. This correction is dictated by the nature of the membrane and solution interaction simply because the ionic exchange membranes do not offer absolute selectivity with respect to each of the anions and cations.

The permselectivity for each of the membranes, α_i is defined as twice the transference number of the selective specie minus one, e.g., for the cationic exchange membrane in sodium chloride solutions; $\alpha_{CEM} = (2t_{Na}-1)$. The mean permselectivity for bench mark membranes is typically in the order of 0.80–0.95, where the CEM usually has a higher permselectivity (0.95+) than the AEM (0.80+) (Dlugolecki, Nymeijer et al. 2008). This gives a unit cell potential of approximately 0.15 V for Eq. (4.3) at 25 °C.

4.2.4 Cell Potentials During Operation

During operation, there are several contributions that will lower the exergy efficiency. In this section, we discuss ohmic losses, concentration polarization, and hydrodynamic losses, in particular, though mixed electrode potential and current leakages may also contribute to lower the exergy efficiency.

4.2.4.1 Cell Charging and Discharging Cycles

The potential across any of these membranes can be described as the sum of the Donnan potentials at the membrane–solution interfaces. When two solutions are separated by a semipermeable membrane such that the free diffusion of some subset ions is impeded, an electrochemical osmotic equilibrium will be set up leading to a potential drop across the membrane (Hamann, Hamnett et al. 1998). In this process, the capacitance of the double layers at the membrane-flow–compartment-solution interfaces is alternated, thus also the response in the Donnan potentials.

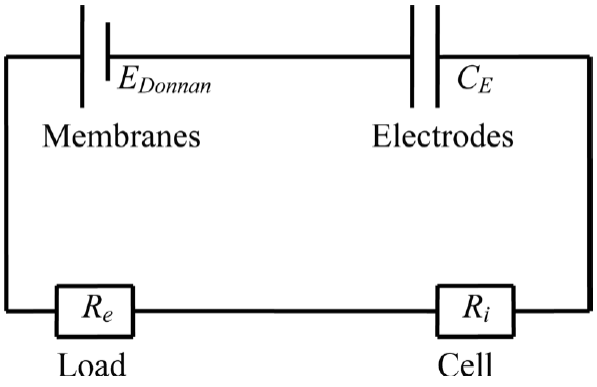

Figure 4.2 Equivalent Electric Circuit for charging/discharging the RC-membrane circuit. Replacing the solutions of the flow compartment converts the chemical potential energy into electric energy by the electrochemical transport processes of the Donnan potentials along the membrane-flow compartment interfaces. Simultaneously, the electrode capacitor double layers are charged/discharged and the flow of electric current in the circuit is dissipated in the resistors.

Alternating the flow of solutions between the pair of membranes can be compared to the analogous process of one capacitor replacing a material with one dielectric constant for a material with a different dielectric constant. By such means, the capacitor will act as a dc potential source. This is illustrated by the Donnan DC

potential source in Fig. 4.2. The double layers of the porous graphite materials separated by membranes from the streaming solutions will thus be cyclically charged and discharged correspondingly, illustrated by C_E in Fig. 4.2. The role of the porous capacitors is to convert the ionic current into electronic current. In this process, a current flows through the circuit while the available electric work is dissipated in the resistors, i.e., the internal ohmic resistance of the cell, R_i, and the external load, R_e. By means of the ohmic potential drop at any given time, t, in the circuit, IR, the initial potential, E° and the dynamic potential, E(t) are given by the following equation (Tipler and Mosca 2007):

$$E(t) = IR = E^\circ \cdot \exp\left(-\frac{t}{\tau}\right) = E^\circ \cdot \exp\left(-\frac{t}{R_{tot} \cdot C_{tot}}\right) \qquad \text{Eq. 4.4}$$

which can be linearized into

$$\ln\left[E(t)\right] = \ln\left[E^\circ\right] - \frac{1}{\tau}t \qquad \text{Eq. 4.5}$$

τ is the time constant of the cell. $R_{tot} = R_i + R_e$ is the resistance of the total circuit, the internal, and external resistance, correspondingly. $C_{tot} = C_E/2$ is the unit cell total capacitance as C_E the capacitance of each porous electrodes of the CPEC in series. When recording the potential relaxation in time plotted in accordance with Eq. (4.5) can thus give the initial potential (the Donnan potential) and the time coefficient (the inverse product of the total capacitance and circuit resistance).

4.2.4.2 Ohmic Potential Losses

Ohmic potential losses are, perhaps, the most obvious loss in exergy efficiency. The power output of an AGCM cell is dictated by the closed circuit potential times the current density, Eq. (4.6). The closed cell potential is dictated by the open circuit potential minus the cell resistivity of the cell, R_{cell} times the current density. The cell resistivity or the inter- nal resistivity, R_{cell} is given by Eq. (4.7)

$$P_{cell} = E_{cell}^{closed} j = E_{cell}^{OCP} \cdot j - R_{cell} \cdot j^2 \qquad \text{Eq. 4.6}$$

where

$$R_{cell} = \sum_{i}^{i=1,2,3,\ldots} \frac{\delta_i}{\kappa_i} \qquad \text{Eq. 4.7}$$

R_{cell} is the internal ohmic resistivity of the unit cell (i.e., Ri in Fig. 4.2), j the current density, and δ_i and κ_i are the thickness and the ionic conductivity of each section i of the unit cell as in Fig. 4.1, respectively. Figures 4.1 and 4.2 and Eqs. (4.6) and (4.7) refer to one unit cell. If the distance between the membranes is increased, the ohmic resistivity associated to the flow compartments – and the river/brackish water, in particular, increases.

4.2.4.3 Concentration Polarization Losses

These losses can occur in the AGCM system and may become particularly pronounced in the case of laminar flow in an open channel. For RED, this phenomenon is well explained by Lacey. As current is drawn, ions of the selected kind are removed or fed from the flowing solution close to the membranes, e.g., cation near the CEM. Due to electroneutrality, the salt concentration, NaCldiss, near the membrane–solution interface is lowered. The effect of such polarization is to a good approximation for stagnant solutions dictated by Fick's first law of diffusion in combination with the Nernst, Eq. (4.8). Correspondingly, the driving force next to the membrane is lowered. This effect will occur symmetrically along the membrane–solution interfaces of each of the flow channels. This loss in exergy efficiency is given by Eq. (4.9). Because the potential work is dictated by the chemical potential difference of the salt, NaCl, at the two interfaces, Eqs. (4.3), (4.6), and (4.9) give Eq.(4.10)

$$j = \frac{D_{NaCl}}{F} \frac{\left(C_{NaCl}^{s.w.,b} - C_{NaCL}^{s.w.,s}\right)}{\delta_{b.l.}} \qquad \text{Eq. 4.8}$$

$$\eta_{u.c}^{conc.pol.} \approx \frac{RT}{F} \ln \frac{C_{NaCl}^{s.w.,b}}{C_{NaCl}^{s.w.,s}} \qquad \text{Eq. 4.9}$$

$$P_{u.c} = \left(\alpha_{mean} \frac{RT}{F} \ln \frac{a_{NaCl}^{s.w.,s.}}{a_{NaCl}^{r.w.,s}} \right) \cdot j - R_{u.c.} \cdot j^2 \qquad \text{Eq. 4.10}$$

where r.w.,s and s.w.,s refer to the membrane–solution interface activities and r.w.,b and s.w.,b refer to the bulk feed solutions.

Due to the nonlinear coupling between current density, concentrations, potential, and power density as described by Eqs. (4.8) – (4.10), further investigation by the use of analytical models is out of the scope of this paper. However, it is important to note the concentration polarization overpotential will lead to a nonlinear behavior for the cell potential as a function of the current density.

4.2.4.4 Flow Pressure Drop

Forcing a fluid through a slit presents a parasitic loss in exergy efficiency. From the equation of momentum (White ; Sorgun, Ozbayoglu et al. 2010), for a one-directional flow in a slit

$$\frac{dp}{dx} = \frac{d\tau}{dy} = \mu\left(\frac{d^2u}{dy^2}\right) \qquad \text{Eq. 4.11}$$

where P is the pressure, x is the flow direction, s is the stress tensor, y is the distance from the wall (membrane surface), and u is the velocity of the fluid. From Eq. (4.11), we obtain the pressure drop in the channel

$$\Delta p = 12\mu\frac{l}{\delta^3 w}Q \qquad \text{Eq. 4.12}$$

Furthermore, the necessary volumetric feed rate, Q, is proportional to the cross-sectional area of a RED stack, i.e., l x w. From a mass balance (considering absolute membrane selectivity), the volume flow, the current density, and the concentration difference between the inlet and outlet are given:

$$Q = \frac{l \cdot w}{F\left(C_{D,outlet} - C_{D,inlet}\right)} j \qquad \text{Eq. 4.13}$$

The pressure drop, Δp, and the pumping power of each compartment, $\overset{\Lambda}{P}$ become

$$\Delta p = 12\mu\frac{j}{F \cdot \left|\Delta C_{i/o}\right|}\frac{l^2}{\delta^3} \qquad \text{Eq. 4.14}$$

$$\hat{P}_{loss} = 12\mu \frac{lQ^2}{\delta^3 w^2} = 12\mu \left(\frac{j}{F\Delta C_{i/o}} \right)^2 \frac{l^4}{\delta^3} \qquad \text{Eq. 4.15}$$

We now see that the pressure drop and the pumping power relate to the flow compartment thickness and length by the same order. Though the exact value of the pressure drop differs in the presence of a spacer, the relation between pressure drop, pumping power, channel length, width, and thickness remains the same. What makes electrochemical reactors, such as AGCM, RED, etc., in particular, different from other processes, such as ED, PRO and FO, is that the flow characteristics, i.e., Re numbers, can only be permitted to be modified by flow-direction velocity, Q/wδ, since increasing the compartment thickness will significantly impede the cell performance by ohmic resistivity.

4.2.4.5 Statistical Analysis

In several cases, linear regression by the sum of least squared residuals is applied to obtain standard deviations. All results reported are given either as raw data or with a 95% confidence interval. In the case of the approach of Eq. (5), the standard deviations are retrieved by the (Gauss) formula of error propagation (Box, Hunter et al. 1978)

$$\sigma_A^2 = \sum_{i=1}^{n} \left(\frac{\delta A}{\delta x_i} \sigma_{x_i} \right)^2 \qquad \text{Eq. 4.16}$$

where A is a function of several variables, i.e., A = f ($x_1 x_2 \ldots x_n$) and σ_{xi} is the standard deviation of the variable x_i.

4.3 Experimental

4.3.1 Apparatus

The cell applied for this investigation was the proof of principle cell, as sketched in Fig. 4.3. Eight cells of 6 x 6 cm^2 were stacked and coupled in parallel. Each cell con- sist of a porous capacitive carbon layer, a 160 µm AEM (Neosepta AMX), a

400 µm polymer spacer, a 160 µm CEM (Neosepta CMX), and a layer of porous capacitive carbon. In the center of the stack, the feed solutions enter through a 1.5 x 1.5 cm^2 hole and leave the cell through one of the gaps on the side (6 cm x 0.4 mm).

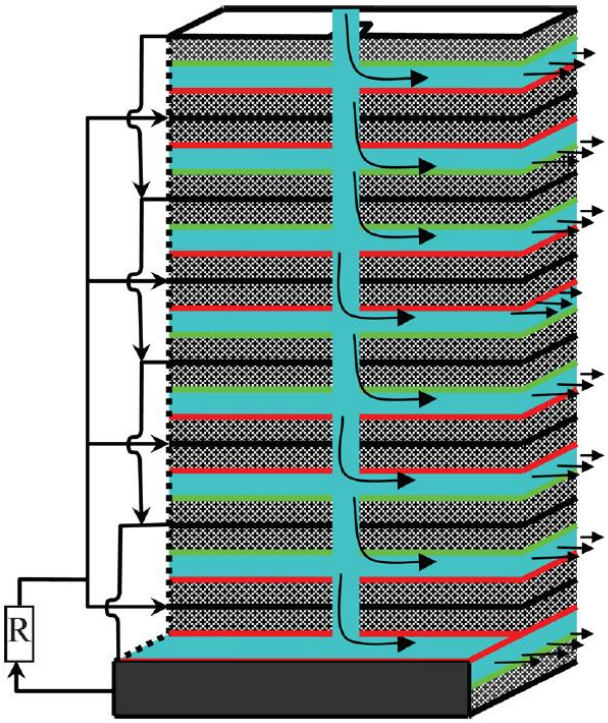

Figure 4.3 A stack of eight cells coupled in parallel. The sketch depicts the stack cut open. The solution feed and exit are indicated by arrows (blue sections in the online color version). AEM and CEM are indicated by (in green and red) lines, respectively. The black and white patterns illustrate the capacitor materials. On the left side of the stack the coupling to the load, R, is illustrated.

The electric measurements were carried out applying standard resistors and a standard multimeter set to dc potential measurements. The resistances of the resistors were 0.5, 1, 11, and 100 Ω.

4.3.2 Procedure

4.3.2.1 Volume Flow Dependency

One important area of studying reactors of different kinds has always been flow rate dependency. Hence three different flow rates were applied in studying the performance of the stack: 25, 50, and 75 mL/min. Standard solutions of 1 and 30 g/ L NaCl were placed in containers in a temperature controlled cupboard and fed to the cell by a pump.

With a total cell volume of 11.5 x 10^{-6} m^3, the minimum residence times become 28, 14, and 9 s for the volumetric flow rates of 25, 50, and 75 mL/min.

4.3.2.2 Polarization Curves

The polarization curves were recorded by applying different loads. The loads were simply standard electric resistors of 0.5, 1, 11, and 100 Ω. The cell potential and the current were logged by measuring the cell potential and the potential drop across these resistors. The presented polarization curve was recorded at the highest volume flow rate, i.e., 75 mL/min.

4.4 Results and Discussion

First, we present the polarization curves retrieved with different loads and the peak power values and peak potential values. Next, we study the impact of changing the volumetric flow rate.

4.4.1 Polarization Curves

In the upper part of Fig. 4.4, we give the absolute value of the potential and current density curves obtained with 0.5 and 11 Ω loads. The gray filled symbols of this upper graph of Fig. 4.4 represent current density and the clear symbols the potential. As can be seen, the potential increases as the sea-like feed water

replaces river-like water in the flow compartment. Next, as shown by Eq. (4), the RC-circuit is discharged.

Among the most classic characterization approaches in the field of electrochemistry, there are the polarization and the power output curves. These are known to characterize regions of activation overpotential (Butler–Volmer), charge transport (ohmic), and mass transport (diffusion) limited regions. Hence, we plot the polarization and power density as functions of the current density in Fig. 4.4 and Table 1. Here, we present the average of the peak values of the charging and discharging cycles obtained with 0.5, 1, 11, and 100 Ω loads in the lower part of Fig. 4.4. The gray filled circles of the lower graph of Fig. 4.4 represent the average cycle peak potential and current density dissipated in an external resistor. As is indicated by Eq. (6), in absence of any mass transport limitations, the cell potential should be linear to the current density. A linear regression by the means of minimum square gives Eq. (17) for the current density given in mA/m^2

$$E_{peak}(j)/V = (0.125 \pm 0.012) - (0.56 \pm 0.010) \cdot j \qquad \text{Eq. 4.17}$$

Seeing the linear trend in the potential curve supports assumptions that diffusion is not, or only to a very small degree, limiting the AGCM process according to the performance reported here. From Eqs. (4.6) and (4.8)–(4.10), one can see that the effective “EOCP” would drop with increased current density and thus not be linear when boundary diffusion becomes pronounced. The intersection point suggests that the maximum potential that we can obtain with this cell is 125 ± 12 mV. Comparing to the best case scenario, open circuit potential of a mixing cell utilizing the membrane induced electrochemical potential, approximately 150 mV, the cell applied here appears able to offer 83 ± 8% of the theoretical open circuit potential value. If considering that the feed solutions enter through a hole in the center and leave through the slits on one side of the square compartments, such that efficient solution replacement is impeded and that there might be current leakages around the edges of the feed entrances, the result of 86 6 8% of the open circuit potential is actually a rather promising value.

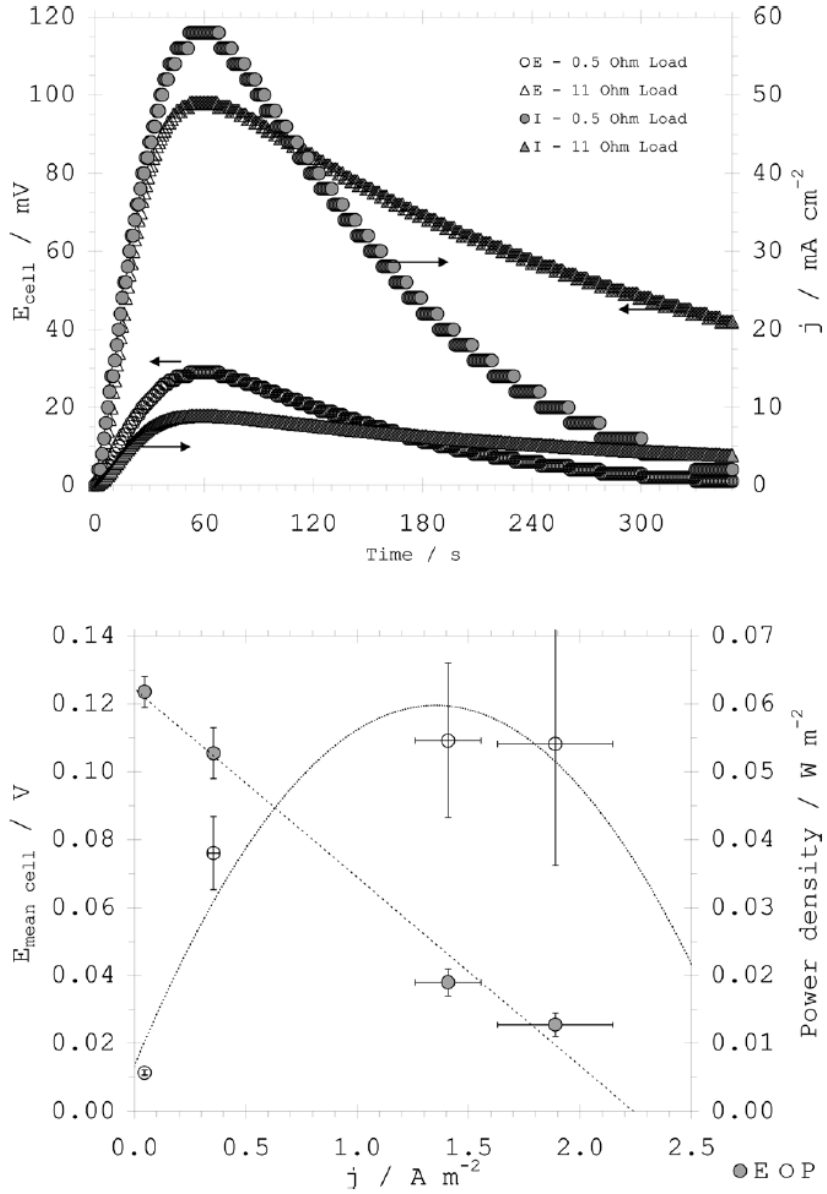

Figure 4.4 Cell potentials and currents of experiments with 11 and 0.5 Ω loads, respectively, (upper) and the peak power densities and potential of the cell as a function of the current density for a constant flow rate (75 mL/min) and for all the different loads applied.

The values that Eq. (4.17) is based on is the average of the charge and discharge cycle of both river and sea water replacement, as given in Table 1.

Table 1 Cell peak potentials and peak power densities averaged for the two cycles as functions of current density and flow rate 75 mL min^{-1}.

E_{peak} (mV)	P_{peak} (mW m^{-2})	j_{peak} (A m^{-2})
124 ± 5	5.7 ± 0.4	0.0458 ± 0.0017
106 ± 8	38 ± 5	0.36 ± 0.03
38 ± 4	55 ± 11	1.41 ± 0.15
26 ± 4	54 ± 18	1.9 ± 0.3

This means that in the average unit cell resistance, $R_{u.c.}$, was 0.56 Ω/m^2 and the open cell potential was 0.125 V. The maximum power reported for the pair of cycles is therefore 55 mW/m^2 though the highest peak observed for this system of one of the peaks was 67 mW/m^2. This cell is the first prototype, so to give an idea of the potential of the technology, consider the following: if the open circuit potential intersection point is increased to 170 mV and the compartment thickness is reduced by a factor two (so that $R_{u.c.}$ would be 0.28 Ω/m^2), the maximum current drawn would, according to Kirchoff's law, be 6.2 A/m^2 and the maximum power density was 0.26 mW/m^2 at a cell potential of 85 mV, respectively. For a RED cell, power densities around 0.93 mW/m^2 have been reported for a stack of fifty cells in series. (Both these power density values relate to membrane area as this is the convention for RED).

4.4.2 Volumetric Flow Rate Dependency

As explained previously, the power is generated as a response to the change in chemical equilibrium in the flow compartment of the cell as the feed solution is replaced and next it decreases as the driving potential gradually vanishes. This far

we have shown that for the higher flow velocity, i.e., 75 mL/s, there is hardly any evidence of mass transportation limitations related to diffusion.

Figure 4.5 gives the charge and discharge cycles when the solutions are replacing each other. The corresponding minimum replacement times, the residence times tres, and the observed pro- cess times, t_{obs}, are given for different volume flow rates, Q, in Table 2, respectively. (The residence time is given by the cell volume divided by the volumetric flow rate and the observed time is the actual charging time of the process.) These results are obtained with a rather small (0.5 Ω) load as to maximize the current density of the cell. As the volumetric feed rate increases, the ratio between the observed time and the estimated time increases as well. This indicates that perhaps the replacement of the electrolyte solution in corners of the cell limits the charging of the two cycles.

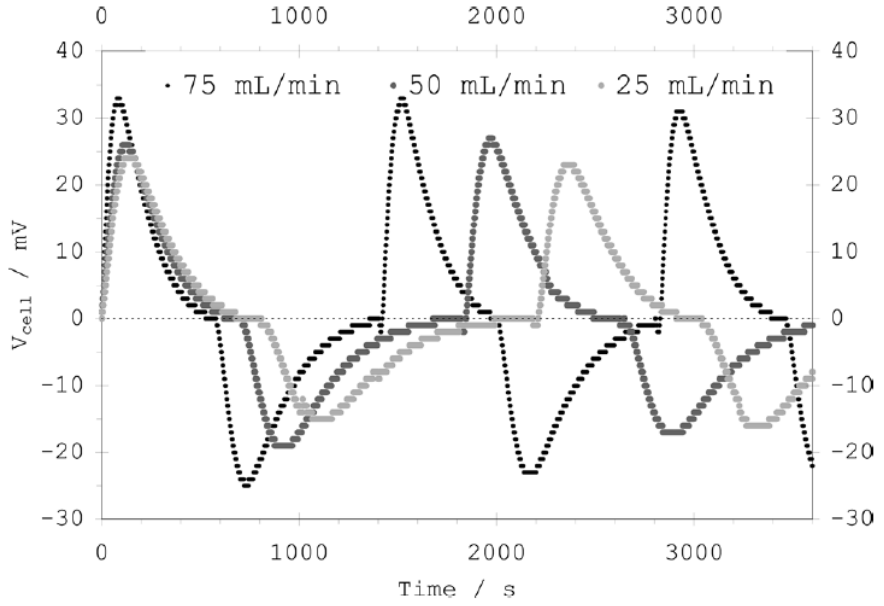

Figure 4.5 Cell potentials of the cell as a function of time for different flow rates (25, 50, 75 mL/min). The available work is continuously dissipated over a 500 mΩ resistor.

Table 2 Estimated residence times, t_{res}, and observed "residence" times, t_{obs}, for the charge processes at different flow rates, Q.

Q(mL min^{-1})	t_{res}(s)	t_{obs}(s)	t_{obs}/t_{res}
25	28	134 ± 19	4.8 ± 0.2
50	14	123 ± 17	8.8 ± 0.5
75	9	90 ± 20	10.0 ± 0.2

By analyzing the cycles with Eqs. (4.4) and (4.5), we can estimate the time dependency factor, τ . By assuming that the starting time, t_0, of Eq. (4) is when the polarization curve crosses 0 V and plotting the results obtained only for the time frame of the potential relaxation of the curves of the curves of Fig. 4.5 we obtain the product of the cell resistivity and the capacitance, τ . These values are given for the cycles driven with sea water like, S.W., and river water like, R.W., solutions, see Table 3. One can see that the time dependency factor, s, increases with the feed water solution resistivity, i.e., higher for the river water like solution but also that it is lowered when the feed velocity increases. With the current cell design, it is difficult to address the latter trend with a good explanation though one possibility is that it is related to a poor electrolyte replacement scenario.

Table 3 Time constant τ and initial potentials, E°, for the cycles given in Fig. 5. Values are estimated by the linear regression, using Eq. (5), and the Gauss propagation of error formula, Eq. (15). Results correspond to Fig. 5.

Q(mL min^{-1})	$\tau_{S.W.}$(s)	$\tau_{R.W.}$(s)	$E^{\circ}_{S.W.}$(mV)	$E^{\circ}_{R.W.}$(mV)
25	156 ± 1	262 ± 1	88 ± 2	71 ± 1
50	140 ± 1	218 ± 1	95 ± 2	73 ± 1
75	117 ± 1	174 ± 1	104 ± 3	84 ± 1

The approach by Eqs. (4.4) and (4.5) allows us to get an estimate of what the initial potential, E°, might be for the different flow rates. Ideally, we would expect this value to be the same for all the flow rates. If considering that the lack of linearity between the fractions of residence times (t_{obs}/t_{res}) and flow rate is due to parts of the cell suffering from impeded electrolyte replacement, then the cell will experience a combination of membrane potentials. This again can lead to charging in one part of the cell and discharging in other parts of the cell. This would again lead to the estimated E° being lower for lower feed rates. This would be so because it takes longer time to change the water at lower flow rates and the relaxation time used in the procedure of Eq. (4.5) would start at a potential that is lower due to longer internal charge exchange. The estimated initial potential values, E° are given in Table 3 in the same manner as the time dependency coefficients, respectively. As the volumetric feed rate is increased, the value increases as well. Considering the lack-of-replacement- effect discussed here, the expected value with an optimal flow and electrolyte replacement could lead to an initial value of 0.15 V, as described by Eq. (3). Thus, we see the performance of this cell as a geometric phenomenon rather than an intrinsic property of the AGCM in general.

4.5 Conclusion

We have seen that AGCM using ionic exchange membranes holds great potential for utilizing the mixing of sea and river water as a viable power source.

The similarities to already established power sources, such as reverse electrodialysis, but with several advantages, place AGCM among the portfolio of competitive salinity power sources.

The most likely limitations of the power density of this first attempt of an AGCM cell appear to be feed solution replacement and ohmic resistances in the feed flow compartment.

Chapter 5

Impact of Wire Geometry in Energy Extraction from Salinity Differences Using Capacitive Technology

Energy extraction based on capacitive Donnan potential (CDP) is a recently suggested technique for sustainable power generation. CDP combines the use of ion-exchange membranes and porous carbon electrodes to convert the Gibbs free energy of mixing sea and river water into electric work. The electrodes geometry has a relevant impact on internal resistance and overall performance in CDP. In this work, we present the first effort to use wire-shaped electrodes and its suitability for improving CDP. Analytical evaluation and electrical measurements confirm a strong nonlinear decrease in internal resistance for distances between electrodes smaller than 3 mm. We also demonstrated that we get more power per material invested when compared to traditional flat plate designs. These findings show the advantages of this design for further development of CDP into a mature technology.

This chapter has been published as:

Sales, B. B.; Burheim, O. S.; Liu, F.; Schaetzle, O.; Buisman, C. J. N.; Hamelers, H. V. M., Impact of Wire Geometry in Energy Extraction from Salinity Differences Using Capacitive Technology. *Environmental Science & Technology* **2012**, 46, (21), 12203-12208.

5.1 Introduction

The oceans have long been considered a great source of energy available in many different forms (Isaacs and Schmitt 1980), but the vast research effort has focused on waves, tidal, and offshore wind power (Gross, Leach et al. 2003). Salinity difference is a frequently overlooked and neglected source of renewable clean energy with a worldwide potential of 2 TW (Post, Hamelers et al. 2008). Yet, this source ranks first in energy density and second place in global power potential when compared to all marine renewable power sources (Wick and Schmitt 1977). Moreover, salinity difference is a steady source of energy much less sensitive to weather conditions than its concurrent renewable energy sources. The production of electricity with this method is obtained from the free energy available when electrolyte solutions of different concentrations are mixed (Veerman, Saakes et al. 2010).

Theoretically, in order to harvest energy from salinity gradients, any of the various seawater desalination techniques at present can be modified and the reverse process implemented (Pattle 1954). Several methods to exploit this potential were proposed and investigated over the last decades (Jones, Finley et al. 2003), with fundamentally different working principles. Currently the most developed technologies (Boon and van Roij 2011; Ramon, Feinberg et al. 2011) for energy conversion from salinity differences are pressure retarded osmosis (PRO) (Achilli, Cath et al. 2009; Thorsen and Holt 2009) and reverse electrodialysis (RED) (Vermaas, Saakes et al. 2011; Burheim, Seland et al. 2012). Nevertheless, a need for different and improved techniques remains due to the engineering complexities (design and hydrodynamic challenges) of these systems and their durability when exposed to local environments (e.g., biofouling) (Lee and Elimelech 2007). Thus, several novel suggestions were reported involving the use of solid-state electrodes (Sales, Saakes et al. 2010; Brogioli, Zhao et al. 2011; La Mantia, Pasta et al. 2011; Liu, Schaetzle et al. 2012) or nanopores (Guo, Cao et al. 2010) to extract and convert this free energy. In particular, Capacitive energy extraction based on

Donnan Potential (CDP) is an electrochemical technique combining the high energy storage and power delivery of porous carbon electrodes (Simon and Gogotsi 2010; Porada, Weinstein et al. 2012) with the selectivity of ion-exchange membranes (Pivonka, Smith et al. 2007). The driving force of this process is directly related to the membrane equilibrium potential also known as the Donnan potential (Sarkar, SenGupta et al. 2010).

One advantage of this technology, where the repeatedly switch between sea and river water causes the consecutive inversion of electrical potential, is that fouling can be drastically reduced (Kerwick, Reddy et al. 2005), which is a common obstacle in membrane systems. Nevertheless, lowering the ohmic losses is one major issue in all electrochemical techniques (Lacey 1980; Veerman, Post et al. 2008). Flow distribution and mass transport issues have also been reported as bottlenecks in this field (Vermaas, Saakes et al. 2011). In this paper, we present a new design using wire-shaped electrodes that reduces significantly the ohmic losses. It also allows the design of closed systems with less mechanical resistance (e.g., spacers between membranes) for water flow (Burheim, Liu et al. 2012; Porada, Sales et al. 2012).

The aim of this work is to demonstrate the advantages of cylindrical wires in CDP with an analytical evaluation, the development of a model, and experimental validations with electrical and power performance measurements.

5.2 Theory

CDP is a two-step cyclic process where we alternate sea and river water between the electrodes. The seawater step consists of ion adsorption on the carbon surface followed by ion release in the river water step. This ion migration generates a spontaneous electron flow via the external circuit where electricity is extracted.

Therefore, our operation method has a constant closed RC circuit joined by the electrodes as the capacitor and an external resistor.

The CDP process is driven by the product of electrochemical potential difference across the compartment containing two membranes covering the carbon electrodes. Figure 5.1 shows the equivalent electrical circuits of CDP during charge and discharge processes. The Donnan potential, E_{Donnan}, acts as the driving force for ionic current. This potential is spontaneously formed at the membrane surface and changes with the solution concentration. When alternating the immersion of the pair of wires in different salinities, E_{Donnan} changes, and the electrical double-layer potential, E_{dl}, on the carbon electrodes builds up to attain the opposite potential. The difference between E_{Donnan} and E_{dl} is named E_{net} and is the actual driving potential for the energy extraction.

The change in adsorbed charge on the capacitive material, C_e, induces a transient current in the external circuit that leads to a voltage drop in the load, R_{ext}. When the equilibrium is reached, there is no electric current anymore, and then, we immerse the cell in a solution with different concentration to continue the cycle of adsorption/desorption. The voltage and power output of this process are given by

$$E^{cell} = E_{donnan} \cdot \exp\left(-\frac{t}{\tau}\right) \cdot \left(\frac{R_{ext}}{R_i + R_{ext}}\right) \qquad \text{Eq. 5.1}$$

$$P^{cell} = \left(E_{net}\right)^2 \cdot \frac{R_{ext}}{\left(R_i + R_{ext}\right)^2} \qquad \text{Eq. 5.2}$$

where R_i is the internal resistance of the cell, t is time and τ is the capacitor constant.

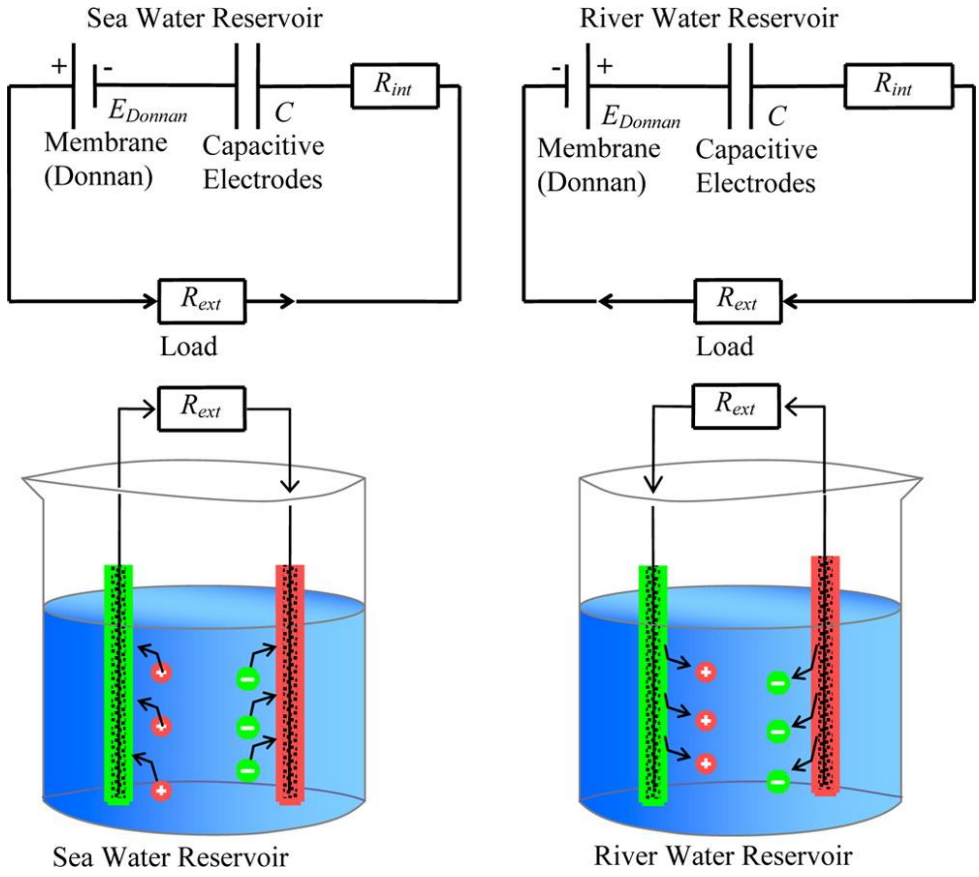

Figure 5.1 Setup schematics and correspondent equivalent circuit.

Different from traditional supercapacitors, where highly concentrated electrolytes are used, the CDP technology in comparison works with much lower conductivities, because it is bound to use sea and in particular river water. Therefore, the electrolyte resistance is included in the total internal resistance of the cell and corresponds to a large fraction of it. In eq 5.2, the dependence of the power output to the ratio of internal and external resistances can be seen. Ideally, for extracting maximum power, R_{ext} should be fixed equal to R_i, and R_i should be minimized as much as possible. Aiming to decrease the R_i without compromise to other losses,

we propose the use of wire-shaped electrodes instead of the usual flat plates design.

For analytical comparison of cell internal resistances between wire and flat plate designs, we focus the study in the region between the two electrodes.

The resistance between electrodes of different shapes can be calculated using mathematical methods described by (Vanýsek 1997). Considering parallel plates with infinite width, w, and length, L, the resistance between the plates is linear to the electrode intermediate distance, x, as given by

$$R^{\parallel} = \frac{x}{\kappa L 2r}, \text{for } w = 2r \qquad \text{Eq. 5.3}$$

where κ is the solution conductivity.

When comparing with the resistance between two wires, we make the following assumptions: (1) the two electrodes, with radius r, have their centers separated by a distance x (horizontally) and immersed in an infinitely large electrolyte volume; (2) the electrodes are separated in a narrow channel of 2r (vertically). The relations are then given by

$$R^{\supset\subset} = \frac{x}{\kappa L 4r}\left(\frac{1}{\sqrt{1-\left(\frac{2r}{x}\right)^2}}\arctan\left[\frac{\left(1+\frac{2r}{x}\right)}{\sqrt{1-\left(\frac{2r}{x}\right)^2}}\right]\right)^{-1} \qquad \text{Eq. 5.4}$$

and

$$R^{\supset\subset} = \frac{x}{\kappa L \pi r}, \text{for } r << x \qquad \text{Eq. 5.5}$$

considering the electrodes interdistance. A more detailed explanation for eq 5.4 can be found in Appendix 5.A of this chapter.

5.3 Materials and Methods

A pair of inert wires coated with activated carbon and ion-selective membranes was alternately dipped in artificial sea and river water in order to deliver electric work. For the theoretical analysis, we modeled the power output as a function of the distance between the wire electrodes in a beaker. In this section, we first give the details of the materials and the experimental setup followed by the details of the applied model.

5.3.1 Electrode Preparation

The porous capacitive electrode solution was made by adding a binder solution to activated carbon (AC). For this, we first dried the AC powder (DLC Super 30, Norit, Amersfoort, The Netherlands) for 24 h in an oven at 105 °C to prevent any adsorbed water in the crude sample. The dried carbon was added to a solution of polyvinilidene fluoride (PVDF) (KYNAR HSV 900, Arkema Inc. Philadelphia, USA) in 1-methyl 2-pyrrolidone (NMP). The mixed solution was put into a ball mill grinder (PM 100, Retsch, Haan, Germany) with 12 agate stone balls for 30 min at 450 rpm to achieve homogeneous mixing. The slurry was then cast onto metal wires composed of titanium coated with platinum (2 mm thick, Magneto Special Anodes BV, Schiedam, The Netherlands) over a length of 6 cm leaving the extremities free for electrical connections and to neglect fringing of the electric field at the ends. After casting, the wires were put in a vacuum oven at 50 °C to let all the NMP evaporate and to achieve a content of 10 wt % PVDF in the electrode. The membrane layer was obtained by painting an ionomer solution over the carbon layer. Anionic ionomer (Fumion FAA, Fumatech, St. Ingbert, Germany) was used to make the anode, and cationic ionomer (Fumion FLNMP-915, Fumatech, St. Ingbert, Germany) was used to make the cathode. Together both layers added in average 120 µm to the wire thickness.

5.3.2 Artificial Sea and River Water

Different salt concentration solutions were made to simulate “sea” and “river” water. The set river concentration Criver consisted of 1 g of NaCl/L, while the sea concentration was 30 g of NaCl/L. All solutions were kept in 1 L containers stored in a incubator (FRIOCELL, MMM Medcenter, Munich, Germany) at 25 °C before all experiments.

5.3.3 Setup and Measurements

The experimental setup used in this study consisted of a rectangular frame in which the wires were positioned parallel to each other. The distance between the wires could be precisely set and changed between 29, 19, 9, and 1 mm. The wires were connected via an external circuit counting a resistor (Figure 5.1).

During the CDP cycle, the setup cell was alternately immersed in sea and river water in large containers, always waiting until the potential reached 0 V before switching to allow a constant flow of ions and electrons. The potential of the setup cell was logged by a precision multimeter (Fluke 8846A 6.5 digit, Everett, USA), and the internal resistance was logged by a high-speed milliohmeter (Agilent 4338A, Santa Clara, USA). This procedure was repeated several times keeping the intermediate distance constant.

5.3.4 Model of Internal Resistance and Power

We have from eq 5.4 that the relation between the electrolyte resistance and the distance between the wires, x, is highly nonlinear. On the other hand, this analytical expression does neither account for the back side of the wire nor the vast additional electrolyte volume in the container of our experiments. Therefore, we modeled the power output for two electrodes of 2.5 mm diameter in a container as a function of x and compared this to the analytical expression and the measured values. We also included different flat plate designs to confirm, in order magnitude consideration, the superiority of wires over plates.

The modeling was done with the finite element mesh (FEM) tool Comsol Multiphysics 2.1. The model was a Faraday one assuming one electrode with an isopotential equal to the ground whereas the other with isopotential of 50 mV (half of the maximal experimentally obtained potential). By analyzing the total current in light of the applied potential, the electrolyte resistance and power were obtained. The model was verified by checking that it was mesh size independent.

5.4 Results and Discussion

We see several consecutive CDP cycles with regular behavior in Figure 5.2, with the distance between electrodes set to 29 mm and Rext to 60 Ω. The CDP cycle starts when immersing a cell with a pair of electrodes, previously equilibrated in river water, into seawater and then returning it to river water to end this adsorption/desorption cycle. Figure 5.2 is in accordance with eq 5.1 that describes in the adsorption step, when the cell is immersed in seawater and t = 0 s, the E_{Donnan} sets instantly the initial and maximum cell voltage. This autogenerated potential drives ion transport through the membranes and into the nanoporous carbon electrodes where they are adsorbed, requiring an external electric current to keep electroneutrality. Over time, one can observe the cell potential decreasing exponentially with the adsorption of ions on the carbon surface electrical double layer. This continues until E^{cell} reaches 0 V (system is in equilibrium) and the charging of the nanoporous supercapacitor reaches saturation.

At the point of equilibrium, the E_{dl} corresponds to E_{donnan} when the membranes are exposed to sea water. We then start the second step of the cycle by switching the cell to river water. Now, the E_{donnan} reverses its sign and the driving force leads to ion desorption. The behavior described is the previous step is also observed here, but with different amplitude of values for E^{cell}. Equations 5.1 and 5.2 successfully predict this difference in voltage and potential obtained in each step, due to much higher R_i in river water than in sea water.

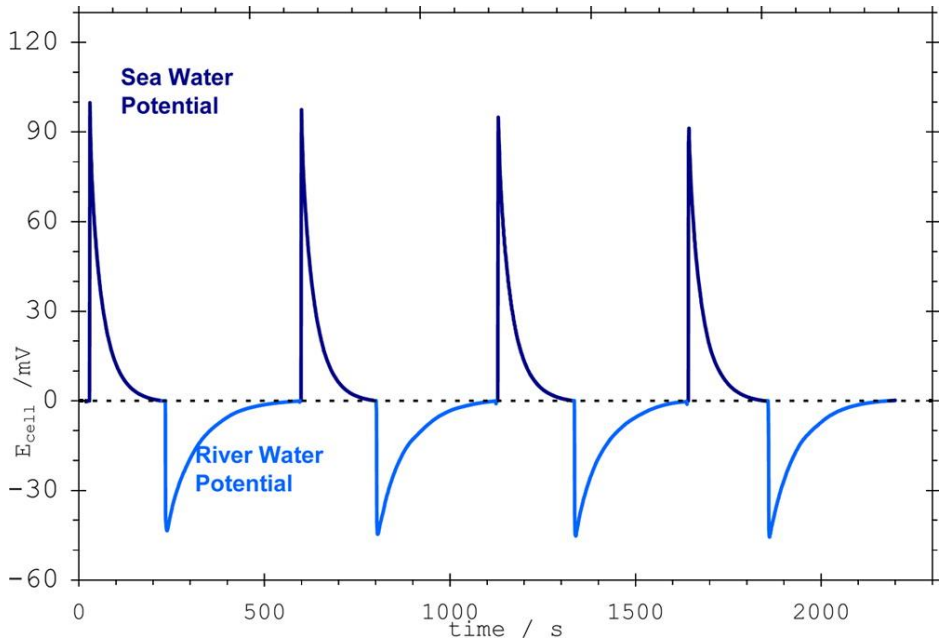

Figure 5.2 Evolution of measured cell potential (mV) over time (s).

The higher and more crucial R_i in river water was modeled in different geometries and the results can be seen in Figure 5.3. The inverse values of x and R_i are plotted in the graphs for convenience, i.e. to emphasize the geometry impact. Also, the positions where we have experimental validation are indicated by dashed rings. In the upper graph we plotted the difference between 3 electrode geometries: wires, double sided plates and one sided plates. One sided plates is the traditional design in supercapacitor technologies, however double sided plates are commonly used when cells are put in parallel (Zhao, Biesheuvel et al. 2009). In our experiments, the double sided plates can be seen as an intermediate, or transition, in comparing wires to single sided plates. We include this to demonstrate that there is hardly any contribution from the single/double sided effect and that, again, the advantage is solely due to the cylindrical shape of the electrode. At large distances in the curves, we observe no substantial difference among the modeled designs. In contrast, when the electrodes are positioned closer to each other, the wire shape

starts to show its advantage. As expected, we see a linear response of R_i with variation of the distance between plates while a strong non-linear relation is observed for wires, especially in the region of 350 m^{-1}.

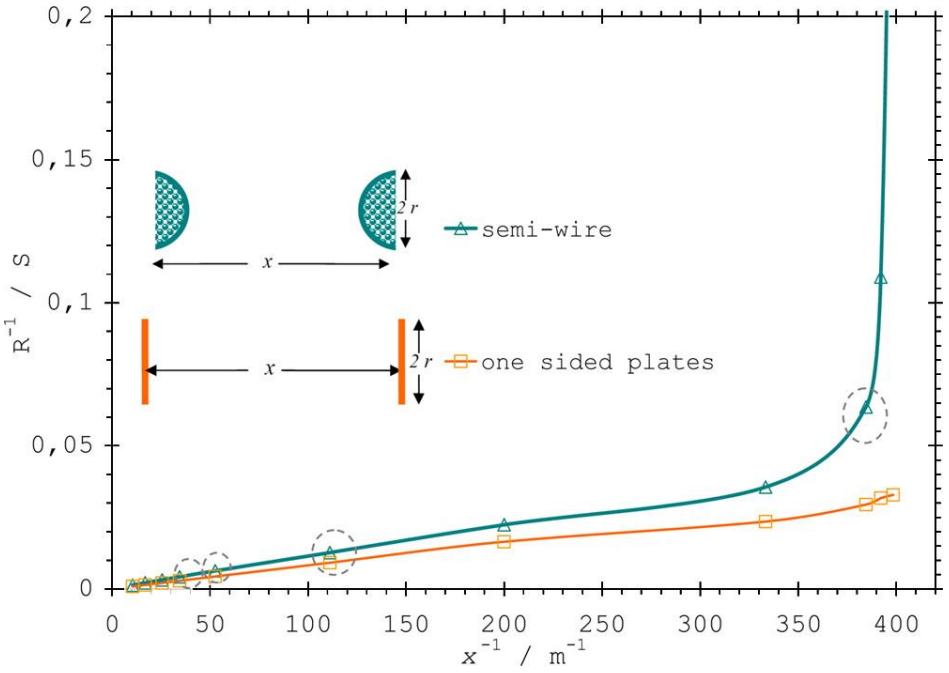

Figure 5.3 Inverse of internal resistance (S) over inverse of electrodes interdistance (m^{-1}) for both wire and plate geometries.

Using the assumptions made to derive the analytical expressions shown in equations 5.3, 5.4 and 5.5, we continue the analysis with focus on the difference of R_i between semi-wires and one sided plates (graph below in Figure 5.3). Already here, we can observe the advantage of wires over one sided plates from the 100 m^{-1} distance region.

The actual R_i measured in river water were 73 Ω for 29 mm, 62 Ω for 19 mm, 47 Ω for 9 mm and 10 Ω for 2.6 mm. One can see the agreement between the measured and modeled resistances. As for the analytical expressions, they give a further

qualitative view of the difference between the two geometries. They describe, and the actual measured values confirm the model, a trend in this particular situation of two electrodes in a large container.

With the cell voltage and the fixed external resistance known, we can calculate the power density (per weight of carbon material) of the whole cycle in this CDP technique. After several cycles logged for each distance set between electrodes, the average power density obtained was 70±5 μW/g for 29 mm, 74±3 μW/g for 19 mm, 163±18 μW/g for 9 mm and 347±12 μW/g for 1 mm. The average value of carbon material per length of wire was 0.85 g/m and it was used in our model to predict the power density for two wire electrodes. Figure 5.4 shows the experimental confirmation of the expected trend in the model (dashed curve) when wire shaped electrodes are used. The power densities do not vary much at large distance, but once again we see the non-linear behavior of the wires when they are put adjacent to each other. The measured values fit nicely to the theoretical curve, except for x = 9 mm. We assume that other neglected ohmic losses, experimental disturbances when holding the wires and partial immersion of the electrodes respond for this deviation. The graph verifies the analysis of superior overall performance of the system when using wires, not only in lowering ohmic losses, but also allowing a higher power density.

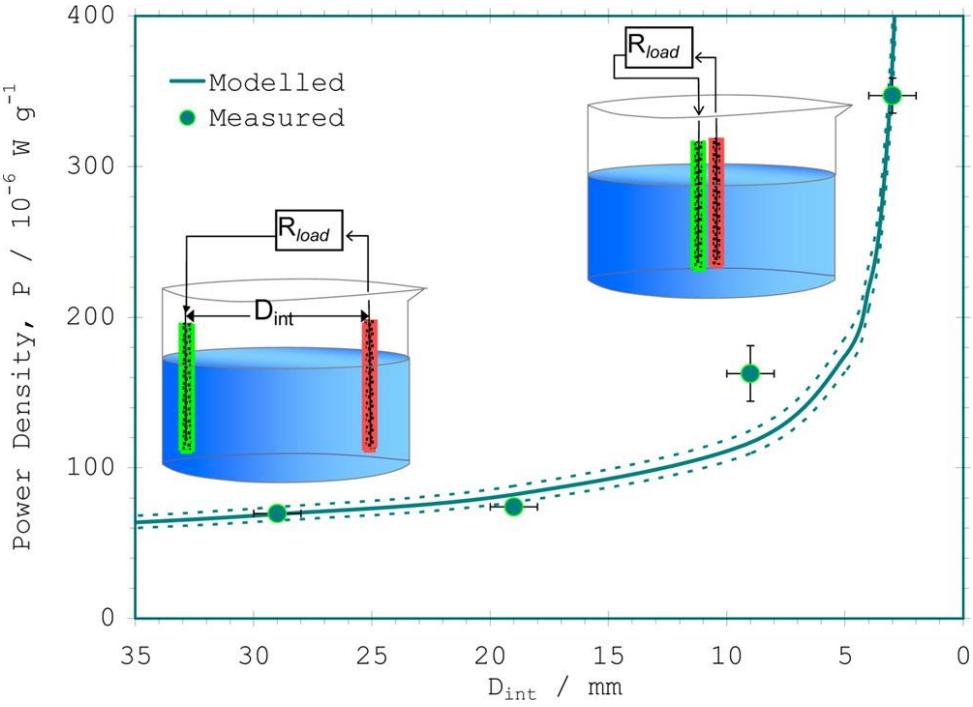

Figure 5.4 Power densities (μW/g) over electrodes interdistance (mm) for both modeled and measured values using wires.

These results present also novel possibilities within salinity gradient technologies. The fact that we are displacing the electrodes, instead of water bodies, opens the door for lowering irreversible losses, for example, pumping. One possible design is to make a carrousel of wire electrodes that alternately is immersed in channels where river and sea water are constantly flowing or batch wise replaced.

Additionally to these advantages, the use of wire-shaped electrodes also brings a better ratio of materials used and the electrode–electrolyte surface area. When we consider a fixed volume of activated carbon slurry and ionomer solutions, by applying the same layer thickness of these materials on the designs, we obtain more surface area with the wires. This way we can increase the performance of ion

adsorption of the whole process, with the same value of financial investment. Therefore, we have another strong argument for applying a wire design in CDP.

This work shows the promising suitability of a wire design for electricity production based on the capacitive Donnan potential principle. We observed fundamental differences in the internal resistance dependence to the distance between electrodes when wire-shaped electrodes are used instead of flat-plate ones. Therefore, the geometry of the electrodes plays an important role in the overall CDP performance.

We have demonstrated that changes in the cell design are a very efficient path for improvement and further development of electrochemical capacitive salinity difference power sources. This was shown analytically and by modeling of the process, in combination with an experimental verification.

In conclusion, with this new geometry of electrodes, it is possible to increase power extraction per mass unit of electrodes, through changes in the cell design, electrode shape, and operating condition.

Acknowledgments

Thanks are due to Dhan Prasam Gautam for assistance with the experiments and to Michel Saakes for valuable discussions. Extra thanks to Raul Rica for commenting on the analytical analysis.

Chapter 5 - Appendix A

The equation of Resistance

The derivation of equation 5.4 is done with the assumption that two wires are placed in a slit with insulating walls adjacent to the wires. We chose to solve the integral for the quarter cylindrical symmetry.

$$\frac{1}{R} = \int \kappa \frac{dA}{l} \text{, where; } dA = rL\,d\phi \tag{A.1}$$

$$\frac{1}{R} = \kappa L \frac{r}{x} \int_0^{\frac{\pi}{2}} \frac{d\phi}{\left(1 - \frac{2r}{x}\cos\phi\right)} \text{, where; } l = x - r\cos\phi \tag{A.2}$$

solving the integral we obtain:

$$\frac{1}{R} = \frac{\kappa L 2r}{x} \frac{2}{\sqrt{1-\left(\frac{2r}{x}\right)^2}} \arctan\left[\frac{\left(1-\frac{2r}{x}\right)}{\sqrt{1-\left(\frac{2r}{x}\right)^2}}\right] \text{, for } r \le x \tag{A.3}$$

Finally, to compare the geometries when the electrodes are remotely distanced:

$$\frac{1}{R} = \frac{\kappa L \pi r}{2x} \Leftrightarrow R = \frac{2x}{\kappa L \pi r} \text{, for r << x} \tag{A.4}$$

$$R^{\supset\subset} = \frac{x}{\kappa L \pi r} \text{, for r << x} \tag{A.5}$$

$$R^{\text{II}} = \frac{x}{\kappa L \varpi} \text{, for r << x} \tag{A.6}$$

Chapter 6

Capacitive Technology for Extracting Power from Low Temperature Waste Heat

We present a new principle for producing electricity from low temperature differences by using an affordable assembly combining ion exchange membranes and supercapacitor carbon electrodes. Our proposed design involves two isolated salty solutions, with equal concentration but different temperatures. The operation consists of an alternately and cyclic exposure of the electrodes to these electrolytes. This difference in temperature generates a thermomembrane potential that acts as a driving force for ionic adsorption/desorption cycles on the electrodes, our simple system is interesting for exploiting the potential of low temperature waste heat. When two volumes with equal concentration have different temperatures, it is possible to immerse a pair of electrodes (anode and cathode) into the low T one and have ion adsorption. An electric current is then generated in the external circuit to achieve electro neutrality. After saturation, the same electrodes are immersed in the high T volume and then ions desorb from the electrodes and are released to the volume, leading to a reverse electric current in the external circuit compared to the first step. These experiments prove the principle and the direct dependence of the temperature gradient for energy extraction.

This chapter has been submitted for publication

6.1 Description of the technology

Creative and modern methods to save and extract energy are in increased need. Technologies with one specific application are improved to demand less energy and produce less waste. Yet, an enormous amount of waste heat is inevitably produced by many established industrial processes (Bell 2008). One possible contribution for improving the energy efficiency is named thermoelectricity, which is the direct conversion between thermal energy into electricity (Chen, Lund et al. 2010; Wongsuwarn, Vigolo et al. 2012). This phenomenon is achieved both in solids and liquids (Bonetti, Nakamae et al. 2011). Conventionally, thermoelectric technology is based on semiconductor charge carriers, and material suitability is analyzed in terms of electrical conductivity and thermopower potentials reported in mV/K units (Piazza 2008; Vining 2009). Established materials such as metals or highly doped semiconductors recently began to share attention with new approaches using composites (Sootsman, Chung et al. 2009), carbon (Yee, Malen et al. 2011), polymers (Crispin 2012) and complex particle/solvent mixtures (Vigolo, Rusconi et al. 2010).

We introduce here a new principle for converting low temperature heat gradients into electricity, between two salty solutions with equal concentration. This is achieved by using the difference of temperature as a driving force for ionic migration through ion exchange membranes, and subsequent adsorption/desorption cycles in supercapacitor carbon electrodes. With our simple and affordable setup we combine traditional ion exchangers and porous activated carbon. The use of ion exchange membranes in systems with temperature gradients leads to a voltage difference known as thermal membrane potential (Ikeda 1958; Tasaka, Hanaoka et al. 1975; Hanaoka, Kiyono et al. 1993), which introduces the driving force. Our design is particularly interesting for generating electricity from the immense low temperature waste heat (Vigolo, Buzzaccaro et al. 2010). Its chief novelty lies on the fact of not having continuous physical contact

between the temperature baths, making it an unconventional thermoelectricity cell capable of insulating the T baths to avoid energy losses via thermal diffusion. The cyclic process is achieved through alternately dipping a pair of supercapacitor carbon electrodes, covered with ion exchange membranes, in insulated far apart cold and hot water bodies. Ion adsorption occurs at lower T, while desorption at high T, allowing a reproducible procedure to extract power via an external resistor. For this proof-of-principle we use a construction currently employed for power extraction from salinity gradients (Sales, Saakes et al. 2010; Bijmans, Burheim et al. 2012; Liu, Schaetzle et al. 2012).

Titanium wires coated with platinum were used as the core of the electrodes (Sales, Burheim et al. 2012). A layer of activated carbon is applied on the surface of the wires, followed by a layer of ion exchange membranes hot pressed around this capacitive layer (Porada, Sales et al. 2012). We use two pairs of anode-cathode electrodes where a pair is connected via electrical cables to the same polarity of the second pair. Two beakers are used containing electrolytes with equal concentration of NaCl, but different temperatures. Figure 6.1 shows the experimental schematics for the performed experiments and an equivalent circuit for the electrical analogue of the system.

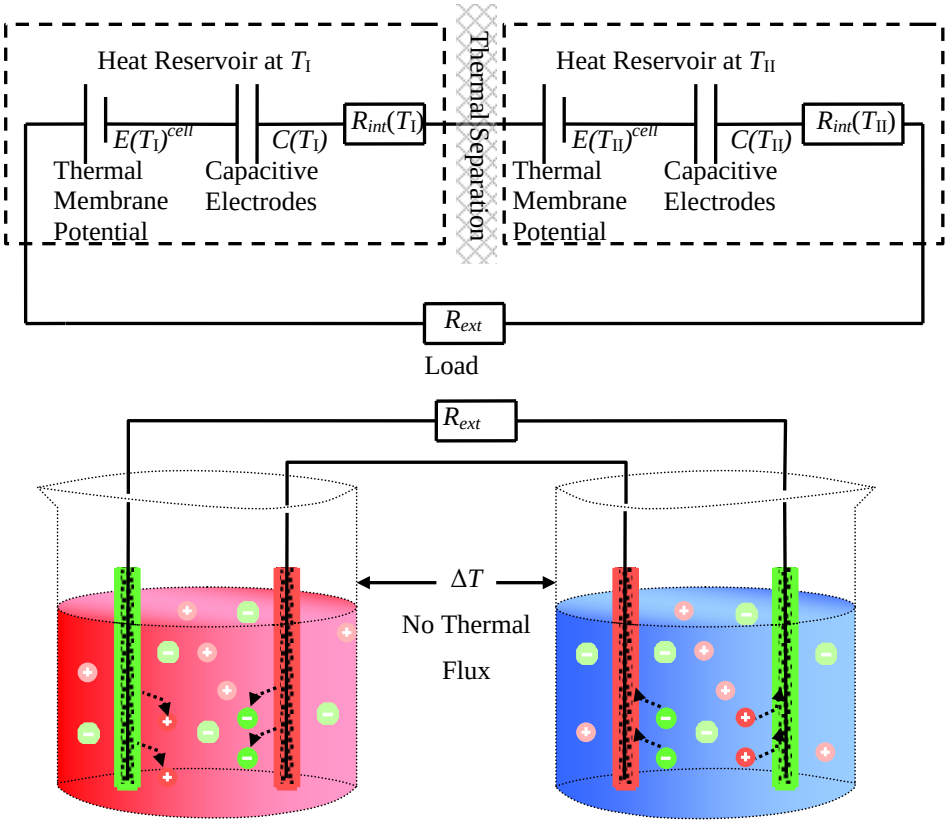

Figure 6.1 Equivalent electric circuit (upper part) with the schematics of the experimental setup (bottom part).

In our system, simultaneous ion adsorption and desorption occur separately in the different beakers. When both pairs are dipped in the beakers, adsorption takes place on the hot beaker, while desorption in the cold beaker. In the cold beaker, when the anode-cathode pair is immersed, a maximum voltage is formed and there is a driving force for the ions to migrate from the beaker through the membranes and be adsorbed in the electric double layer. At this point, a decrease of this potential over time occurs, mainly due to the thermal dissipation making the same temperature in both sides of the membranes (electrode side and electrolyte side) and secondly the increase of the electric double layer potential acting as a counter

driving force. While in the hot beaker, the reverse occurs and the ions are released from the electrodes until a new thermal equilibrium is achieved. The system halts and no more electricity is extracted via the external resistor. To restart the cycle, we switch the pairs to the opposite beakers and the process restarts as described. The typical voltage measurement for this process is observed in Figure 6.2.

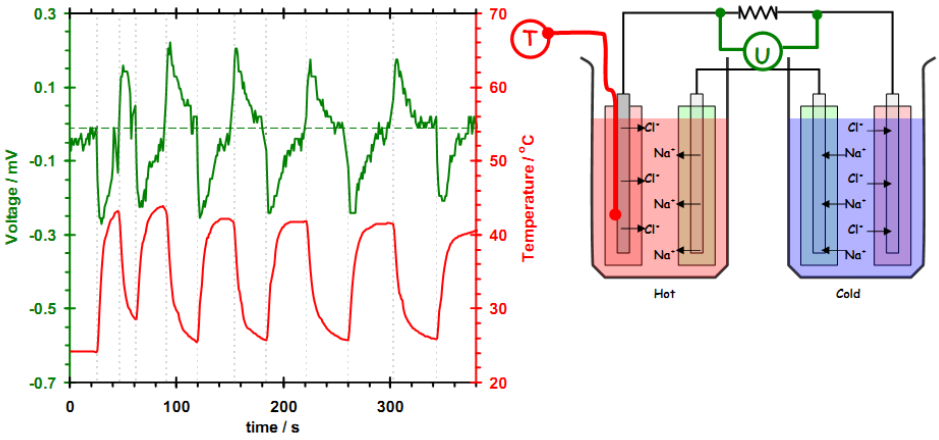

Figure 6.2 Typical voltage behavior (upper) during adsorption/desorption cycles for 30 g/L NaCl solution and temperature (bottom) evolution in the core of the wire.

To demonstrate the proposition of the temperature gradient across the membranes being the driving force for the process, we started by performing experiments without membranes in the setup and no effect was observed. Later we added thermocouples (schematics in Figure 6.2) between the electrode and the membrane to record the temperature evolution over time (Figure 6.2 – red line). We observe that in every time we switch the electrodes to the water body in another temperature, there is an abrupt voltage peak and rapid decrease. The same is seen for the temperature, which rapidly changes and generates the driving force. After sometime, it reaches equilibrium with the temperature of the surrounding electrolyte, causing the driving force to vanish and bringing the process to a halt until the electrodes are switched among the different beakers.

As a second experiment, we looked into the direct relation between amount of energy extracted and temperature difference. For that we chose an electrolyte concentration of 30g/L NaCl, an external circuit of 15Ω and we varied the difference of temperature between both water bodies. We performed several energy extraction cycles in every fixed ΔT. Figure 6.3 shows the reproducible measurements of energy over temperature. The data behavior clearly shows the dependence of energy available to electric work on temperature gradient, while further confirming the assumption of the driving force for the ion adsorption/desorption cycle being indeed the thermomembrane potential created by the temperature profile over the electrodes. Its major role is also evident when varying the electrolyte concentration from 0,05 M to 1,03 M and yet no significant variation in energy extracted for each ΔT was observed.

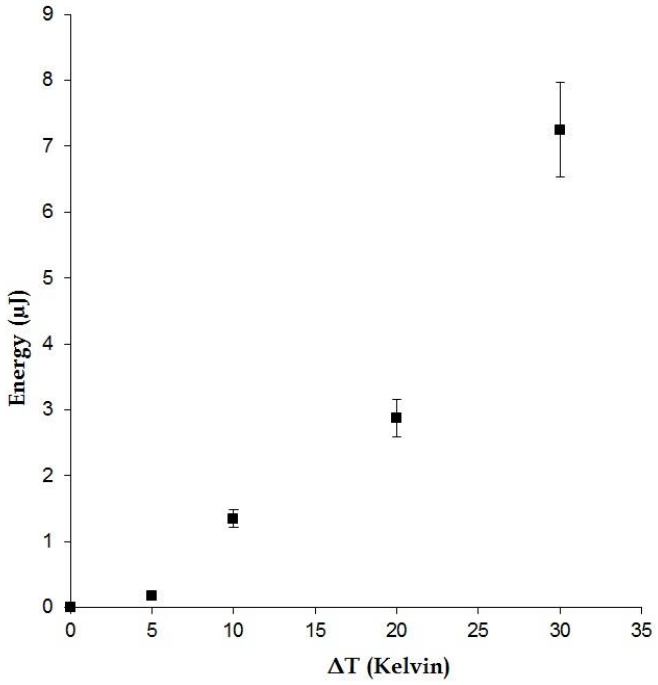

Figure 6.3 Energy extracted (nJ) over the difference of temperature (ΔT) between the water bodies. Experiment set on 30g/L NaCl with an external resistor of 15Ω.

Finally, we investigated the relation between amount of electrode material and charge transferred. Q was calculated by integrating the electric current passing through the external resistor. The intention of this experiment was to demonstrate that the measured electric current was related to the amount of ions adsorbed/desorbed in the capacitive layer of our electrodes. For this we first fully immersed the electrodes in the volumes as previous experiments, and compared to a partial immersion. The results are shown in Table 1. Considering the standard deviation of the experiments, we observe a good agreement between available electrode material and charge during a half cycle. The additional charge present in half immersion can be originated from the solution still present in the bulk of the electrodes or additional water contact with the electrode due to capillary forces.

Table 1 – Measured values for immersion Q when ΔT = 20K and Rext = 6Ω.

Immersion (%)	**Q (μC)**
100	209 ± 12
54	163 ± 20

After this initial investigation, we propose this new construction for an unconventional thermoelectric cell to take advantage of the low temperature waste heat in many factories world wide. The results show the principle behind the use of an affordable capacitive materials combined with traditional ion exchangers to guide ionic migration, quickly converting thermal energy into electricity. The benefits vary from no thermal diffusion due to possibility of using insulated far apart heat baths; adding to regular voltage peaks, in comparison to conventional thermoelectric technology; till affordable and simpler materials for upscale instead of current semiconductors.

A wide variety of possibilities leading to the improvement of this new process could be explored, e.g. the membranes were not optimally selected for this application, the electrolytes play major role in the overall performance and more complex solutions could yield major benefits, etc. The potential for this kind of technology

also extends to natural waters, since oceans have also a temperature gradient between the surface and the bottom of their profile.

Acknowledgments

Thanks are due to Natalia Grzywaczewska, Sebastien Ars, Dhan Prasam Gautam, Fei Liu and Olivier Schaetzle for assistance with the experiments and to Michel Saakes for valuable discussions.

Chapter 7

General Discussion and Perspectives

7.1 Introduction

This thesis introduces the new principle of Capacitive energy extraction using the Donnan Potential (CDP) as driving force. In this chapter we will summarize the results reported in this thesis and discuss the steps for improvement.

The very first results of CDP (Chapter 2) gave the proof-of-concept of using capacitive porous electrodes combined with ion exchange membranes for a direct conversion from salinity differences into electricity. To improve the low average power density in this study, subsequent work aimed at a better understanding of the process to be able to improve process performance.

Initially, we performed an electrochemical characterization (Chapter 3) to identify the contribution of each individual component in overall performance. Here, we found that the use of ion exchange membranes in our setup did not influence the capacitance of the carbon layer. The anion exchange membrane showed a limiting factor during the discharge step in river water.

Next we studied a stack of 8 cells coupled in parallel (Chapter 4) and observed that 83 ± 8 % of the theoretical driving force was achieved during operation. However, very low values of power density (peaks of 55 mW/m^2) were achieved. This led us to look carefully at the hydrodynamics in the apparatus, from which we concluded that optimizing the feed fluid flow and lowering the internal ohmic resistances were the most beneficial paths to improve CDP performance.

Finally, a novel design was tested (Chapter 5) tackling both limitations: fluid flow and internal resistance. A system was built with wire shaped electrodes and we studied the influence of this geometry. Analytical and simulation analysis were performed to confirm the advantages of using wire-shaped constructions. We then show the good agreement between our expected and measured power densities.

In addition to studies of CDP applied to salinity gradients, a novel application was proposed to exploit thermal gradients (Chapter 6). In here we showed the suitability of our capacitive technology to directly convert temperature differences into electricity. This opens a new research field where further studies are needed.

7.2 Energy extraction in CDP

We used power density as the prime metric for system performance, this choice facilitated the comparison with the reported values of other salinity gradient technologies. The power density of the CDP system has increased from an average power of 13 mW/m^2 of surface area to 200 mW/m^2. This improvement is a result of increased insight, better materials choice, design modification and optimized operation. An open question is if CDP still has technical possibilities to increase its power density in a substantial way. In the following we want to discuss the various factors influencing the CDP performance and the road to further improvement.

7.2.1 Materials

The major components of a CDP cell are the porous carbon electrode and ion exchange membranes. We performed a series of preliminary tests with commercially available activated carbons, choosing DLC Super 30 (Norit, Amersfoort, the Netherlands) as our standard. This carbon is consistently used for supercapacitor research and application, with reports found in the literature showing high values (> 100 F/g) of specific capacitance depending on the type and concentration of the electrolyte used. However, in our characterization studies (Chapter 3), the specific capacitance of our electrodes ranges around 4.5 F/g during the adsorption step in artificial sea water (~ 0.5 M of NaCl). Although not relevant for power density, a high capacitance of the system allows longer

adsorption/desorption steps in a full cycle, requiring less electrolyte switching to achieve a certain amount of energy. A further development of carbon material more suitable to Salinity Gradients conditions is needed to achieve higher energy density, approaching this way a more feasible technology.

The other key component, the ion exchange membranes, are directly responsible for the driving force in the system. The membrane permselectivity determines how high and stable the cell potential is, and we show in this thesis to be around 83% of the theoretical maximum. It was also found that the anion exchange membrane is a limiting factor at low current densities, since its lower permselectivity compared to the cation exchange membrane leads to a larger contribution of self discharge. This can be explained by the lower selectivity of AEM compared to CEM and the relative larger contribution of the leakage current in a slow process. Improving either the membrane quality or increasing the current density could improve the overall performance. The membrane quality varies from low electric resistance to durability. In the case of wire electrodes, a robust adherence to the capacitive layer is of great importance to guarantee mechanical and chemical stability, therefore different ideas for better integration of these components are needed. These parameters are still pending fundamental observation on long-term experiments and real-life conditions.

7.2.2 Cell Operation

Besides the cell configuration, the operation of a CDP cell also brings significant optimization routes. The energy extraction cycles can be operated with a constant load like most of the experiments in this thesis, or in an alternative manner with a determined current density (Liu, Schaetzle et al. 2012). The ideas are to galvanostatically charge and discharge the electrodes with a preset constant current, and to expand the energy cycle of the system by “forcing” extra charge beyond the limits of the Donnan potential. By controlling the current rather than the

constant load, we can optimize the charging and discharging rate to achieve the best balance between power density and internal ohmic losses. The cycle duration period can also be maximized to decrease the ratio of electrolyte switching time and complete cycle time. This methodology resulted in the highest average power density reported by a CDP system, 200 mW/m^2, and further improvements are possible by finding the optimal charging and discharging current densities.

In terms of electrolyte accessibility, an option for optimized technique is to step away from the approach of using an stationary system where river and sea water are alternately pumped into it the cell, and operate a mobile system by dipping it intermittently in continuous water streams with different salinity (Burheim, Liu et al. 2012; Porada, Sales et al. 2012).

7.2.3 Internal Energy losses

We categorized these internal energy losses in hydraulic and ohmic based. The hydraulic loss is the energy needed for pumping water between the electrodes, and can be estimated with the volumetric flow rate and the pressure drop across the cell. The use of a spacer between the membranes in a CDP cell increases significantly the pressure drop, therefore an spacerless construction is preferred (Chapter 3). However such an open construction retains also a certain hydraulic resistance determined by the volumetric flow rate and channel dimensions (length, width and thickness).. The straightforward solution to minimize this loss would be to increase the distance between the electrodes but that would imply a substantial increase in ohmic losses due to higher resistivity.

The internal ohmic losses are divided in: (i) the electric resistance of each individual component in a CDP cell (current collector, porous carbon and membrane); (ii) contact resistance, between the interfaces of the different components; (iii) the electrolyte resistance contribution, proportional to the distance

between the electrodes; and (iv) concentration polarization, increase of concentration in the retained solution on the surface of the membranes. As initial step, we used cell components with low electric resistance in separate layers: a metallic current collector (TiPt), carbon electrodes with low ratio (10%) of nonconductive binder, and selected commercial membranes. Then we utilized an integration of the layers to minimize the contact resistance (Chapter 5), which meant the carbon electrode being casted directly on the top of the current collector, followed by the application of an ion selective solution over the carbon layer, acting as a thin ion exchange membrane. Then to further minimize these ohmic losses, we identified the major contributor as being the electrolyte resistance, therefore a cell design modification was proposed as solution.

7.3 Cell Design

Wire shaped electrodes were suggested as a route to decrease the cell internal resistance (Chapter 5). The electrical resistance between electrodes is dependent on their geometry. After analytical evaluation, and numerical calculations, we were convinced that a cylindrical construction can reach a lower internal resistance than the traditional flat plate supercapacitors. The experimental results fitted nicely to the expected theoretical behavior of the resistance when the electrodes are in the immediate vicinity of each other. This geometry also causes a faster Donnan potential response when the electrodes change solution. (Burheim 2012). These results showed for the first time the possibility of achieving the minimum electrolyte resistance possible when the electrodes are touched (Fig 7.1). Theoretically, ideal ion exchange membranes would shield the system from a short-circuit since they are electrically non-conductive, but due to our current irregular application method of an ion exchange layer around our wires, this scenario could not be tested yet. We also preferred to report our power densities per weight of activated carbon, since the precise surface area of the membranes was difficult to estimate. The

maximum average value obtained was 350 μW/g, an order of magnitude higher compared to the 41 μW/g obtained in Chapter 2.

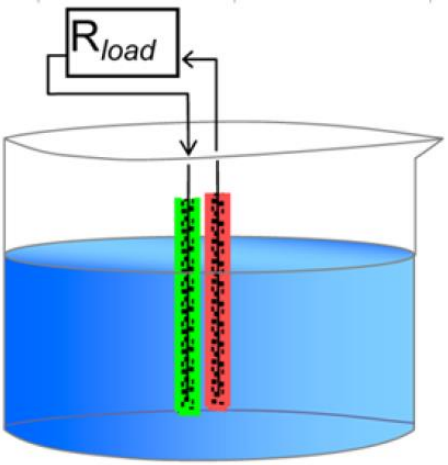

Figure 7.1 Schematics of wires electrodes dipped in a water reservoir

In this system we also applied for the first time the idea of displacing the electrodes instead of water bodies (Fig 7.1). A possible operation for this technique would make use of a carrousel of wire electrodes that alternately is immersed in reservoirs where river and sea water are constantly flowing or batch wise replaced. Further research to evaluate the association of wires in parallel and in series is necessary to choose the path for system upscale.

7.4 Alternative application

Even though the salinity difference between river and sea waters was the initial goal for the CDP technology, alternative applications are feasible and also desired. For example, the capacitance and energy density of our system is strongly dependent on the type and concentration of the electrolytes. An alternative application was studied in this thesis (Chapter 6). The suggestion was to use a CDP system to exploit temperature differences between electrolytes with the same

concentration. The driving force in this case is the thermal membrane potential, present when a membrane is exposed to a difference of temperature between its interfaces. The initial proof-of-principle was introduced, but further investigations are required for improved electricity generation. The absolute value of the thermal membrane potential is known to decrease with the increase of electrolyte concentration. This suggests a good suitability of this technique for solutions with concentrations lower than 1 M, e.g. natural river and sea water concentrations vary from 0.02 M (river) and 0.5 M (sea).

7.6 Final remarks

This chapter summarized the principle, characterization and initial developments of CDP since 2009. With the identification of the key factors for CDP performance, we proposed routes leading to one order of magnitude improvement and room for further substantial gains. Additional focus in the improvement of power generation, material integration and component durability will make CDP achieve better results and make it a key competitor for energy extraction from naturally occurring gradients. For this purpose, an increase of one order of magnitude in power density, making it in the range of units of W/m^2 is required. A good understanding and enhanced performance were reached with artificial solutions in the lab, but limited knowledge remains over the interaction between the system and more complex electrolytes, i.e. real sea and river water, therefore the next steps should be in the direction of long-term experiments in real world conditions. The current restricting factors continue to be the internal resistance, storage capacities in the capacitive layer and appropriate design for up-scaling, but alternative applications seem to be also a positive route to hinder these limitations.

References

Achilli, A., T. Y. Cath, et al. (2009). "Power generation with pressure retarded osmosis: An experimental and theoretical investigation." Journal of Membrane Science **343**(1-2): 42-52.

Achilli, A. and A. E. Childress (2010). "Pressure retarded osmosis: From the vision of Sidney Loeb to the first prototype installation—Review." Desalination **261**(3): 205-211.

Bazant, M. Z., K. Thornton, et al. (2004). "Diffuse-charge dynamics in electrochemical systems." Physical Review E **70**(2): 021506.

Bell, L. E. (2008). "Cooling, Heating, Generating Power, and Recovering Waste Heat with Thermoelectric Systems." Science **321**(5895): 1457-1461.

Biesheuvel, P. M. (2004). "Electrostatic free energy of interacting ionizable double layers." Journal of Colloid and Interface Science **275**(2): 514-522.

Biesheuvel, P. M. and M. Z. Bazant (2010). "Nonlinear dynamics of capacitive charging and desalination by porous electrodes." Physical Review E **81**(3): 031502.

Biesheuvel, P. M. and A. van der Wal (2010). "Membrane capacitive deionization." Journal of membrane science **346**(2): 256-262.

Bijmans, M. F. M., O. S. Burheim, et al. (2012). "CAPMIX -Deploying Capacitors for Salt Gradient Power Extraction." Energy Procedia **20**(0): 108-115.

Birol, F. (2013). "Europe's energy crossroads is dangerously close." Europe's world: the only Europe-wide policy journal(23): 104-107.

Björnbom, P. (2007). "Charge/discharge of an electrochemical supercapacitor electrode pore; non-uniqueness of mathematical models." Electrochemistry Communications **9**(2): 211-215.

Bonetti, M., S. Nakamae, et al. (2011). "Huge Seebeck coefficients in nonaqueous electrolytes." The Journal of Chemical Physics **134**(11): 114513-114518.

Boon, N. and R. van Roij (2011). "'Blue energy' from ion adsorption and electrode charging in sea and river water." Molecular Physics **109**(7-10): 1229-1241.

Box, G. E., W. G. Hunter, et al. (1978). "Statistics for experimenters: an introduction to design, data analysis, and model building."

Brogioli, D. (2009). "Extracting Renewable Energy from a Salinity Difference Using a Capacitor." Physical Review Letters **103**(5): 058501-058504.

Brogioli, D., R. Zhao, et al. (2011). "A prototype cell for extracting energy from a water salinity difference by means of double layer expansion in nanoporous carbon electrodes." Energy & Environmental Science **4**(3): 772-777.

Burheim, O. S., F. Liu, et al. (2012). "Faster Time Response by the Use of Wire Electrodes in Capacitive Salinity Gradient Energy Systems." The Journal of Physical Chemistry C **116**(36): 19203-19210.

Burheim, O. S., F. Seland, et al. (2012). "Improved electrode systems for reverse electro-dialysis and electro-dialysis." Desalination **285**(0): 147-152.

Campbell, C. (2002). "Petroleum and People." Population and Environment **24**(2): 193-207.
Chen, M., H. Lund, et al. (2010). "Energy efficiency analysis and impact evaluation of the application of thermoelectric power cycle to today's CHP systems." Applied Energy **87**(4): 1231-1238.
Chmiola, J., G. Yushin, et al. (2006). "Anomalous Increase in Carbon Capacitance at Pore Sizes Less Than 1 Nanometer." Science **313**(5794): 1760-1763.
Choi, J.-Y. and J.-H. Choi (2010). "A carbon electrode fabricated using a poly(vinylidene fluoride) binder controlled the Faradaic reaction of carbon powder." Journal of Industrial and Engineering Chemistry **16**(3): 401-405.
Conway, B. (1999). Electrochemical supercapacitors: scientific fundamentals and technological applications (POD), Kluwer Academic/Plenum: New York.
Crispin, D. X. (2012). "Towards Polymer-based Organic Thermoelectric Generators." Energy & Environmental Science.
Demarconnay, L., E. Raymundo-Piñero, et al. (2011). "Adjustment of electrodes potential window in an asymmetric carbon/MnO2 supercapacitor." Journal of Power Sources **196**(1): 580-586.
Demirkaya, G., S. Besarati, et al. (2012). "Multi-objective optimization of a combined power and cooling cycle for low-grade and midgrade heat sources." ASME J Energ Resour Tech **134**: 032002.
Dincer, I. (2000). "Renewable energy and sustainable development: a crucial review." Renewable and Sustainable Energy Reviews **4**(2): 157-175.
Długołęcki, P., A. Gambier, et al. (2009). "Practical Potential of Reverse Electrodialysis As Process for Sustainable Energy Generation." Environmental Science & Technology **43**(17): 6888-6894.
Dlugolecki, P., K. Nymeijer, et al. (2008). "Current status of ion exchange membranes for power generation from salinity gradients." Journal of Membrane Science **319**(1-2): 214-222.
Donnan, F. G. (1911). "Theorie der Membrangleichgewichte und Membranpotentiale bei Vorhandensein von nicht dialysierenden Elektrolyten. Ein Beitrag zur physikalisch-chemischen Physiologie." Zeitschrift für Elektrochemie und angewandte physikalische Chemie **17**(14): 572-581.
Frackowiak, E., S. Delpeux, et al. (2002). "Enhanced capacitance of carbon nanotubes through chemical activation." Chemical Physics Letters **361**(1-2): 35-41.
Fronk, B. M., R. Neal, et al. (2010). "Evolution of the transition to a world driven by renewable energy." J Energy Res Technol **132**(2): 21009-21015.
Gerstandt, K., K. V. Peinemann, et al. (2008). "Membrane processes in energy supply for an osmotic power plant." Desalination **224**(1-3): 64-70.
Grahame, D. C. (1947). "The Electrical Double Layer and the Theory of Electrocapillarity." Chemical Reviews **41**(3): 441-501.
Gross, R., M. Leach, et al. (2003). "Progress in renewable energy." Environment International **29**(1): 105-122.

Guo, W., L. Cao, et al. (2010). "Energy Harvesting with Single-Ion-Selective Nanopores: A Concentration-Gradient-Driven Nanofluidic Power Source." Advanced Functional Materials **20**(8): 1339-1344.

Hamann, C. H., A. Hamnett, et al. (1998). Electrochemistry. 1998, Wiley-VCH.

Hanaoka, K., R. Kiyono, et al. (1993). "Thermal membrane potential across anion-exchange membranes in KCl and KIO< sub> 3</sub> solutions and the transported entropy of ions." Journal of membrane science **82**(3): 255-263.

Hayes, R. and S. Kolaczkowski (1994). "Mass and heat transfer effects in catalytic monolith reactors." Chemical Engineering Science **49**(21): 3587-3599.

Himelic, J. B. and F. Kreith (2011). "Potential Benefits of Plug-In Hybrid Electric Vehicles for Consumers and Electric Power Utilities." Journal of Energy Resources Technology **133**(3).

Hoffert, M. I., K. Caldeira, et al. (2002). "Advanced Technology Paths to Global Climate Stability: Energy for a Greenhouse Planet." Science **298**(5595): 981-987.

Huys, Q. J. M., N. Eshel, et al. (2012). "Bonsai Trees in Your Head: How the Pavlovian System Sculpts Goal-Directed Choices by Pruning Decision Trees." PLoS Comput Biol **8**(3): e1002410.

Ikeda, T. (1958). "Thermal Membrane Potential." The Journal of Chemical Physics **28**(1): 166-167.

Isaacs, J. D. and W. R. Schmitt (1980). "Ocean Energy: Forms and Prospects." Science **207**(4428): 265-273.

Jiang, Z. and D. Stein (2010). "Electrofluidic Gating of a Chemically Reactive Surface." Langmuir **26**(11): 8161-8173.

Jones, A. T., W. Finley, et al. (2003). Recent development in salinity gradient power. Oceans 2003. Proceedings.

Jones, A. T. and W. Rowley (2002). "Global Perspective: Economic Forecast for Renewable Ocean Energy Technologies." Marine Technology Society Journal **36**: 85-90.

Kamat, P. V. (2007). "Meeting the Clean Energy Demand: Nanostructure Architectures for Solar Energy Conversion." The Journal of Physical Chemistry C **111**(7): 2834-2860.

Kerwick, M. I., S. M. Reddy, et al. (2005). "Electrochemical disinfection, an environmentally acceptable method of drinking water disinfection?" Electrochimica Acta **50**(25–26): 5270-5277.

Khazaee, I. (2012). "Experimental Investigation of Irreversibility of a Proton Exchange Membrane Fuel Cell." Journal of Energy Resources Technology **134**(2).

Khomenko, V., E. Raymundo-Piñero, et al. (2010). "A new type of high energy asymmetric capacitor with nanoporous carbon electrodes in aqueous electrolyte." Journal of Power Sources **195**(13): 4234-4241.

Kim, J.-S. and J.-H. Choi (2010). "Fabrication and characterization of a carbon electrode coated with cation-exchange polymer for the membrane capacitive deionization applications." Journal of membrane science **355**(1-2): 85-90.

Kjelstrup, S. and D. Bedeaux (2008). Non-equilibrium thermodynamics of heterogeneous systems, World Scientific Singapore.
Kostevšek, A., L. Cizelj, et al. (2013). "A novel concept for a renewable network within municipal energy systems." Renewable Energy **60**(0): 79-87.
Kotas, T. J. (2012). The exergy method of thermal plant analysis, Exergon Publishing Company.
La Mantia, F., M. Pasta, et al. (2011). "Batteries for Efficient Energy Extraction from a Water Salinity Difference." Nano Letters **11**(4): 1810-1813.
Lacey, R. E. (1980). "Energy by reverse electrodialysis." Ocean Engineering **7**(1): 1-47.
Lee, S. and M. Elimelech (2007). "Salt cleaning of organic-fouled reverse osmosis membranes." Water Research **41**(5): 1134-1142.
Levenspiel, O. and N. d. Nevers (1974). "The Osmotic Pump." Science **183**(4121): 157-160.
Levi, M. D., G. Salitra, et al. (2009). "Application of a quartz-crystal microbalance to measure ionic fluxes in microporous carbons for energy storage." Nat Mater **8**(11): 872-875.
Liu, F., O. Schaetzle, et al. (2012). "Effect of additional charging and current density on the performance of Capacitive energy extraction based on Donnan Potential." Energy & Environmental Science **5**(9): 8642-8650.
Loeb, S. and R. S. Norman (1975). "Osmotic Power Plants." Science **189**(4203): 654-655.
Logan, B. E. and M. Elimelech (2012). "Membrane-based processes for sustainable power generation using water." Nature **488**(7411): 313-319.
Mann, M. E., R. S. Bradley, et al. (1998). "Global-scale temperature patterns and climate forcing over the past six centuries." Nature **392**(6678): 779-787.
Margarone, M., S. Magi, et al. (2011). "Revamping, Energy Efficiency, and Exergy Analysis of an Existing Upstream Gas Treatment Facility." Journal of Energy Resources Technology **133**(1).
Mi, B. and M. Elimelech (2010). "Organic fouling of forward osmosis membranes: Fouling reversibility and cleaning without chemical reagents." Journal of membrane science **348**(1-2): 337-345.
Myers, N. and J. Kent (2003). "New consumers: The influence of affluence on the environment." Proceedings of the National Academy of Sciences **100**(8): 4963-4968.
Newman, J. and K. E. Thomas-Alyea (2012). Electrochemical systems, John Wiley & Sons.
Nijmeijer, K. and S. Metz (2010). Chapter 5 Salinity Gradient Energy. Sustainability Science and Engineering. C. E. Isabel and I. S. Andrea, Elsevier. **Volume 2:** 95-139.
Norman, R. S. (1974). "Water Salination: A Source of Energy." Science **186**(4161): 350-352.
Pattle, R. E. (1954). "Production of Electric Power by mixing Fresh and Salt Water in the Hydroelectric Pile." Nature **174**(4431): 660-660.

Piazza, R. (2008). "Thermophoresis: moving particles with thermal gradients." Soft Matter **4**(9): 1740-1744.
Pivonka, P., D. Smith, et al. (2007). "Investigation of Donnan equilibrium in charged porous materials—a scale transition analysis." Transport in Porous Media **69**(2): 215-237.
Porada, S., B. B. Sales, et al. (2012). "Water Desalination with Wires." The Journal of Physical Chemistry Letters **3**(12): 1613-1618.
Porada, S., L. Weinstein, et al. (2012). "Water Desalination Using Capacitive Deionization with Microporous Carbon Electrodes." ACS Applied Materials & Interfaces.
Post, J., C. Goeting, et al. (2010). "Towards implementation of reverse electrodialysis for power generation from salinity gradients." Desalination and Water Treatment **16**(1-3): 182-193.
Post, J. W., H. V. M. Hamelers, et al. (2008). "Energy Recovery from Controlled Mixing Salt and Fresh Water with a Reverse Electrodialysis System." Environmental Science & Technology **42**(15): 5785-5790.
Post, J. W., J. Veerman, et al. (2007). "Salinity-gradient power: Evaluation of pressure-retarded osmosis and reverse electrodialysis." Journal of Membrane Science **288**(1-2): 218-230.
Ramon, G. Z., B. J. Feinberg, et al. (2011). "Membrane-based production of salinity-gradient power." Energy & Environmental Science **4**(11).
Ratkje, S., T. Holt, et al. (1986). "Effect of biofilm formation on salinity power plant output on laboratory scale." Industrial membrane processes, AIChE.
Rica, R. l. A., D. Brogioli, et al. (2012). "Ions transport and adsorption mechanisms in porous electrodes during capacitive-mixing double layer expansion (CDLE)." The Journal of Physical Chemistry C **116**(32): 16934-16938.
Ricketts, B. W. and C. Ton-That (2000). "Self-discharge of carbon-based supercapacitors with organic electrolytes." Journal of Power Sources **89**(1): 64-69.
Sales, B. B., O. S. Burheim, et al. (2012). "Impact of Wire Geometry in Energy Extraction from Salinity Differences Using Capacitive Technology." Environmental Science & Technology **46**(21): 12203-12208.
Sales, B. B., M. Saakes, et al. (2010). "Direct Power Production from a Water Salinity Difference in a Membrane-Modified Supercapacitor Flow Cell." Environmental Science & Technology **44**(14): 5661-5665.
Samson, E., J. Marchand, et al. (2003). "Calculation of ionic diffusion coefficients on the basis of migration test results." Materials and Structures **36**(3): 156-165.
Sarkar, S., A. K. SenGupta, et al. (2010). "The Donnan Membrane Principle: Opportunities for Sustainable Engineered Processes and Materials." Environmental Science & Technology **44**(4): 1161-1166.
Simon, P. and Y. Gogotsi (2008). "Materials for electrochemical capacitors." Nat Mater **7**(11): 845-854.
Simon, P. and Y. Gogotsi (2010). "Charge storage mechanism in nanoporous carbons and its consequence for electrical double layer capacitors."

Philosophical Transactions of the Royal Society A: Mathematical, Physical and Engineering Sciences **368**(1923): 3457-3467.

Sootsman, J. R., D. Y. Chung, et al. (2009). "New and Old Concepts in Thermoelectric Materials." Angewandte Chemie International Edition **48**(46): 8616-8639.

Sorgun, M., M. E. Ozbayoglu, et al. (2010). "Modeling and Experimental Study of Newtonian Fluid Flow in Annulus." Journal of Energy Resources Technology **132**: 033102.

Stoller, M. D., S. Park, et al. (2008). "Graphene-Based Ultracapacitors." Nano Letters **8**(10): 3498-3502.

Stoller, M. D. and R. S. Ruoff (2010). "Best practice methods for determining an electrode material's performance for ultracapacitors." Energy & Environmental Science **3**(9): 1294-1301.

Tasaka, M., K. Hanaoka, et al. (1975). "Thermal membrane potential through charged membranes in electrolyte solutions." Biophysical Chemistry **3**(4): 331-337.

Thorsen, T. and T. Holt (2009). "The potential for power production from salinity gradients by pressure retarded osmosis." Journal of Membrane Science **335**(1-2): 103-110.

Tipler, P. A. and G. Mosca (2007). Physics for scientists and engineers, Macmillan.

Turner, J. A. (1999). "A Realizable Renewable Energy Future." Science **285**(5428): 687-689.

Vanýsek, P. (1997). "Impact of electrode geometry, depth of immersion, and size on impedance measurements." Canadian Journal of Chemistry **75**(11): 1635-1642.

Veerman, J., J. W. Post, et al. (2008). "Reducing power losses caused by ionic shortcut currents in reverse electrodialysis stacks by a validated model." Journal of Membrane Science **310**(1-2): 418-430.

Veerman, J., M. Saakes, et al. (2010). "Reverse electrodialysis: evaluation of suitable electrode systems." Journal of Applied Electrochemistry **40**(8): 1461-1474.

Veerman, J., M. Saakes, et al. (2011). "Reverse electrodialysis: A validated process model for design and optimization." Chemical Engineering Journal **166**(1): 256-268.

Veerman, J., M. Saakes, et al. (2009). "Reverse electrodialysis: Performance of a stack with 50 cells on the mixing of sea and river water." Journal of Membrane Science **327**(1-2): 136-144.

Veerman, J., M. Saakes, et al. (2010). "Electrical Power from Sea and River Water by Reverse Electrodialysis: A First Step from the Laboratory to a Real Power Plant." Environmental Science & Technology **44**(23): 9207-9212.

Vellini, M. and J. Tonziello (2010). "Hydrogen use in an urban district: energy and environmental comparisons." Journal of Energy Resources Technology **132**(4).

Vermaas, D. A., M. Saakes, et al. (2011). "Doubled Power Density from Salinity Gradients at Reduced Intermembrane Distance." Environmental Science & Technology **45**(16): 7089-7095.

Vermaas, D. A., M. Saakes, et al. (2011). "Power generation using profiled membranes in reverse electrodialysis." Journal of membrane science **385–386**(0): 234-242.

Vigolo, D., S. Buzzaccaro, et al. (2010). "Thermophoresis and Thermoelectricity in Surfactant Solutions." Langmuir **26**(11): 7792-7801.

Vigolo, D., R. Rusconi, et al. (2010). "Thermophoresis: microfluidics characterization and separation." Soft Matter **6**(15): 3489-3493.

Vining, C. B. (2009). "An inconvenient truth about thermoelectrics." Nat Mater **8**(2): 83-85.

Weinstein, J. N. and F. B. Leitz (1976). "Electric Power from Differences in Salinity: The Dialytic Battery." Science **191**(4227): 557-559.

White, F. Fluid mechanics, 1986, McGraw-Hill, New York.

Wick, G. L. and J. D. Isaacs (1978). "Salt Domes: Is There More Energy Available from Their Salt than from Their Oil?" Science **199**(4336): 1436-1437.

Wick, G. L. and W. R. Schmitt (1977). "Prospects For Renewable Energy from the Sea." Marine Technology Society Journal **11**(5-6): 16-21.

Wongsuwarn, S., D. Vigolo, et al. (2012). "Giant thermophoresis of poly(N-isopropylacrylamide) microgel particles." Soft Matter **8**(21): 5857-5863.

Yee, S. K., J. A. Malen, et al. (2011). "Thermoelectricity in Fullerene–Metal Heterojunctions." Nano Letters **11**(10): 4089-4094.

Zhao, R., P. M. Biesheuvel, et al. (2009). "Charge Efficiency: A Functional Tool to Probe the Double-Layer Structure Inside of Porous Electrodes and Application in the Modeling of Capacitive Deionization." The Journal of Physical Chemistry Letters **1**(1): 205-210.

Summary

This thesis introduces the principle of Capacitive energy extraction based on Donnan Potential (CDP) to exploit salinity gradients. It also shows the fundamental characterization and improvements of CDP. An alternative application of this technology aimed at thermal gradients was tested.

Chapter 2 introduces the principle and initial tests. The entropy increase of mixing two solutions of different salt concentrations can be harnessed to generate electrical energy. Worldwide, the potential of this resource, the controlled mixing of river and seawater, is enormous, but existing conversion technologies are still complex and expensive. Here we present a small-scale device that directly generates electrical power from the sequential flow of fresh and saline water, without the need of auxiliary processes or converters. The device consists of a sandwich of porous “supercapacitor” electrodes, ion-exchange membranes, and a spacer and can be further miniaturized or scaled-out. Our results demonstrate that alternating the flow of saline and fresh water through a capacitive cell allows direct autogeneration of voltage and current and consequently leads to power generation. Theoretical calculations aid in providing directions for further optimization of the properties of membranes and electrodes.

In **Chapter 3**, traditional electrochemical techniques (galvanostatic charge–discharge and cyclic voltammetry) were used to investigate intrinsic properties of this open system. This study demonstrates the feasibility to characterize the capacitive behavior of the cell in low concentration (0.5 M). Presence of membranes, as well as the possibility of having the electrolyte flowing through the cell was investigated. In the studied cell, the presence of membranes showed a limitation by the anion exchange membrane at low current densities but no effect at high current densities. The flow rate did not influence the capacitance of the system either.

Chapter 4 uses again a stack of eight cells coupled in parallel to investigate the viability of this technology. An average power density of 0.055W/m^2 was obtained during the peak of the different cycles, though reasonable optimization suggests an expectation of 0.26W/m^2 at 6.2 A/m^2. It was found that 83 ± 8% of the theoretical driving potential was obtained during the operating process. By studying the polarization curves during charging and discharging cycles, it was found that optimizing the feed fluid flow is currently among the most beneficial paths to make CDP a viable salinity difference power source. Another parallel route for increasing the efficiency is lowering the internal ohmic resistances of the cell by design modifications.

A modification is proposed in **Chapter 5**, approaching the electrodes geometry that has a relevant impact on internal resistance and overall performance in CDP. In this work, we present the first effort to use wire-shaped electrodes and its suitability for improving CDP. Analytical evaluation and electrical measurements confirm a strong nonlinear decrease in internal resistance for distances between electrodes smaller than 3 mm. We also demonstrate that we get more power per material invested when compared to traditional flat plate designs. These findings show the advantages of this design for further development of CDP into a mature technology.

Alternatively, in **Chapter 6**, we present a new principle for producing electricity from low temperature differences by using an affordable assembly combining ion exchange membranes and supercapacitor carbon electrodes. Our proposed design involves two isolated salty solutions, with equal concentration but different temperatures. The operation consists of an alternately and cyclic exposure of the electrodes to these electrolytes. This difference in temperature generates a thermomembrane potential that acts as a driving force for ionic adsorption/desorption cycles on the electrodes. Our simple system is interesting for exploiting the potential of low temperature waste heat. When two volumes with

equal concentration have different temperatures, it is possible to immerse a pair of electrodes (anode and cathode) into the low temperature one and have ion adsorption. An electric current is then generated in the external circuit to achieve electro neutrality. After saturation, the same electrodes are immersed in the high T volume and then ions desorb from the electrodes and are released to the volume, leading to a reverse electric current in the external circuit compared to the first step. These experiments prove the principle and the direct dependence of the temperature gradient for energy extraction.

Finally, **Chapter 7** discusses the internal energy losses identified and faced throughout this thesis. We summarize the solutions encountered for the major contributions hindering the CDP performance and give suggestions to further develop the technology.

Samenvatting

Dit proefschrift introduceert het principe van Capacitieve energie-extractie gebaseerd op Donnan Potential (CDP) voor de exploitatie van zoutgradiënten. Daarnaast wordt ook de fundamentele karakterisatie en verbeteringen van CDP besproken. Tevens is een alternatieve toepassing onderzocht, gericht op thermische gradiënten..

Hoofdstuk 2 introduceert het principe en het beginnende onderzoek. De toename in entropie van het mengen van twee oplossingen van verschillende zoutconcentraties kan worden benut om elektrische energie op te wekken. De wereldwijde potentiaal van de gecontroleerde menging van rivier -en zeewater is enorm, maar de bestaande technologie voor de omzetting is nog steeds complex en duur. Hier presenteren we een kleinschalig apparaat dat rechtstreeks elektrische stroom van de opeenvolgende stroom van zoet en zout water genereert, zonder de noodzaak van ondersteunende processen of omzetters. Het apparaat bestaat uit lagen van poreuze "supercondensator" elektroden, ionuitwisselingsmembranen, en een spacer, en kan verder worden verkleind of opgeschaald. Onze resultaten tonen aan dat het afwisselend toevoeren van zout en zoet water door een capacitieve cel direct resulteert in een opwekking van spanning en stroom en dus tot opwekking van elektriciteit. Theoretische berekeningen dragen bij aan verdere optimalisatie van de eigenschappen van de membranen en elektroden.

In **hoofdstuk 3** worden traditionele elektrochemische technieken (galvanostatische lading-ontlading en cyclische voltammetrie) gebruikt om de intrinsieke eigenschappen van dit open systeem te onderzoeken. Deze studie toont aan dat het karakteriseren van het capacitieve gedrag van de cel in lage concentratie (0,5 M) haalbaar is. Zowel de aanwezigheid van membranen als de mogelijkheid om het elektrolyt door de cel te later stromen werd onderzocht. De aanwezigheid van

membranen in de bestudeerde cel zorgde voor een limitatie veroorzaakt door het anion-uitwisselingsmembraan bij lage stroomdichtheden. Er was echter geen effect geconstateerd bij hoge stroomdichtheden. De vloeistof stroomsnelheid had geen invloed op de capaciteit van het system.

Hoofdstuk 4 wordt wederom een stapel van acht cellen parallel gekoppeld om de uitvoerbaarheid van deze technologie te onderzoeken. Bij de piek van de verschillende cycli werd een gemiddelde vermogensdichtheid van 0.055 W/m2 verkregen. Berekeningen laten zien dat bij experimentele optimalisatie 0.26 W/m2 bij 6.2 A/m2 behaald kan worden. Het bleek dat 83 ± 8 % van theoretisch kracht werd verkregen tijdens het proces. Door het bestuderen van de polarisatie curves tijdens laad- en ontlaadcycli werd vastgesteld dat de optimalisatie van de toevoer van de vloeistofstroom momenteel het meest gunstige pad is om CDP technisch haalbaar te maken als stroombron door een verschil in zoutgehalte. Een andere parallelle route voor het verhogen van de efficiëntie is het verlagen van de interne ohmse weerstanden van de cel door wijzigingen in het ontwerp.

In **hoofdstuk 5**, wordt er een wijziging voorgesteld van de elektroden geometrie. Dit heeft een relevante invloed op de interne weerstand en de algemene prestaties in CDP. In dit werk presenteren we de eerste poging om een draadvormige electrode te gebruiken voor het verbeteren van CDP. Analytische evaluatie en elektrische metingen bevestigen een sterke lineaire afname in interne weerstand voor een afstand kleiner dan 3 mm tussen de elektroden. We toonden ook aan dat we meer vermogen genereren per materiaal volume in vergelijking met traditionele vlakke plaat ontwerpen. Deze bevindingen tonen de voordelen van dit ontwerp voor de verdere ontwikkeling van CDP richting een volwassen technologie.

Als alternatief presenteren we in **hoofdstuk 6** een nieuw principe voor de productie van elektriciteit uit kleine temperatuurverschillen door middel van een betaalbare constructie die ionwisselingsmembranen en supercondensator koolstof elektroden

combineert. Ons voorgestelde ontwerp bestaat uit twee geïsoleerde zoutoplossingen, met gelijke concentratie maar verschillende temperatuur. De werking bestaat uit een afwisselende en cyclische blootstelling van de elektroden aan deze elektrolyten. Dit verschil in temperatuur genereert een thermomembraan potentiaal dat fungeert als een drijvende kracht voor ionische adsorptie / desorptie cycli van de elektroden. Ons eenvoudige systeem is interessant voor het benutten van het potentieel van laag-calorische restwarmte. Wanneer twee volumes met dezelfde concentratie verschillende temperatuur hebben en een paar elektroden (anode en kathode) in de lage T oplossing wordt gedompeld vindt ion adsorptie plaats. Hierdoor wordt een elektrische stroom opgewekt in het externe circuit om elektro-neutraliteit te bereiken. Na verzadiging worden dezelfde elektroden ondergedompeld in de hoge T oplossing en vervolgens desorberen ionen van de elektroden. Deze ionen worden vrijgegeven in de oplossing, waardoor een omgekeerde elektrische stroom in het externe circuit ontstaat ten opzichte van de eerste stap. Deze experimenten bewijzen het principe, en de directe relatie, van de temperatuurgradiënt voor energiewinning.

Tenslotte worden in **Hoofdstuk 7** de interne energieverliezen besproken die geïdentificeerd en beschreven zijn in dit proefschrift. We vatten de oplossingen voor de belangrijke belemmeringen in de prestatie van CDP samen en geven suggesties voor de verdere ontwikkeling van de technologie.

Acknowledgements

I find writing my gratitude to everybody involved in this thesis simply ineffable. All my efforts to finish my PhD were immeasurably amplified by far too many individuals to list. I stare at all the memories of the last years and I disastrously fail to tame a gale of myriad feelings. Family, friends, colleagues and acquaintances gave paramount alms to my otherwise meager journey. Muito obrigado!

Rita, mano pupuluka, myliu tave labiau už viską pasaulyje, nes tu esi priežastis, dėl kurios aš gyvenu!

About the author

Bruno Bastos Sales was born in Fortaleza, Brazil. There he lived till graduating with a B.Sc. in Physics at the Federal University of Ceara. He subsequently moved to Recife, Brazil to pursue a M.Sc. in Energetic and Nuclear Technologies at the Federal University of Pernambuco. His interest in sustainability led to his move to Leeuwarden, the Netherlands, where he worked on the topic of Blue Energy: Renewable Energy from Mixing River and Sea water as his PhD project at Wetsus and Wageningen University.

Netherlands Research School for the
Socio-Economic and Natural Sciences of the Environment

C E R T I F I C A T E

The Netherlands Research School for the
Socio-Economic and Natural Sciences of the Environment
(SENSE), declares that

Bruno Bastos Sales

born on 21 October 1981 in Fortaleza, Brazil

has successfully fulfilled all requirements of the
Educational Programme of SENSE.

Leeuwarden, 1 November 2013

the Chairman of the SENSE board	the SENSE Director of Education
Prof. dr. Rik Leemans	Dr. Ad van Dommelen

The SENSE Research School has been accredited by the Royal Netherlands Academy of Arts and Sciences (KNAW)

KONINKLIJKE NEDERLANDSE
AKADEMIE VAN WETENSCHAPPEN

The SENSE Research School declares that **Mr. Bruno Bastos Sales** has successfully fulfilled all requirements of the Educational PhD Programme of SENSE with a work load of 56 ECTS, including the following activities:

SENSE PhD Courses

- Environmental Research in Context
- Research Context Activity: Chair of SENSE PhD Council and Co-organizing scientific programme of Wetsus Water Challenge 2009, 1-5 May 2009, Leeuwarden

Other PhD Courses

- Mathematical Models in Ecology and Evolution
- Hunger defeated? Long-term dynamics of global food security
- Bath Electrochemistry Winter School
- International Workshop on Salinity Gradient Energy
- Scientific publishing: introductory workshop for PhD students
- Career Orientation

Management and Didactic Skills Training

- Membership of the WIMEK PhD Council
- Supervision of three MSc Theses and three Research Internships

Oral Presentations

- *Blue Energy: Sustainable Power Production from Salinity Gradients* . 2nd International Symposium on Enhanced Electrochemical Capacitors (ISEEC2011), 12-16 June 2011, Poznan, Poland
- *Cylindrical Design Suitability for CAPMIX.* International Workshop on Salinity Gradient Energy, 4-6 September 2012, Milan, Italy
- *Materials Suitability for Capacitive Mixing (CAPMIX).* 9th European Congress of Chemical Engineering , 21-25 April 2013, The Hague, the Netherlands
- *Capacitive Technologies applied to Energy Extraction and Water Treatment.* 3rd International Symposium on Enhanced Electrochemical Capacitors (ISEEC2013), 3-7 June 2013, Taormina, Italy
- *Ion Exchange Membranes preparation for Energy Extraction via CAPMIX.* Engineering with Membranes Towards a Sustainable Future, 3-7 September 2013, Saint-Pierre d'Oleron, France

SENSE Coordinator PhD Education

Drs. Serge Stalpers

This work was performed in the TTIW-cooperation framework of Wetsus, Centre of Excellence for Sustainable Water Technology (www.wetsus.nl). Wetsus is funded by the Dutch Ministry of Economic Affairs, the European Union Regional Development Fund, the Province of Friesland, the City of Leeuwarden, and the EZ/Kompas program of the “Samenwerkingsverband Noord-Nederland”. Thanks are due to the members of the research theme “Blue Energy” in Wetsus for their participation and contributions.

Cover designed by Dr. Ran Zhao. Drawings in wax by Anna Casadellà Muní.
Printed by Drukkerij Macula B.V.